Identification and production of cardio-inductive extracellular matrix proteins for applications in regenerative medicine

Von der Fakultät Energie-, Verfahrens- und Biotechnik der

Universität Stuttgart zur Erlangung der Würde eines

Doktors der Naturwissenschaften (Dr. rer. nat.) genehmigte Abhandlung

Vorgelegt von

Monika Holeiter

aus Sathmar

Hauptberichter:	Prof. Dr. Günter Tovar
Mitberichter:	Prof. Dr. Thomas Hirth
	Prof. Dr. Katja Schenke-Layland
Tag der mündlichen Prüfung:	07.11.2014

Institut für Grenzflächenverfahrenstechnik

und Plasmatechnologie IGVP der Universität Stuttgart

2014

The person who says it cannot be done should not interrupt the person doing it.

Chinese saying

Table of contents

Abbreviations

BMSC	bone marrow-derived stem cell
BSA	bovine serum albumine
Co-IP	Co-Immunoprecipitation
CPC	cardiac progenitor cell
CVD	cardiovascular disease
DAPI	4’,6-diamidin-2-phenylindol
DHFR	dihydrofolate reductase
Dox	doxycycline
EB	embryoid body
ECM	extracellular matrix
EF	ejection fraction
EHS sarcoma	Engelbreth-Holm-Swarm sarcoma
ELISA	enzyme-linked immunosorbent assay
EMT	epithelial-to-mesenchymal transition
FACS	fluorescence activated cell sorter
FBS	fetal bovine serum
FPLC	fast protein liquid chromatography
G418	geneticin
GAG	glycosaminoglycan
GAPDH	glyceraldehyde 3-phosphate dehydrogenase
GFP	green fluorescent protein
GMP	good manufacturing practice
GVI	gray value intensity
hESC	human embryonic stem cell
HRP	horseradish peroxidase

IF	immunofluorescence
IMAC	immobilized metal affinity chromatography
LRR	leucine-rich repeat
LV	left ventricle/ left ventricular
mAU	milli absorbance unit
MEF	mouse embryonic fibroblast
MEM	minimum essential medium
MI	myocardial infarct
MI/R	myocardial ischemia and reperfusion
MMP	matrix metalloproteinase
MTX	methotrexate
Pen/Strep	penicillin-streptomycin
PFA	paraformaldehyde
PBMC	peripheral blood mononuclear cell
qPCR	real-time polymerase chain reaction
RGD	tripeptide L-arginine, glycine and L-aspartic acid
rpm	rotations per minute
RT	room temperature
RT-PCR	reverse transcription polymerase chain reaction
SDS-PAGE	sodium dodecyl sulfate polyacrylamide gel electrophoresis
SLRP	small leucine-rich proteoglycan
TGF-β1	transforming growth factor-β1
TMB	3,3',5,5'-tetramethylebenzidine
TNF-α	tumor necrosis factor-α
WHO	World Health Organization
wt	wild type

Summary

Cardiovascular disease (CVD) remains one of the leading causes of death in the world, despite significant advances that have been made in cardiology and cardiac surgery in order to change this fact. The most common cause of acute damage to the heart is a myocardial infarction (MI) event. Oxygen depletion during MI leads to a rapid loss of cardiomyocytes at the site of injury, which drastically and permanently impairs the heart's contractile force and the patients' quality of life. Limited regeneration potential of the heart precludes appropriate functional tissue repair. Instead, a scar is formed due to ongoing adverse compensatory mechanisms that are not only focused on the site of injury, but also exert their effects in remote areas [1, 2]. Unlike in the highly organized extracellular matrix (ECM) microenvironment in healthy myocardium, this remodeling process is characterized by an imbalanced turnover of ECM proteins and interstitial fibrosis. It has a major impact on ECM composition and organization that leads to cardiac stiffness [3, 4] and impaired electrical signal transduction and over years can cause pathological deformation and eventually heart failure. To address this major health problem, the regeneration of functional cardiac tissue and restoration of heart function is the driving goal for researchers worldwide.

In early human development, wounds heal rapidly and without the formation of a scar. Fetal wound healing has the potential to not only close the wound, but to regenerate functional tissue and therefore be a blueprint for ideal tissue repair. The fetal wound healing process is fundamentally different from its counterpart in adults, which often is accompanied by pathological fibrosis. A reason for this difference might be found in the unique fetal ECM organization and composition.

These findings provided the basis for the hypothesis of this work, which describes how a specific cardiovascular ECM at the onset of human cardiogenesis could contain key ECM proteins to promote cardioinduction and increase the heart's potential for functional tissue regeneration. In order to identify specific ECM proteins that provide cardiovascular microenvironmental cues during human embryogenesis, we used embryoid bodies (EBs) generated from human embryonic stem cell (hESC) line H9 as a model for early human development.

The results of this work show that an efficient cardiovascular differentiation protocol could be designed that generates a high number of spontaneously beating EBs (85% ± 17.6%) containing a high percentage of cardiomyocytes (49.4% ± 11.4% MF20-positive cells) within only 10 days of differentiation. These beating EBs represent an early stage in human cardiovascular differentiation and they secrete their own ECM. The expression patterns of the non-fibrillar ECM

proteins decorin and nidogen-1 were identified by real-time polymerase chain reaction (qPCR) analysis. Decorin and nidogen-1 expression is significantly increased during cardiovascular differentiation of hESCs in EBs, suggesting an important role of these proteins in early cardiac development. This result is supported by semi-quantitative analysis of immunofluorescence (IF) images that revealed a significantly higher amount of decorin and nidogen-1 in the beating EB samples at day 10 of cardiovascular differentiation compared to fibronectin, periostin, laminins, collagen types I and IV.

In order to test the potential of these proteins to support cardiovascular differentiation in vitro or to serve as potential therapeutic candidates, stable clones for the recombinant expression of active human decorin and nidogen-1 were generated. Production plasmids were designed utilizing I) a permanent and II) an inducible production system. Mutant Chinese Hamster Ovary (CHO) cells, deficient in the dihydrofolate reductase (DHFR) were transfected and selected with methotrexate (MTX) to enable genomic co-amplification, which resulted in a significantly increased decorin and nidogen-1 production with concentrations of up to 42.8 µg/ml decorin and 4.2 µg/ml nidogen-1 in the production media. The production clones that provided the highest yields were adapted to suspension culture and serum depletion, followed by production up-scaling and protein purification using fast protein liquid chromatography (FPLC)-controlled methods, retaining 73% -78% of the initial protein content. The identity and purity of the decorin and nidogen-1 concentrates was verified with specific antibodies. Glycosylation status and activity of these purified ECM proteins could be confirmed utilizing deglycosylation enzymes and Co-Immunoprecipitation (Co-IP) with known interaction partners.

The hypothesis of this work was tested in vitro, using the purified decorin and nidogen-1 as coatings on cell culture dishes. A cardio-inductive effect of nidogen-1 on hESC-derived EBs could be shown for the first time, as identified by a significant increase of cardiovascular differentiation efficiency on the coating containing nidogen-1. The effects of both decorin and nidogen-1 on the human immune reaction were tested in vitro and a protein concentration of 50 µg/ml had no impact on immune cell proliferation and activation. Therefore, this concentration was chosen to test the effect of decorin and nidogen-1 in vivo in a mouse MI and reperfusion (MI/R) model. Conscious echocardiography of the mice was conducted on three different time points after MI/R and injections in the infarct border zone. The echocardiography revealed a significant increase of the ejection fraction (EF), an important physiological parameter for heart function, in the mice that received nidogen-1 injections or combined decorin and nidogen-1 injections compared to the control mice two weeks post MI/R. At the latest analyzed time point, four weeks post MI/R, the significant positive effect of the nidogen-1 injections on heart function compared to the control mice remained consistently high. This effect of the nidogen-1 injections

resulted in a remarkable difference of 14.5% EF to the control mice. H&E and Russel-Movat Pentachrome staining as well as IF staining of the cardiomyocyte marker protein cTnT, were conducted on the explanted mouse hearts four weeks post MI/R. The qualitative histological analyses revealed that the cardiac morphology was better preserved and showed less pathological remodeling due to the nidogen-1 treatment compared to controls.

The results presented in this thesis include the identification of the potentially cardio-inductive hESC-derived cardiovascular ECM proteins decorin and nidogen-1, their recombinant production in CHO cells and the establishment of an in vitro hESC-based test system, with which we showed for the first time a cardio-inductive effect of nidogen-1. In addition, utilization of a small animal MI/R model revealed a significantly improved heart function and qualitative histological analyses showed a better preservation of cardiac morphology and lower degree of pathological remodeling after peri-infarct injections of nidogen-1 compared to controls. These results provide a direct reference towards the development of an early-stage nidogen-1-based therapy for the prevention of heart failure.

Zusammenfassung

Kardiovaskuläre Erkrankungen bleiben trotz großer Fortschritte in der Kardiologie und Herzchirurgie eine der häufigsten Todesursachen weltweit. Meist entstehen akute Schädigungen des Herzens durch myokardiale Infarkte (MI). Sauerstoffmangel während eines akuten Herzinfarktes führt innerhalb kurzer Zeit zum Absterben von Herzmuskelzellen, den Kardiomyozyten, in der Infarktregion, was eine drastische und anhaltende Beeinträchtigung der Kontraktionsfähigkeit des Herzen verursacht und somit die Lebensqualität des Patienten stark einschränkt. Durch das kaum bis nicht vorhandene Regenerationspotential des Herzens ist kein angemessener Wiederaufbau von funktionalem Gewebe möglich. Anstatt dessen entsteht eine Narbe aufgrund anhaltender Ausgleichsmechanismen, die sich nicht nur auf den Infarktbereich beschränken, sondern auch in entfernten Bereichen des Herzens ihre Effekte ausüben [1, 2]. Während sich gesundes Myokardium durch eine hoch organisierte extrazelluläre Matrix (ECM) auszeichnet, verursacht der MI-induzierte, pathologische Remodellierungsprozess den gestörten Umsatz von ECM-Proteinen und Fibrose. Er hat einen erheblichen Einfluss auf die ECM-Zusammensetzung und Organisation, die zunächst zu kardialer Versteifung und beeinträchtigter elektrischer Signalweiterleitung führen, und über Jahre hinweg krankhafte Verformungen und Herzversagen verursachen können [3, 4]. Das antreibende Ziel von Wissenschaftlern weltweit um dieses große Gesundheitsproblem zu bekämpfen ist die Regeneration gesunden Herzgewebes und der Herzfunktion.

In der frühen menschlichen Entwicklung heilen Wunden schnell und ohne die Entstehung von Narben. Fetale Wundheilung hat das Potential Wunden nicht nur zu schließen, sondern funktionales Gewebe wiederherzustellen und dient daher als Vorbild für ideale Gewebereparatur. Somit unterscheidet sich der fetale Wundheilungsprozess grundlegend vom entsprechenden Prozess im adulten Organismus, der häufig mit pathologischer Fibrose verbunden ist. Ein möglicher Grund für diesen Unterschied könnte die einzigartige fetale ECM Organisation und Zusammensetzung sein.

Vor diesem Hintergrund wurde die Hypothese dieser Arbeit formuliert, die besagt, dass die spezifische kardiovaskuläre ECM zu Beginn der humanen Kardiogenese Proteine enthält, welche eine kardioinduktive Schlüsselfunktion besitzen und das Potential des Herzens für funktionale Geweberegeneration erhöhen könnten. Um diese ECM Proteine zu identifizieren, haben wir aus der humanen embryonalen Stammzelllinie H9 (hESC H9) embryoid bodies (EBs) hergestellt, die als Modell der frühen menschlichen Entwicklung dienen.

Die Ergebnisse dieser Arbeit zeigen, dass ein effizientes kardiovaskuläres Differenzierungsprotokoll entwickelt werden konnte, mit welchem innerhalb von 10 Tagen spontan-schlagende EBs erzeugt werden konnten (85% ± 17.6%), die einen hohen Prozentsatz an Kardiomyozyten enthalten (49.4% ± 11.4% MF20-positive Zellen). Die schlagenden EBs repräsentieren eine frühe Stufe der humanen kardiovaskulären Differenzierung und sekretieren ihre eigene ECM. Mittels qPCR Analyse wurde die signifikant erhöhte Expression der nicht-fibrillären ECM Proteine Decorin und Nidogen-1 während der kardiovaskulären Differenzierung der hESCs in EBs gezeigt. Dies deutet auf eine wichtige Rolle dieser Proteine in der frühen Herzentwicklung hin. Die semi-quantitative Analyse von Immunfluoreszenzbildern unterstützt dieses Ergebnis, da sie eine signifikant höhere Menge von Decorin und Nidogen-1 in den schlagenden EBs an Tag 10 der kardiovaskulären Differenzierung im Vergleich zu Fibronektin, Periostin, den Lamininen, Kollagen Typ IV und Typ I aufdeckt.

Um das Potential dieser Proteine für die Erhöhung der kardiovaskulären Differenzierung in vitro oder als Therapie nach einem Herzinfarkt testen zu können, mussten zunächst stabile Zellklone für die rekombinante Produktion von humanem Decorin und Nidogen-1 hergestellt werden. Plasmide für I) ein permanentes und II) ein induzierbares Produktionssystem wurden konzipiert und in eine Dihydrofolatreduktase-defiziente Zelllinie aus dem Ovarium des Chinesischen Hamsters (CHO Zellen) transfiziert. Die Selektion mit Methotrexat (MTX) ermöglichte eine signifikante Steigerung der Decorin und Nidogen-1 Produktion, mit Konzentrationen im Kulturmedium bis zu 42.8 µg/ml Decorin und 4.2 µg/ml Nidogen-1. Die Produktionsklone, die den höchsten Ertrag brachten, konnten an Suspensionskultur und Serumreduktion angepasst werden. Anschließend folgte die Produktion in größerem Maßstab und die FPLC-gesteuerte Aufreinigung, bei der 73% - 78% der Proteinausgangsmenge erhalten wurde. Die Identität und Reinheit der Decorin und Nidogen-1 Konzentrate konnte mit spezifischen Antikörpern nachgewiesen werden. Der Glykosylierungsstatus und die Aktivität dieser aufgereinigten ECM Proteine wurden mit Hilfe von Deglykosylierungsenzymen und Co-Immunpräzipitationen mit bekannten Interkationspartnern bestätigt.

Die Hypothese dieser Arbeit wurde in vitro mit Beschichtungen von Zellkulturplatten mit aufgereinigtem Decorin und Nidogen-1 getestet. Ein signifikanter Anstieg der kardiovaskulären Differenzierungseffizienz durch die Nidogen-1 Beschichtung zeigte den kardioinduktiven Effekt von Nidogen-1 auf EBs aus hESCs. In vitro Tests ergaben, dass die Auswirkung von Decorin und Nidogen-1 auf die humane Immunzell-Proliferation und Aktivierung bei der Konzentration 50 µg/ml unbedenklich war. Daher wählten wir diese Konzentration für den Test von Decorin und Nidogen-1 Injektionen im Anschluss an einen Myokardinfarkt in einem in vivo Maus Modell.

Nach dem Infarkt und den Injektionen in den Infarkt-umgrenzenden Bereich folgten an drei verschiedenen Zeitpunkten echokardiographische Untersuchungen der Mäuse. Diese Untersuchungen zeigten bei den Mäusen denen Nidogen-1 oder eine Kombination von Decorin und Nidogen-1 injiziert wurde zum Zeitpunkt zwei Wochen nach dem Myokardinfarkt eine signifikante Erhöhung der Auswurfsfraktion (EF), einem wichtigen Parameter für die Herzfunktion, im Vergleich zu den Kontrollgeweben. Zum letzten untersuchten Zeitpunkt, vier Wochen nach dem Infarkt, blieb der positive Effekt der Nidogen-1 Injektionen auf die Herzfunktion mit einer Erhöhung um 14.5% EF verglichen mit den Kontrollmäusen ähnlich hoch. Vier Wochen nach dem Myokardinfarkt wurden an den entnommenen Herzen der Mäuse H&E und Russel-Movat Pentachrom Färbungen, sowie IF Färbungen des Kardiomyozyten Marker Proteins cTnT durchgeführt. Eine qualitative Auswertung der histologischen Untersuchungen ergab, dass die Morphologie der mit Nidogen-1 behandelten Herzen besser erhalten war und diese weniger krankhafte Remodellierung aufwiesen als die Kontrollherzen.

Die in dieser Doktorarbeit dargestellten Ergebnisse umfassen die Identifizierung der potentiell kardioinduktiven ECM Proteine Decorin und Nidogen-1 aus einer von hESCs gebildeten, kardiovaskulären Matrix, sowie deren rekombinante Herstellung in CHO Zellen. Zudem konnte ein in vitro Testsystem aufgebaut werden, welches zum ersten Mal die kardioinduktive Wirkung von Nidogen-1 zeigt. In einem Kleintiermodell, bei dem nach einem induzierten MI Nidogen-1 Injektionen in den Infarkt umgebenden Bereich verabreicht wurden, ergab sich eine signifikante Verbesserung der Herzfunktion und qualitative histologische Analysen zeigten einen verbesserten Erhalt der kardialen Morphologie und ein geringeres Ausmaß an krankhafter Remodellierung im Vergleich zu den Kontrollgeweben. Diese Ergebnisse stellen den ersten Schritt auf dem Weg zur Entwicklung einer frühzeitigen, Nidogen-1 basierten Therapie gegen Herzversagen dar.

1 Introduction

For many years the biological functions of organs and tissues were attributed to the different cell types within these entities, while the extracellular matrix (ECM) was believed to be merely an inert supporting scaffold. But recently besides the obvious function of the ECM as structural support or its influence on physical characteristics of the tissue like stretch or strain, scientists started to unravel the complexity of the interplay between cells and their specific ECM microenvironment. Its role in tissue regeneration can be used for therapeutic approaches with natural ECM proteins.

1.1 ECM in the heart

The human heart's highly organized myocardium is composed of cardiomyocytes, fibroblasts, endothelial cells and vascular as well as neuronal networks that are arranged in this organized structure. The heart is a complex organ that is the first to develop and function during embryogenesis, which underlines its vital importance. The complex and dynamic myocardial ECM is expressed in precise temporal as well as spatial patterns and is mainly produced by the cardiac fibroblasts. Due to remodeling events in the cardiac development as well as in diseased states, the ECM undergoes constant change. It comprises structural proteins like collagens and elastin, adhesion proteins like fibronectin, laminins and tenascins as well as matricellular proteins in a hydrated environment that is rich in proteoglycans and glycosaminoglycans (GAGs) [5], which is constantly communicating with the embedded cells. Utilizing cell-matrix interactions, the ECM can transmit information on the occurring physical forces to the cells, thereby activating intracellular signaling pathways [6]. This can lead to a change in cell function, for example by supporting transdifferentiation of a cell type to another, which conversely can induce changes in the ECM structure, typically due to altered matrix deposition or the release of remodeling enzymes like matrix metalloproteinases (MMPs) [7].

1.2 Cardiovascular disease

Cardiovascular disease (CVD) is the leading cause of death in industrialized countries, affecting every one in five men and women during a lifetime [8, 9]. Despite medical progress a cure to CVD could not be found to this point. It continues to have an exceptional relevance to society

and causes exceedingly high costs for the healthcare system. The occurrence of deaths caused by CVD in different age groups is shown in **Figure 1**.

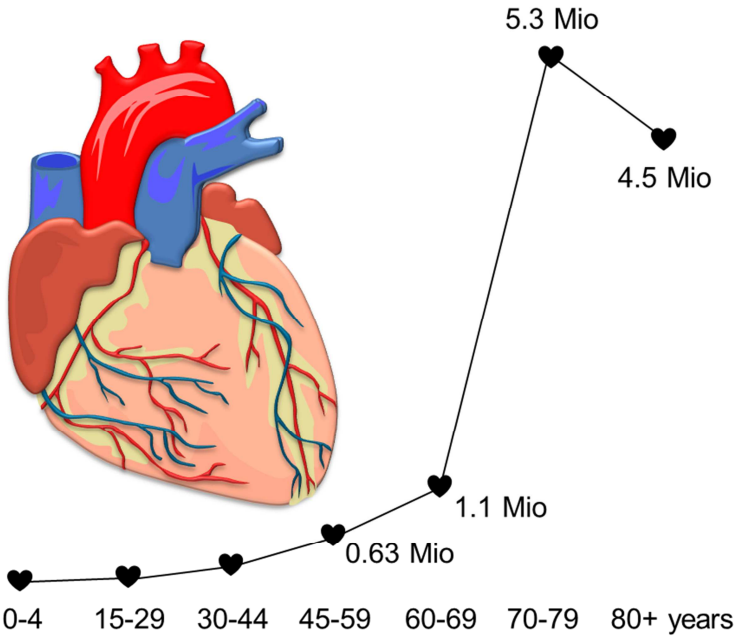

Figure 1: Global deaths per year caused by CVD in the age groups 0 – 4 years, 15 - 29 years, 30 - 44 years, 45 - 59 years, 60 - 69 years, 70 - 79 years and 80 + years. Modified from the World Health Organization (WHO); http://www.who.int/mediacentre/factsheets/fs317/en/.

With the highest occurrence of CVD in the older age groups and our increasingly aging society, the negative impact of CVD on society and healthcare systems is expected to rise. Often this major health risk manifests as an acute myocardial infarct (MI), which is an ischemic event that is caused by an inadequate arterial oxygen supply to the myocardium. Similar to other injuries a MI is accompanied by cell death and inflammation [4], raising the need for a wound healing process. Cardiomyocytes, the contracting cells that are responsible for the heart's pumping function, are especially sensitive to ischemic conditions and die within hours [10, 11]. The wound healing process after a MI shares many characteristics with wound healing processes that occur after physical trauma in other [6], even fundamentally different tissues [12, 13]. Wound healing in the heart induces scarring, a prominent alteration of the ECM [14].

1.3 Development of heart failure

Fibroblasts in the healthy, uninjured myocardium are protected from mechanical stress in the beating heart by the cross-linked ECM surrounding them [4]. In the aftermath of a MI, fibroblasts are exposed to mechanical stress as their ECM microenvironment is significantly damaged. Mechanical stress induces the differentiation of fibroblasts to proto-myofibroblasts, the first stage in the two-stage model of myofibroblast transdifferentiation [15]. The proto-myofibroblasts already can generate contractile force [15]. Continuing exposure to stress as well as the presence of transforming growth factor-β1 (TGF-β1) that is mainly produced by cardiac fibroblasts [16], stimulates the transdifferentiation of proto-myofibroblasts to myofibroblast [17]. These cells express the contractile protein α-smooth muscle actin in more extensively developed stress fibers and thereby generate a greater contractile force than proto-myofibroblasts [15, 18]. Transdifferentiation of cardiac fibroblasts to myofibroblasts does not occur in the protected microenvirnonment of a healthy heart [15], therefore this cell type only emerges in the heart after injury. The transdifferentiation process contributes to the formation of a granulation tissue following wounding that is mainly composed of small vessels, fibroblasts, myofibroblasts as well as inflammatory cells [19]. In this environment, myofibroblasts are mainly responsible for the contraction of the granulation tissue to reduce the scar size [20]. Contraction generated by cardiomyocytes and myofibroblasts is fundamentally different [4]. While cardiomyocytes contract and relax cyclically upon electrical activation from the cardiac conduction system [15], myofibroblasts generate a tonic, sustained contraction. The replacement of the necrotic tissue post MI with granulation tissue and finally with a scar, the so-called replacement fibrosis, initially has a positive effect, as it helps support the ventricular morphology by reinforcing the injured myocardium [4]. This can prevent dilatation leading to heart failure [4]. These early modifications of the dynamic cardiac ECM to adapt to a cardiac injury event are still reversible. Later irreversible changes to the collagen network affect collagen amount and phenotype and are mainly characterized by a higher degree of collagen crosslinking.

Differences in the mode of cardiac ischemic wound healing and normal wound healing of the skin become apparent after the initial wound stabilization. In the skin, the wounded contracted area is similarly stabilized by ECM mainly deposited by myofibroblasts [14, 21]. Subsequently the amount of cellular elements, especially myofibroblasts, in the granulation tissue decreases significantly, leaving an ECM-rich, poorly cellularized skin scar [12, 22]. Unlike wound healing in the skin, myofibroblasts can persist in the human heart for decades after a MI [23], even in areas

remote from the site of injury. This is probably due to a lack of apoptotic decellularization [22, 24] in the final phase of wound healing.

The remaining myofibroblasts continue to influence matrix turnover in the post-injury state, which is the result of the synthesis and degradation processes of ECM during cardiac remodeling [25, 26]. Due to their accelerated production and deposition of collagens, myofibroblasts are mainly responsible for the unbalanced matrix turnover post MI, which causes fibrosis [25, 26]. Fibrosis is a common outcome of an imperfect healing process, not only in the heart, but in various tissues, for example in kidney, lung or liver [27-29]. In the heart the remaining myofibroblasts cause persisting adverse ECM changes. Their excessive deposition of interstitial collagen type I with a high degree of cross linking in areas remote from the original site of injury increases cardiac stiffness [14] and can contribute to pathological cardiac remodeling, deformation and malfunction. Especially left ventricular (LV) remodeling, characterized by LV dilatation and diminished cardiac performance, predicts the progression of heart failure and increased mortality [30, 31].

1.4 Therapeutic approaches

Over a course of years, patients gradually develop heart failure due to pathological remodeling processes described above. For these patients no therapy is available to regulate the underlying ongoing process of pathological ECM turnover and therefore prevent heart failure. Bypass surgery or LV assist devices can help the patients, but to date, heart failure has no cure. Heart transplantation is still the only therapy that can stop the progression of the disease. For most patients however, limited donor supply and organ rejection preclude its widespread use [32].

The body has an innate ability to mobilize and release endothelial progenitor cells like bone marrow-derived stem cells (BMSCs). Through the blood flow these cells reach the heart. It could be shown that the magnitude of progenitor cell mobilization after an acute MI can be correlated with regional and global left ventricular functional improvement [33]. But confronted with a large MI, the body's innate regeneration ability cannot meet the required extent.

Still, the idea to make up for the lost cardiomyocytes post MI with a potent cell population, has led to the development of various cell replacement approaches [34-37]. The aim of these therapies is to apply cells (usually via injection) into the myocardium that have the capacity to restore the heart's blood-pumping function in the infarcted area. Unfortunately, over the last decade, cell replacement therapies alone have proven unable to fulfill the high expectations scientists had of this revolutionary therapy [38-46]. To date, cardiac stem cell transplantation

showed only modest results with restricted therapeutic effectiveness. There are various reasons for these disappointing results of cell-based therapies, including the lack of safe and easily identifiable cell populations for transplantation, inefficient cell delivery with the method of injection as well as low retention, survival, engraftment and differentiation of the implanted cells in the hostile microenvironment post MI are the most important hurdles [47-49].

To prevent high mortality due to the body's inadequate regeneration post MI, modern approaches should not only rely on cell replacement therapies to replenish for the loss of cardiomyocytes. It is crucial that they also provide a healthy ECM that combines structural integrity with cardio-inductive microenvironmental cues to support a true regeneration of the infarct area. Contrary to an infected and scarred microenvironment in the post MI myocardium, normal cardiac ECM would have the capacity to guide the cell fate of the heart's resident adult stem cells to potentially differentiate into cardiomyocytes. Also, it could be used to inhibit the adverse changes in ECM turnover and especially LV remodeling post MI or support the success of an additional cell transplantation therapy. Searching for such cardio-inductive ECM, this PhD thesis was guided by various reports from the field of ECM research. Over two decades ago, scientists observed in human fetuses with progressive and life-threatening anatomic defects that fetal wound healing is fundamentally different from the wound healing process in adults [50, 51]. While scarring and fibrosis are a common outcome of imperfect tissue and organ repair in adults, this was not the case in the fetus [50]. Here, wound healing occurred rapidly and without the formation of a scar. This 'true regeneration' of the wounded tissue can be considered as a blueprint for ideal wound healing. The authors hypothesized that the extraordinary regeneration potential of the fetus may be attributed to its ECM, which shows a unique organization and different composition compared to adult ECM [50].

To date, a multitude of beneficial functions attributed to the ECM generate the interest to use specific ECM compositions for applications in tissue engineering and regenerative medicine [52-54]. It has been shown that the injection of an ECM hydrogel containing decellularized porcine cardiac tissue post MI has a positive effect in a large animal study [55]. In this study, upon injection of infarcted pigs with a digested ECM hydrogel, an improvement in cardiac function, ventricular volumes, and global wall motion scores was achieved. Furthermore, the ECM-treated hearts were distinguishable from the untreated control hearts by a significantly larger zone of cardiac muscle at the endocardium. Unfortunately, there are many limitations for the transfer of ECM products generated with decellularization methods to clinic. The loss of the biologically important proteoglycans (such as decorin) or other non-structural ECM proteins (such as nidogen-1) in the decellularization process, animal origin and possible immunological rejections

as well as uncertain reproducibility of the decellularization process and undefined composition of the ECM product are only some of the important limitations [56].

1.5 ECM and stem cells

As early as the very beginning of human embryonic stem cell (hESC) research, scientists had high expectations of the impact these cells would have on transplantation therapies [57]. This new and promising cell source seemed to be predestined for the successful treatment of diseases that affect only one or few cell types like Parkinson's disease, juvenile-onset diabetes mellitus or cardiac disease. The reasons for these high expectations are the intriguing properties of hESCs. Derived from the inner cell mass of the blastocyst [57-59], hESCs have the potential to differentiate into any specialized cell type from all the three germ layers or to self-renew and thereby maintain their undifferentiated pluripotent state in vitro for more than one year [60]. The self-renewal mechanism allows the expansion of hESCs in their karyotypically and phenotypically stable state. It became clear that the mechanisms that determine the fate of hESCs needed to be understood and controlled in order to direct the differentiation of these cells to a specific cell type. Only an efficient, guided differentiation protocol can produce large populations of purified cell types such as cardiomyocytes for applications in drug discovery or regenerative medicine (**Fig. 2**).

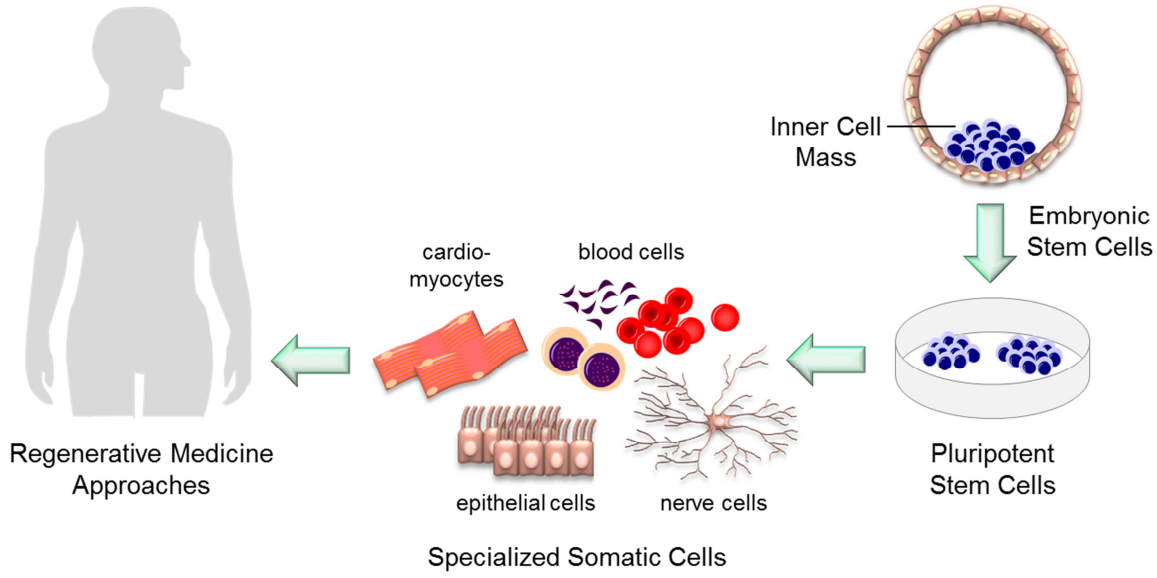

Figure 2: Schematic of the most important steps and cell types for regenerative medicine approaches.

It is known that cell fate decisions in vitro are determined by signals the hESCs are exposed to from adjacent cells in the ESC colonies or in co-cultures [61, 62], as well as from soluble factors in the media and insoluble factors [63, 64], like the ECM that is in contact with the cells via integrin receptors on the cell surface [65]. While the use of ECM has been recognized and utilized in many different ways for the maintenance of ESC pluripotency, like for the culture on ECM secreting feeder layers of mouse embryonic fibroblasts (MEFs) [58, 62, 66], on the ECM extract Matrigel [67], or on coatings of ECM mixtures [68], single ECM proteins like laminins, collagen type I, fibronectin, vitronectin or E-cadherin [67, 69-76], or synthetic peptide-acrylate surfaces [77], there are only a few examples that use a specific ECM in order to guide the differentiation of pluripotent cells to tissue-specific cell types, such as cardiomyocytes [63, 78-83]. Insufficient knowledge of the changing composition and organization of the developing cardiac ECM in human embryogenesis restrains the promising application of a cardiac-specific cardio-inductive ECM in regenerative medicine for the diseased heart.

1.6 Differentiation of embryoid bodies

Embryoid bodies (EBs) are cell aggregates that form spontaneously when ESCs are cultured in suspension [84]. Another protocol for EB generation uses the spin EB method, where the ESC suspension is centrifuged in conical well plates [85]. In EBs, the differentiation of pluripotent ESCs into cells from the three germ layers is triggered [86]. Using hESCs, the resulting 3-dimensional cell spheroids recapitulate early human embryogenesis to a certain extent [84, 87, 88], and therefore are an accessible in vitro model to investigate early differentiation events in various tissues [57, 58, 86, 89]. EBs are a powerful tool for the investigation of ECM deposition in the earliest stage of human cardiogenesis in order to elucidate the initial signals that drive cardiac differentiation.

Current differentiation protocols of hESCs combine the formation of EBs with staged growth factor addition to the media [85, 90-92]. HESCs that differentiate to the three cardiovascular cell phenotypes (endothelial cells, smooth muscle cells and cardiomyocytes) deposit their own ECM, that is different from the ECM deposited by undifferentiated hESCs [93]. We expect the changed composition of the secreted ECM to hold specific information for cardiovascular differentiation. In a combined ECM and cell therapy, this cardio-inductive ECM could be used to generate a microenvironment that supports the directed cell fate decision to cardiomyocytes (**Fig. 3**).

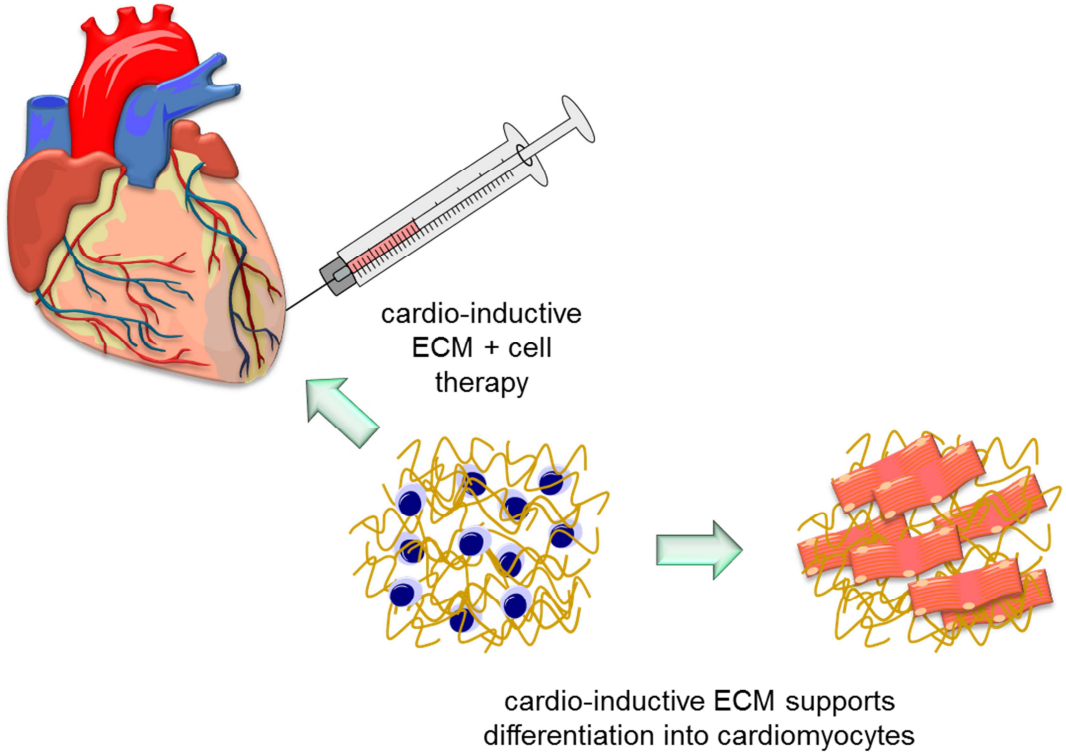

Figure 3: Schematic of a cardio-inductive ECM + cell therapy. The microenvironment generated by this ECM can support the differentiation of transplanted cells into cardiomyocytes.

1.7 Requirements for an ECM protein product

For the safety and efficacy of a high-quality protein product like an injectable hydrogel with defined composition and protein concentration, several points must be taken into account. For a safe clinical application, the identity of the potential cardio-inductive ECM proteins must be human. Protein sequences among different species may show high homology to the human sequence, but even slight differences might be detected and trigger a response from the immune system of the patient [94-96]. This precludes the extraction and purification of the identified proteins of interest from animal tissue. With regard to a possible protein extraction from human tissue, it should be noted that these tissues are rare, of varying origin and quality and with uncertain infection background. Also, the purification of a specific protein from a tissue with complex protein composition can require harsh methods [97]. These can damage the protein and impair or abolish its natural activity. Therefore the recombinant production of a protein of interest is much preferred compared to its extraction from human or animal tissue. Progress in

genetics allowed a higher understanding of protein production and the possibilities of genetic manipulation [98-100]. One of the most important accomplishments of this development is recombinant protein production in high-yield host cell lines [99, 100]. Recombinant production of protein therapeutics is an important branch of the pharmaceutical industry, which achieves turnovers measured in the billions worldwide. Compared to protein extractions from tissues, recombinant protein production has the advantage to grant the secured availability of the human protein of interest in a reproducible high quality [101].

In order to generate high-quality protein products, the recombinant production of the human ECM proteins of interest by a safe host cell line under defined conditions and in defined media is preferable to other options. The careful selection of the host cell line, transfection, clone selection, production and purification method needs to be based on the requirements for recombinant human ECM protein production under good manufacturing practice (GMP)-translatable conditions. For proteins to be synthesized in biologically active forms, they need to be properly folded and post-translationally modified. There are more than 200 different post-translational protein modifications possible in mammalian cells. Glycosylation is one of the most common and important post-translational modifications [102, 103]. When glycans are attached to asparagine residues on the core protein this is defined as N-linked glycosylation and when glycans are attached to serine or threonine residues as O-linked glycosylation [103]. This post-translational modification cannot be done in microbial hosts like Escherichia coli because these organisms lack the required machinery to synthesize the appropriate mammalian glycoforms [100, 102, 104]. Many ECM proteins carry complex glycosylations that are important for activities like growth factor sequestering and can enable interactions with cells or other ECM components. Therefore an adequate host with the required enzymes for post-translational modification of human proteins needs to be chosen. In this work, we chose Chinese Hamster Ovary (CHO) cells, the most commonly used cell line for the production of recombinant protein therapeutics in the pharmaceutical industry [101, 105].

1.8 Strategies to increase recombinant protein production

The CHO cell line is a robust protein expression host that is easy to maintain and has the ability to adapt to suspension culture [106]. Suspension culture results in enhanced cell density and cell productivity levels compared to cultures employing adherent cells and therefore is the most common cell culture format for recombinant protein production with CHO cells [101]. By using a mutant CHO cell line deficient in the dihydrofolate reductase (DHFR) enzyme, an improved

selection of stable clones and co-amplification of the gene of interest can be achieved with rising methotrexate (MTX) levels [107, 108]. The increased number of copies of the gene of interest in the host genome due to co-amplification with the DHFR gene results in a higher productivity of the production clone. The DHFR enzyme catalyzes the reaction of dihydrofolate to tetrahydrofolate, thereby playing a central role in the synthesis of this nucleic acid precursor in all organisms and eventually for DNA replication and cell growth (**Fig. 4 A**). MTX is a potent competitive inhibitor of the DHFR enzyme, with a one thousand-fold higher affinity to DHFR than folate (**Fig. 4 B**). Making use of this co-amplification system, specific productivity levels are expected to be highly increased [101, 109].

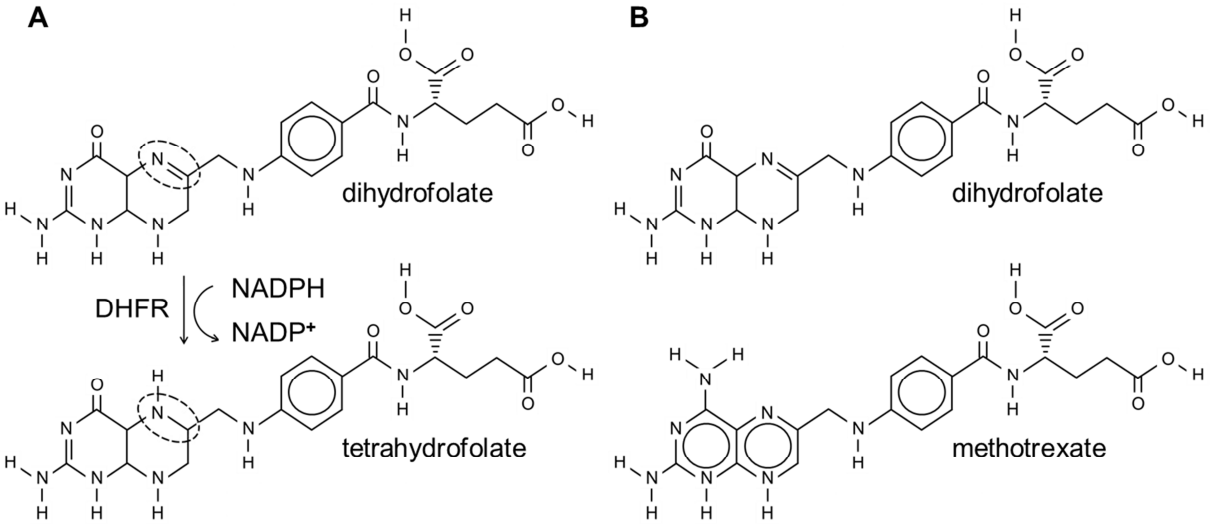

Figure 4: Function of the DHFR enzyme. **A**) The DHFR enzyme catalyzes the transfer of a hydride from NADPH to dihydrofolate, thereby reducing dihydrofolate to tetrahydrofolate while NADPH is oxidized to NADP+ [110]. **B**) MTX is a very tight binding inhibitor of the DHFR enzyme and shares similar structures with dihydrofolate [110].

For a further increase of product expression, codon adaptation can be applied to the gene sequence of the potentially cardio-inductive ECM proteins [111]. The genetic code is degenerated, which means that many amino acids are encoded by more than one triplet codon. The concept of codon adaptation is based on the usage of the most frequently used triplet code for an amino acid, resulting in an optimized gene sequence, matching the codon usage of the rodent host while still encoding the same human protein [112]. This is how codon adaptation can bypass predictable bottlenecks in tRNA availability for a certain codon in the host cell line.

Additional to permanent recombinant protein production, an inducible production of the potentially cardio-inductive ECM proteins can be beneficial. This is the case if the permanent amplified recombinant protein production causes a metabolic burden to the host cell, leading to reduced proliferation [113]. Undesired inhibition of the host cell proliferation during the clone selection phase could also be caused by the biological effects of the protein of interest [114]. Therefore instead of conventionally designed plasmids for the permanent protein production, the inducible production system uses plasmids with the protein of interest under the transcriptional control of an inducible promoter [115]. For this system it is necessary to stably transfect the host cells with a plasmid for the permanent production of an activator protein [115, 116]. Subsequently this stable activator clone is transfected with the plasmid for inducible production of the protein of interest. In this plasmid an inducible promoter controls the transcription of the gene of interest and can only be activated by the permanently produced activator protein in the presence of doxycycline (Dox) [115, 116].

1.9 Purification of recombinant ECM proteins

For easier protein purification without the need for a lysis step as well as intact protein activity, the recombinant ECM proteins should be secreted to the culture media by the host cells, just like these ECM proteins are secreted into the interstitial space in the human body [101, 117]. For secretion purposes the ECM protein's natural secretion peptide needs to be included in the ECM gene sequence on the production plasmid. Incomplete protein secretion of the recombinant ECM proteins could cause protein aggregate formation in the host cell, impairing its metabolism as well as the protein purification and protein activity [117]. Protein purification of secreted proteins from the culture media leads to higher yields with maintained protein activity as no cell lysis, chemical extraction of the protein-containing cell compartment or refolding of the protein to bioactive conformation needs to be performed [117, 118].

Affinity chromatography is one of the most efficient and selective chromatographic protein purification methods [104]. Several small affinity tags are widely used as an efficient tool for recombinant protein purification, histidine-tags being one of the most known and favored [119, 120]. The main step in the purification of a secreted, histidine-tagged protein is based on a specific type of affinity chromatography, the so-called immobilized metal affinity chromatography (IMAC) [121]. In this case the natural affinity of the amino acid histidine to immobilized nickel ions on an affinity chromatography column is used for the protein purification [120, 122]. A nickel

ion charged sepharose bead matrix ensures a high binding capacity for histidine-tagged proteins [120]. The molecular interaction, which is the basis of this affinity chromatography is shown in **Figure 5**.

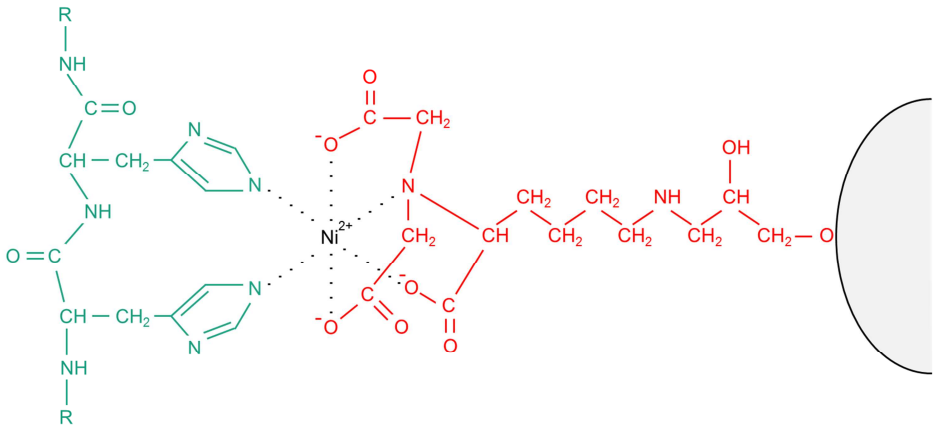

Figure 5: Basis of IMAC with a poly histidine-tag. A protein with poly histidine-tag (in green) is bound to a nickel ion (Ni^{2+}). The nickel ion is immobilized to a solid support (sepharose bead) by the chelating agent nitrilotriacetic acid (NTA, in red) and a linker (in red).

Reproducible IMAC purification with defined equilibration, wash and elution buffers, constant flow rates through the affinity chromatography column and monitoring of important measurement data can be accomplished with a fast protein liquid chromatography (FPLC) system [117]. Monitoring and recording of flow rate, conductivity, pressure and absorption at 280 nm and 256 nm provide an informative basis of the different sections of the purification process. Automated elution fraction collection and subsequent desalting and buffer exchange, concentration, wash and sterile filtration of the protein solution result in a high-quality pure protein product that can be stored until use at -80°C [117].

1.10 Aims of this study

In diseased states, the ECM turnover, composition and crosslinking characteristics in the heart are drastically changed, mainly due to the effects of a cell type that cannot be found in the healthy heart – the myofibroblast. Despite huge efforts, the great expectations scientists had of cell replacement therapies to replenish the lost cardiomyocytes after a MI did not prove realistic, as these therapies alone remained disappointing.

A multitude of functions attributed to the ECM so far generate the interest to use specific ECM compositions for applications in tissue engineering and regenerative medicine for the diseased heart. First results of ECM injections in large animal models for MI are promising, but such undefined ECM products that are generated by decellularization of tissues have many limitations for an application in clinic.

Over two decades ago the unique organization and composition of fetal ECM was implied to hold the key for the outstanding ability of ideal fetal wound healing, which is a blueprint for scar-free functional tissue regeneration [50]. This background lead to the hypothesis of this work, that the ECM microenvironment in the early healthy cardiovascular development holds the key cardio-inductive signals that are necessary for an increased regeneration potential of the diseased heart. This cardio-inductive ECM could trigger a higher regenerative potential from the heart's own adult stem cells or circulating stem cells of the body. In addition, the ECM provides structural integrity with microenvironmental cues, and when combined with a cell replacement therapy, the ECM could support a successful cell delivery, engraftment, survival as well as differentiation of transplanted cells to cardiomyocytes. A healthy cardiovascular ECM composition and the biological activities of its components can regulate the imbalanced ECM turnover post MI, prevent fibrosis, pathological remodeling of the heart and finally heart failure.

In this study, we identified the key ECM proteins in early human cardiogenesis utilizing EBs, generated from hESC line H9. We modified a staged protocol for the efficient differentiation of spin EBs towards the cardiac lineage and analyzed the cardiac-specific ECM that the EBs deposited during differentiation. In a next step, we produced these human ECM proteins under GMP-translatable conditions. The cardio-inductive effect of the chosen cardiac ECM proteins was tested in vitro with hESC cells, and their impact on heart regeneration post MI was examined after ECM protein and hydrogel injections in a mouse myocardial ischemia and reperfusion (MI/R) model. We believe that the influence that specific ECM components or mixtures exert on cell fate decisions can be used to give the right stimuli to drive cardiac cell fate decisions. The implementation of cardiac-inducing ECM proteins in tissue engineering strategies might help to provide crucial microenvironments for regenerative medicine applications for the diseased heart.

2 Material and methods

2.1 Identification of hESC-derived cardiovascular ECM proteins

2.1.1 HESC culture and generation of embryoid bodies

HESCs (H9) [62] were cultured according to current protocols (WiCell Research Institute, Inc.) on MEF cells (PMEF-CFL, Millipore, USA). HESC culture media was prepared from 200 ml DMEM/F12 media (11330-032, Life Technologies, USA), 50 ml serum replacer (10828-028, Lot 1253363, Life Technologies, USA), 1.25ml L-glutamine (35050-061, Life Technologies, USA), 1.75 µl 2-mercaptoethanol (M7522, Sigma Aldrich, USA), 2.5 ml 100x MEM non-essential amino acids (11140-050, Life Technologies, USA) and 0.5 ml b-FGF solution (PHG0261, Life Technologies, USA). For single cell suspension, the H9 cell colonies were washed with phosphate buffered saline (PBS) (BE17-512F, Lonza, Switzerland), incubated with TrypLE Select (12563-011, Life Technologies, USA) 5 min at 37°C, resuspended with a 1 ml pipette and passed through a cell strainer with 40 µm wide pores (352340, BD Biosciences, USA). The cell suspension was mixed with PBS in the ratio 1:1 and centrifuged (5 min, 1000 rpm). The cell pellet was resuspended in mTeSR1 (05850, STEMCELL Technologies, Inc., Canada) with 10 ng/ml BMP4 (314-BP-010, R&D Systems, USA) and 10 ng/ml Rho-associated kinase (ROCK) inhibitor (Y-27632, Sigma Aldrich, USA) to make a 6 x 10^5 cells/ml suspension. 3 x 10^4 cells (50 µl of the cell suspension) were dispensed per well in a 96-well plate with conical wells (249952, 96-Well Microplates, non-treated, conical bottom, Fisher Scientific, USA). The cell suspension in the 96-well plate was centrifuged at 1000 rpm for 5 min and the plate was incubated overnight in a cell culture incubator.

2.1.2 Modified cardiac differentiation protocol

For cardiac differentiation, a modification of the differentiation protocols described in Yang 2008 and Willems 2011 [64, 92] was used. On day 1 of differentiation, after the overnight incubation, EBs formed due to cell aggregation and were carefully transferred to ultra-low attachment 6-well plates (3471, Corning incorporated, USA) with 1 ml pipettes. One 6-well can hold up to 200 EBs in 3 ml of StemPro 34 (10639-011, Life Technologies, USA) + 3 ng/ml Activin A (338-AC-010/CF, Life Technologies, USA) + 5 ng/ml bFGF (233-FB-025/CF, R&D Systems, USA) + 10 ng/ml BMP4 (314-BP-010, R&D Systems, USA) (stage 1 media). A change of the same media is required on day 2 or 3 of differentiation. The floating EBs were transferred to a 0.1% gelatin

coated 6-well on day 4 with 2 ml of stage 1 media + 5 µM IWR-1 (I0161-5MG, Sigma Aldrich, USA) (as replacement of 150 ng/ml DKK-1). The EBs were incubated without moving the plate until the next day. On day 5, most of the EBs had attached to the dish, cells outgrew the EBs and spread on the coated 6-well. From day 5 to day 10 the attached EBs were differentiated in stage 2 media, consisting of StemPro 34 (10639-011, Life Technologies, USA) + 5 ng/ml VEGF (293-VE-010/CF, R&D Systems, USA) + 10 ng/ml bFGF (233-FB-025/CF, R&D Systems, USA) + 5 µM IWR-1 (I0161-5MG, Sigma Aldrich, USA). A change of the same media was required on day 8 of differentiation. The attached EBs started beating on day 7 or 8 and were harvested for further analysis on day 10.

2.1.3 Counting and dissection of beating EBs

On day 10 of cardiovascular differentiation, the beating and non-beating attached EBs were inspected under a IX51 inverted microscope (Olympus Corporation, Japan). Beating EBs were marked from underneath with a pen. The percentage of spontaneously beating EBs was calculated for the different cultures. A 23-gauge needle and a dissection microscope (SMZ1000, Nikon, Japan) with a heatable plate (MATS-USMZSL, Tokai HIT Co. Ltd, Japan) set to 37°C were utilized for dissecting beating EBs from the surrounding non-beating cells that have grown out of the attached EBs. The needle was used to cut the cells on the border between the beating EBs and the surrounding non-beating cells and to thereby detach the EBs from the plate. At room temperature, the EBs stop beating after few minutes, therefore, dissection on a heated plate increased the beating time and facilitated the dissection of the beating from the non-beating cells. Prior to further analysis, the detached EBs as well as the non-beating cells were transferred to reaction tubes and were washed with PBS.

2.1.4 Flow cytometric analysis

For the intracellular fluorescence activated cell sorter (FACS) analysis on day 10 of cardiovascular differentiation approximately 30 beating EBs as well as non-beating surrounding cells from one 6-well were prepared according to the following protocol. The samples were transferred to FACS tubes, washed with PBS, incubated with TrypLE Select (12563-011, Life Technologies, USA) and mechanically resuspended by pipetting to receive a single cell suspension. The cell suspension was passed through a cell strainer (352340, BD Biosciences,

USA), PBS was added to the samples and they were centrifuged at 1300 rpm for 5 min. The supernatant was discarded, and the cells were resuspended in 50 µl of PBS. 950 µl 4% paraformaldehyde (PFA) in PBS (19943 1 LT, Affymetrix, USA) were added. The cells were resuspended and incubated on ice for 15 min. 57 µl of 2.5 M Glycine (50046-50G, Sigma Aldrich, USA) were added per 1000 µl cell suspension in 4% PFA. The suspension was agitated for 30' at RT. The cells were spun at 1500 rpm for 5 min and then permeabilized with 1x Perm/Wash buffer (554723, prepared from 10x solution, BD Biosciences, USA) for 15 min at 4°C. Afterwards, the cells were centrifuged at 2000 rpm for 7 min and the supernatant was removed. The pellet was resuspended in 1600 µl 1x Perm/Wash buffer, and the cells could rehydrate on ice for 5 min. The primary antibody MF20 (MF20 antibody concentrate, Developmental Studies Hybridoma Bank (DSHB)-university of Iowa, USA) was added to the cells in a dilution of 1:100 and incubated for 30 min on ice. The cells were washed with Perm/Wash buffer and spun at 2000 rpm for 7 min. The last step was repeated 3 times before the secondary antibody (1:250, A21203, Alexa Fluor AB, 594 nm, donkey against mouse, Life Technologies, USA) was added and incubated for 20 min in the dark on ice. The cells were again washed with 1x Perm/Wash buffer and spun at 2000 rpm for 7 min three times. Subsequently the samples were analyzed using the BD LSRFortessa cell analyzer (BD Biosciences, USA) and MF20$^-$positive cells were detected with Texas PE.

2.1.5 Immunofluorescence (IF) staining

EBs were fixed in 4% PFA (19943 1 LT, Affymetrix, USA) for 24h. The PFA was removed and some drops of liquefied Histogel (EMHGECS, American MasterTech, USA) were dispensed onto the EBs. After cooling, the Histogel solidified and the samples could be processed and paraffin-embedded. Immunofluorescence staining on paraffin-embedded 3 µm tissue sections of EBs on day 10 of cardiovascular differentiation and human fetal heart (17 weeks) was performed to detect cardiac-specific proteins (cardiac Troponin T (cTnT, TNNT2) and sarcomeric myosin (MF20 antibody)) as well as ECM proteins (decorin, nidogen-1, laminins and collagen type IV). The study of human fetal hearts, obtained from elective abortions, was performed in accordance with institutional guidelines and received approval by the local research ethics committee at the University of California Los Angeles (IRB #05-10-093). The sections were deparaffinized in xylene and hydrated in baths of decreasing ethanol concentrations. Antigen retrieval was performed consecutively in Tris-EDTA and citrate buffer in a steam cooker. For the intracellular antigens, the sections were treated with 1% Triton X-100 for permeabilization of the cell

membrane. A goat block solution was used to block unspecific binding sites. Primary antibodies to sarcomeric myosin (1:50, MF20 antibody concentrate, Developmental Studies Hybridoma Bank (DSHB)-University of Iowa, USA), decorin (1:250, GTX 101250, Genetex, USA), nidogen-1 (1:100, sc-33141, Santa Cruz, USA), laminins (1:50, ab11575, Abcam, UK) and collagen type IV (1:250, ab6586, Abcam, UK), as well as cTnT (1:3000, HPA015774, Sigma Aldrich, USA) were diluted in antibody dilution buffer (PBS containing 1% bovine serum albumin (BSA), 0.1% TritonX-100, 0.1% cold-water fish skin gelatin and 0.05% Tween20) and samples were incubated overnight. After several washes, the secondary antibody was applied to the samples. For sarcomeric myosin the secondary antibody was anti-mouse IgG 2b (1:250, A-21145, Alexa Fluor 594, Life Technologies, USA), for the other proteins the secondary antibody anti-rabbit IgG (H+L) (1:250, A-11034, Alexa Fluor 488, Life Technologies, USA) was used. The secondary antibody was incubated for 30 min and after several washes the sections were exposed to a 4′,6-Diamidin-2-phenylindol (DAPI) solution (10236276001, 5 mg/ml in PBS, Roche, Germany). Fluorescent images were acquired using the laser scanning microscope (LSM710 Meta, Carl Zeiss AG, Germany). The acquired images were processed with Adobe Photoshop CS3 (Adobe System Inc., USA).

2.1.6 Semi-quantification of IF staining

Semi-quantification of the gray value intensities of IF images of beating EBs at day 10 of cardiovascular differentiation was performed with focus on the ECM proteins decorin, nidogen-1, fibronectin, periostin, collagen type IV and laminins using the ImageJ software. For each of these ECM proteins 3 IF images were analyzed (n = 3) and the gray value intensities were normalized to the laser power of the LSM710 (Carl Zeiss AG, Germany) applied for the ideal exposure of the individual proteins.

2.1.7 Real-time PCR (qPCR)

RNA was isolated from the samples on different stages of differentiation (day 0, day 4 and day 10 (beating and non-beating)) according to the description in the RNA isolation kit (74004, RNeasy Micro Kit 50, Quiagen, Netherlands). Reverse transcription was performed with the Omniscript RT Kit (10) (205110, Qiagen, Netherlands) in the PCR machine MyCycler (Bio-Rad, USA) (protocol: 37°C, 1h, then hold on 4°C) to receive cDNA. After cDNA synthesis the amount

of ssDNA was measured by using the Qubit fluorometer (Q32866, Life technologies, USA) and the Qubit ssDNA assay kit (Q32852, Life technologies, USA). The measurement was performed according to manual using 1 µl of cDNA. QPCR was performed using the Bio-Rad CFX96 machine and the QuantiFast SYBR Green PCR Kit (204054, Qiagen, Netherlands). The cycling conditions included the activation of HotStarTaq Plus DNA Polymerase at 95°C for 5 minutes followed by 40 cycles of denaturation (95°C for 10 seconds) and combined annealing/extension (60°C or 62°C depending on primer). Primer sequences and annealing temperatures are presented in **Table 1**. After qPCR a melt curve analysis was performed from 65°C to 90°C in increasing steps of 0.5°C. Fluorescence data were collected after every increase of temperature. Glyceraldehyde 3-phosphate dehydrogenase (GAPDH) (QT01192646, Hs_GAPDH_2_SG QuantiTect Primer Assay (200), Qiagen, Netherlands) was used as the reference gene. All samples were performed as triplicates. 2 µl of cDNA were added as template for each qPCR reaction.

Table 1: Primer sequences and annealing temperatures for qPCR.

Primer	Sequence	Annealing Temperature
Tbx5	Forward: GACCATCCCTATAAGAAGCCCT Reverse: TGTGCCGACTCTGTCCTGTA	62°C
cTnT	Forward: TGTTCTCCGAAACAGGATCAAC Reverse: CCGGTGACTTTAGCCTTCCC	60°C
MYH6	Forward: CAACAATCCCTACGACTAC Reverse: TCTCCTCTGAAGTGAAGC	60°C
decorin	Forward: AGTTGGAACGACTTTATCTGTCC Reverse: GTGCCCAGTTCTATGACAATCA	60°C
nidogen-1	Forward: CCGCTTCTACGACAGATCCG Reverse: GCGACTGCACCGAATGTTG	62°C

2.1.8 Statistical analysis

For the quantification of the qPCR data, the 2-ΔΔCt (2 to the power of minus Delta Delta CT) method [123] was applied. QPCR data as well as data from semi-quantification of immunofluorescence staining are presented as mean ± standard deviation. Results were assessed by one-way ANOVA, using the Fisher LSD test with statistical significance at a p-value *$p<0.05$ or **$p<0.01$.

2.2 Generation of stable decorin and nidogen-1 production clones

2.2.1 DCN and NID1 production plasmid construction

Commercially available plasmids utilized for pTet and pTD DCN and Nid1 production plasmid construction

For the construction of the inducible pTet and non-inducible pTD DCN and NID1 vectors, several sections of commercially available vectors were used (**Table 2**). Codon-optimized sequence of human decorin (GenBank accession number: BT019800.1, 1080 bp) and human nidogen-1 (GenBank accession number: BC045606.1, 5406 bp) with a histidine/ asparagine tag at the C-terminus were synthesized from GeneArt (Life Technologies, USA).

Table 2: Commercially available vectors utilized for pTet and pTD DCN and Nid1 production plasmid construction.

Utilized section	pTet	pTD	vector, company and order information
main backbone	x	x	pcDNA™3.1, pcDNA™3.1 Directional TOPO® Expression Kit, K490040, Life Technologies, USA
TK promoter for DHFR expression	x	x	pGL4.74(hRluc/TK), E6921, Promega, USA
TRE promotor for DCN or NID1 expression	x		pTRE3G, Tet-On 3G Inducible Expression System Bicistronic, 631166, Clontech Laboratories, USA
GFP	x	x	pEGFP-C1, 632470, Clontech Laboratories, USA
activator protein Expression cassette for TRE activation	x		pCMV-Tet3G, 631166, Clontech Laboratories, USA

Reverse transcription polymerase chain reaction (RT-PCR)

Primer pairs that have been used for RT-PCR are listed in **Table 3**. If not stated otherwise, for RT-PCR RNA was isolated with the RNeasy Mini Kit (74104, Qiagen, Netherlands), according to the protocol. 1 µg of RNA was reverse transcribed using the ABI High Capacity cDNA Synthesis Kit (4387406, Life Technologies, USA) in 20 µL final reaction volume. If the PCR template was an existing vector, the vector DNA could be directly used for PCR. All PCR reactions for cloning had a final volume of 50 µL, composed of 10 µL 5x buffer, 1 µL dNTP (10 mM), 1 µL of each primer (forward and reverse, 10 µM), 0.5 µL DNA polymerase (M0530 L, Phusion® High-Fidelity

DNA Polymerase, New England Biolabs, USA), 25 ng DNA template (variable volume) and H_2O to bring the reaction mix to a final volume of 50 µL.

Table 3: Sequences of primer pairs for pTet and pTD DCN and NID1 production plasmid construction using RT-PCR.

Primer	Sequence
GFPfor	CACCATGGTGAGCAAGGGCGAGGAGC
GFPrev	GAGATCTAGATCACTTGTACAGCTCGTCCATGCCGAGAGTG
CgDhfrHind3For	GTCGACAAGCTTGCCACCATGGTTCGACCGCTGAACTGCATCGTC
CgDhfrSpeIRev	AGATCTAGACTAGTTTAGCCTTTCTTCTCATAGACTTC
TKPromDra3For	CACGTGCACGTAGTGAATGAGTCTTCGGACCTCGCGGGGGCCGC
SV40Rev	TTTACCACATTTGTAGAGGTTTTACTTGCTTTAA
DCN-NID1Rev	CCCGGGTTTAAACTCGAGTTAATGATTATGATTGTG
Wt-DCN F2	CTCCTTCTGCTTGCACAAGTTTCCTGGGCTGGCCCCTTCCAGCAGCG GGGCC TGTTCGAC
Wt-NID1 F3	GCCGCTGCTGCTGGCGGGGCCTGTGGGCTGCCTGTCCCGGCAGGA ACTGTT CCCATTCGG
Wt-DCN F1	GGTACCGGATCCGCTAGCATGAAGGCCACTATCATCCTCCTTCTGCT TGCACA AGTTTCC
Wt-NID1 F2	GATCCGGGCTGCGTGGACGCGGGCGCTGCTGCTGCCGCTGCTGCTG GCGGG GCCTGTGGG
Wt-NID1 F1	GATGGTACCGCTAGCATGTTGGCCTCGAGCAGCCGGATCCGGGCTG CGTGG ACGCGGGCG
TRE3Gfor2	CTCGAGGATCCGAATTCCTCGAGTTTACTCCCTATCAGTG
TRE3Grev2	CTCGAGGTACCTCCAGGCGATCTGACGGTTCACTAAACGAGC

Digestion with restriction enzymes

The reaction for enzymatic digestions with restriction enzymes had a final volume of 50 µL. The reaction mix contained 5 µL of the 10x digestion buffer (different buffers need to be chosen according to the restriction enzymes), 5 µL 10x BSA, 1 µL of each restriction enzyme, as well as 2 µg of plasmid DNA and H_2O for a final volume of 50 µL. The reaction mix was incubated at 37°C overnight. Prior to the digestion of PCR products with restriction enzymes, a cleanup of the

PCR products was done using the QIAquick PCR Purification Kit (28104, Qiagene, Netherlands) as instructed.

Ligation and transformation of competent bacteria

The molar ratio of the DNA fragments for ligation of approximately 3:1 of insert:vector was chosen. To minimize exposure to UV and damage to the DNA no agarose gel pictures were taken prior to ligation. The ligation mixture contained 2 µL T4 DNA Ligase Reaction Buffer (B0202S, New England Biolabs, USA), 1 µL T4 DNA Ligase (M0202S, New England Biolabs, USA), digested vector DNA, digested insert DNA and H_2O to a final volume of 20 µL. Ligations of restriction products with the pcDNA3.1D TOPO kit (K4900-01) were performed according to the instructions of the kit. The ligation products were used to transform competent bacteria (DH5α or Top10 cells for the TOPO ligation product) with the standard transformation protocol: incubate competent bacteria with 1 µL ligation product for 30 minutes on ice, heat shock for 45 seconds at 42°C, cool down on ice for 5 minutes, incubate at 37°C for 1 hour with 1 mL of LB nutrient broth. Plate the bacteria onto an LB agar plate and grow them overnight at 37°C. Pick colonies of transformed bacteria and inoculate 2 mL of LB broth with 100 µg/mL ampicillin.

Miniprep, Maxiprep and Miniprep digestions

Minipreps of transformed bacterial overnight cultures (1.5 mL) were prepared with the QIAprep Spin Miniprep Kit (27106, Qiagen, Netherlands) per instruction to purify 100 ng/µL to 200 ng/µL plasmid DNA. All miniprep digestions to screen had a final volume of 20 µL. A Miniprep digestion mixture contained 2 µL 10x buffer, 2 µL 10x BSA, 0.25 µL of each restriction enzyme, 4 µL miniprep DNA and 11.5 µL H_2O. The digestion mixture was incubated at 37°C for 3 hours.
Maxipreps were prepared with the Plasmid Maxi Kit (12163, Quiagen, Netherlands) according to the instructions in the kit.

2.2.2 Culture of CHO DHFR-negative cells prior to transfection

The CHO DHFR-negative mutant cells (DSMZ no.: ACC 126) were cultured in culture media composed of minimum essential medium (MEM) α without nucleosides (22561-021, Life Technologies, USA) supplemented with 10% fetal bovine serum (FBS) (10270106, Gibco, Life Technologies, USA) and hypoxanthine and thymidine supplement (11067-030, Gibco, Life Technologies, USA) to support the adherent growth of the DHFR-negative CHO mutant.

Confluent cultures were split 1:3 or higher every 2-4 days using 0.25% trypsin-EDTA (1x) with phenol red (25200-072, Life Technologies, USA). Aliquots of cells were frozen with cryo media (C-29910, Promo Cell, Germany) at about 4 x 10^6 cells/ampoule.

2.2.3 Transfection of activator clones

The inducible expression system required a CHO clone that stably expresses the activator protein for activation of the TRE promoter [115, 116]. This CHO clone was generated by transfecting CHO DHFR-negative mutant cells with the pCMV-Tet3G plasmid (631166, Clontech Laboratories, USA) and selecting for Geneticin (G418) (345810, G418 Sulfate, Calbiochem, USA) resistance. 48 hours prior to transfection, the CHO DHFR-negative mutant cells were plated in a 6-well plate in order to reach 70% - 80% confluency at the day of transfection. 2 µg of the pCMV-Tet3G plasmid was complexed with 5 µL of Lipofectamine® 2000 Transfection Reagent (11668-019, Life Technologies, USA) and added to the cells. 24 hours post transfection the cells from the 6-well were trypsinized and replated into a 10 cm dish. These cells were selected 3 – 4 weeks in culture media with the addition of 500 µg/ml G418 Sulfate, then they were split to a very low concentration in order to let the single cells grow to a colony and transfer stable clones to a 24-well plate.

2.2.4 Identification of the best activator clone

To identify the best activator-producing clone, all the activator clones were transfected with the constructed pTet-GFP plasmid (similar to the transfection with the pCMV-Tet3G plasmid) and as a control, one of the activator clones was additionally transfected with the constructed pTD-GFP plasmid. The pTet-GFP plasmid only can express the GFP product in the presence of a sufficient amount of the activator protein, produced by the activator clones, and after induction with Dox (10224633, Doxycycline hydrochloride, Fisher Scientific, USA). 24 hours post-transfection the activator-clones were induced with 100 ng/ml Dox, after another 24 hours the GFP expression of the activator-clones could be analyzed using the fluorescent microscope Axio Observer Z1 (Carl Zeiss AG, Germany). The pTD-GFP plasmid serves as a positive control as GFP can be expressed from this plasmid independent on the presence of the activator protein or doxycycline. The best activator-clone (acCHO) can be identified by the highest GFP expression.

2.2.5 DCN and NID1 expression plasmid transfection and stable clone selection

CHO DHFR-negative mutant cells for pTD transfection or acCHO cells for pTet transfection were plated in 6 well plates 48 hours prior to transfection. 2 µg of the inducible (pTet) or non-inducible (pTD) plasmid DNA for DCN or NID1 expression, was complexed with 5 µL of Lipofectamine® 2000 Transfection Reagent (11668-019, Life Technologies, USA) and added to the cells in one 6-well (657160, Greiner bio-one GmbH, Germany) at 70% – 80% confluency. 24 hours post transfection, cells from each well were trypsinized and replated into 10 cm dishes with selection media (MEM α (22561-021, Life Technologies, USA), 10% FBS dialyzed (26400, Gibco, Life Technologies, USA), no HT-supplement) that does not support the growth of DHFR-negative cells. The media for cells that were transfected with the inducible expression plasmids additionally contained 500 µg/ml of G418 (345810, G418 Sulfate, Calbiochem, USA) for selection purposes. This selection continued for two weeks with changes of fresh media every 2 to 3 days. The cells were trypsinized and seeded in a low cell concentration into 6-well plates in order to separate single cells spatially in the culture. The single cells were grown to foci and multiple foci were picked and expanded individually in 12-well plates. When these cloned cells reached 100% confluency, media was collected to measure the concentration of human decorin or nidogen-1and the cells were replated into 10 cm dishes. Decorin or nidogen-1 concentrations were measured using an enzyme-linked immunosorbent assay (ELISA) system (described in 2.2.6), and only clones with the highest measured levels of these proteins underwent MTX selection for genomic amplification.

2.2.6 Human decorin and nidogen-1 ELISA

The concentration of human decorin and nidogen-1 was measured according to the instructions of the manufacturer of the ELISA kits DuoSet® Human Decorin and DuoSet® Human Nidogen-1/Entactin (DY143 and DY2570, R&D Systems, USA). The ELISA was conducted in a transparent 96-well plate with flat bottom (442404, Nunc, USA). The plate was blocked with reagent diluent (DPBS (BE17-512F, Lonza, Switzerland) with 1% BSA (5479, Sigma-Aldrich, USA) and 3,3′,5,5′-tetramethylebenzidine (TMB) (T8665 -100ML, Sigma Aldrich, USa) was used as the specific substrate for the horseradish peroxidase (HRP) in the ELISA kit. The color development was stopped by adding 1 M H_2SO_4 and the absorption at 450 nm with a reference at 540 nm was measured in the Infinite M200 PRO photometer (Tecan, Switzerland).

2.2.7 Genomic amplification

To select the DCN or NID1 clones that underwent genomic amplification the cells were cultured in selection medium (containing 500 µg/ml of G418 (345810, G418 Sulfate, Calbiochem, USA) for the inducible clones) and 0.065 µM MTX (A6770-100MG, Sigma-Aldrich, USA). Cells were selected for 2-3 weeks with regular changes of the same media every 2 - 3 days. Foci were picked and expanded individually in 12-well plates. At 100% confluency, media were collected for ELISA and the cells were expanded further for cryo preservation using cryo media (C-29910, Promo Cell, Germany) and storage. Clones with inducible promoter were treated with 100 ng/ml Dox (10224633, Doxycycline hydrochloride, Fisher Scientific, USA) to induce expression and production. Media were collected 48 hours after induction. ELISA was performed to measure the amount of secreted decorin or nidogen-1. This selection process was repeated several times with clones with the highest production levels, each time with increasing concentrations of MTX: 0.065 µM, 0.13 µM, 0.275 µM, 0.55 µM, 1.0 µM and 2.5 µM.

2.2.8 QPCR

QPCR was performed to measure the relative level of DCN or NID1 mRNA and assess the relative copy number of genome amplified DCN or NID1.

mRNA QPCR: RNA was isolated using RNeasy columns (74104, Qiagen, Netherlands) with a slight modification. Cells were lysed in QIAzol (79306, Qiagen, Netherlands) and phase separated after addition of chloroform. The aqueous phase was removed, mixed with an equal volume of 70% ethanol, and loaded onto RNeasy columns. Washes and DNaseI on-column treatment were performed per instructions from the RNeasy kit. Phase separation and DNase I treatment were necessary to remove genomic contamination, which is especially important in clones that had underwent several selection rounds for genomic amplification. These would theoretically have significantly higher copy numbers of the cDNA due to their elevated amount of the DCN or NID1 expression cassette. 1 µg of RNA was reverse transcribed using the ABI High Capacity cDNA Synthesis Kit (4387406, Life Technologies, USA). QPCR was performed on the Roche LightCycler 480 II using the LightCycler 480 SYBR Green I Master (04887352001, Roche, Germany). An aliquot of cDNA from all samples were pooled and serially diluted (5-fold) to prepare a set of standard curve samples. QPCR was performed with 2 pairs each of human DCN or human NID1 specific primers, along with B-Actin as housekeeping gene of CHO cells for RNA input normalization (**Table 4**).

Genomic DNA (gDNA) qPCR: gDNA was isolated using DNeasy columns (69581, Qiagen, USA). 10 ng of gDNA were used per reaction. A set of standard curve samples was prepared by pooling a part of all DCN or NID1 samples and serial dilution of the mixture. For genomic DNA qPCR the same DCN and NID1 primers were used as for QPCR of mRNA (**Table 4**). Amplification of CHO p53 was used to normalize for gDNA input.

Table 4: Primer sequences for CHO clone selection.

Primer		Sequence
human DCN 5’	QhDCN279F	ACCACCCTGCTGGACCTGCA
	QhDCN409R	GTGAAGGCGCCAGGGGACAC
human DCN 3’	QhDCN1054F	CCTCCACCTTCCGCTGCGTG
	QhDCN1107R	GAGCCACGCGGAACCAGCTT
human NID1 5’	QhNID1-389F	CCGCTGAGTGCGTGCACAGA
	QhNID1-495R	GTCCCGAGAAGGGCCCTGGT
human NID1 3’	QhNID1-2015F	CCACGGCTGCGATACCAACGCCGCC
	QhNID1-2160R	CAGGATGTGCTCTCTCTCGTGCTGG
hamster B-Actin	QhamB-Actin-F	GGCGCTTTTGACTCAGGACTTTA
	QhamB-Actin-R	GGGATGTTTGCTCCAACCGA
hamster p53	Qham-p53-F	CATGCCGAATACCTGGATGACAAG
	Qham-p53-R	GCAAATCAAACCCTGTCTTCAACC

2.2.9 Adaptation to suspension growth and serum reduction

Four of the best clones for decorin or nidogen-1 production were chosen for adaptation to suspension growth in 250 ml Erlenmeyer flasks (5506250S, Witeg, Germany). These clones were chosen based on ELISA results for decorin and nidogen-1 on the protein level. The CHO clones in T175 flasks were grown to 50% confluency and the medium was changed to suspension medium consisting of DMEM/Ham’s F12 basal medium (FG 4815, Biochrom AG, Germany) with 10% FBS dialyzed (26400, Gibco, Life Technologies, USA), 2.5 µM MTX (A6770-100MG, Sigma-Aldrich, USA), 2 mM L-Glutamine (25030-081, Gibco, Life Technologies, USA), 1% penicillin-streptomycin (Pen/Strep) (15070, Gibco, Life Technologies, USA) and additional 250 µg/ml G418 (345810, G418 Sulfate, Calbiochem, USA) in the inducible clones. At 90% confluency the cells were trypsinized and 10 x 10^6 cells were resuspended in 100 ml of fresh

suspension media for an inoculation concentration of 1 x 10^5 cells/ml. The media was previously pre-incubated in the incubation shaker (Minitron, Infors GmbH, Switzerland) at 37°C and 5% CO_2, and the cell suspension was cultured in a 250 ml Erlenmeyer flask (5506250S, Witeg, Germany) at 85 rotations per minute (rpm) in the incubation shaker. The suspension cells were passaged every 4-5 days. For inoculation of a defined cell concentration and cell growth monitoring, samples of the cell suspension were counted after mixing 1:1 with trypane blue in a Neubauer counting chamber (T729.1, Carl Roth, Germany). The cells were passaged 5 to 10 times in the suspension media containing 10% FBS dialyzed for adaptation to suspension growth. Adaptation was visible due to lower clump formation and lower adherence to the wall of the Erlenmeyer flask. Serum depletion occurred in several steps of reduced FBS dialyzed content in the suspension media: 5%, 3%, 1% and 0.5% FBS dialyzed. Prior to adaptation serum reduction caused a decrease in cell growth. The cells were ready for the next step in serum depletion when the cell growth had increased and reached a constant value. Depending on the cell clone, additional steps of serum content were necessary to avoid permanent growth depression (4% and 2% FBS dialyzed). Also depending on the cell clone, a reduction to 0.5% FBS dialyzed was not successful due to complete growth arrest. In this case serum depletion was stopped at 1% FBS dialyzed.

2.3 Decorin and nidogen-1 protein production, purification and characterization

2.3.1 Protein production and storage

Protein production and storage started when the clones were adapted to suspension growth with the final reduced content of FBS dialyzed (26400, Gibco, Life Technologies, USA). In the permanent expression system protein production occurred in the suspension medium without any further additions to the medium. For the passaging of the suspension cultures every 4-5 days the cell suspension was centrifuged for 5 min at 1000 rpm. The media supernatant with the secreted proteins was harvested under sterile conditions and stored until use at -20 °C. A slightly different approach was necessary with the permanent protein expression system, as this required the induction with 100 ng/ml Dox (10224633, Doxycycline hydrochloride, Fisher Scientific, USA) for protein production. Therefore Dox was added to the suspension media at each passage and similar to the protein production in the permanent system, the secreted protein was harvested 4-5 days later under sterile conditions during the next passage and stored

at -20°C. The cells were only induced for production once and then discarded, therefore in parallel another culture needed to be maintained to support the need for production cells in the inducible system.

2.3.2 Protein purification with chromatography methods

The IMAC purification of the histidine-tagged secreted ECM proteins is based on the affinity of the amino acid histidine to nickel ions on the affinity chromatography column [120, 122]. The reproducible purification with constant pressure and flow rates through the column was controlled by the FPLC system Äkta Explorer 10 (GE Healthcare, USA). Important measurement data like flow rate, conductivity, pressure and absorption at 280 nm and 256 nm were monitored and recorded. To avoid gas bubbles in the Äkta Explorer 10 system all fluids and buffers that were needed for the purification were degassed for 15 min in a sonification bath (Sonorex Super RK 510 H, Bandelin, Germany) prior to their use on the system. Buffer compositions are shown in **Table 5**. At the beginning of the purification process the HisPrep FF 16/10 affinity chromatography column (28-9365-51, GE Healthcare, USA) was equilibrated with five column volumes, which equals 100 ml, of the 1x equilibration and wash buffer at a flow rate of 3.5 ml/min. Different ECM proteins were purified with separate affinity chromatography columns to ensure the purity of the elution. The suspension culture supernatants were thawed, filtered through a Stericup-GP 500 mL sterile filter unit (SCGPU05RE, Millipore, USA) with 0.22 µm pores to remove cell debris and mixed with 9x concentrated binding buffer in order to generate the salt concentration of a 1x binding buffer in the sample. Subsequently 300 ml – 600 ml of the protein-containing samples were loaded onto the column at a flow rate of 3 ml/min. A wash step with 5 column volumes of the 1x equilibration and wash buffer at the flow rate 3.5 ml/min cleaned the column of media residues. Subsequently the elution of the histidine-tagged proteins with five column volumes of the elution buffer at a flow rate of 3.5 ml/min was monitored by the increased absorption at the wavelengths 280 nm and 256 nm. Several elution fractions of 6 ml each were collected with the automated fraction collector and the fractions that contain the eluted protein were pooled and subsequently processed in the next purification step.

Table 5: Buffer compositions for IMAC purification with the HisPrep FF 16/10 affinity chromatography column on a FPLC system.

Buffer	$NaH_2PO_4 \cdot H_2O$	Imidazole	NaCl
Equilibration and wash buffer (1x), pH 7.4	20 mM	10 mM	100 mM
Binding buffer (9x), pH 7.4	180 mM	180 mM	4500 mM
Elution buffer (1x), pH 7.4	20 mM	300 mM	250 mM

2.3.3 Desalting and buffer exchange of the protein elution fractions

The desalting process is based on size separation of proteins and salts [117] on the 53 ml HiPrep™ 26/10 desalting column (17-5087-01, GE Healthcare, USA) controlled by the Äkta Purifier 100 System (GE Healthcare, USA). Compared to salts, proteins have a high molecular weight and pass the column first while molecules with low molecular weight enter the matrix pores in the desalting column. This takes up more time and therefore these small molecules pass the column later. On the Äkta Purifier 100 System the buffer of the highly salt- and immidazol-containing protein elution fractions is exchanged to DPBS (BE17-512F, Lonza, Switzerland). Therefore 6 ml of elution fraction from the IMAC purification containing the protein was loaded onto a sample loop with a syringe. Loading onto the desalting column with a flow rate of 5 ml/min was controlled by the Äkta Purifier 100 System. After passing through the column the protein-containing solution was manually collected as the UV absorption reading at 280 nm started to rise, indicating a protein peak. The manual protein harvest was stopped when the UV curve had decreased to the original level. The conductivity curve peaks after the protein curve, representing the presence of salts in the elution buffer that pass the desalting column after the proteins. Subsequently further protein-containing elution fractions could be loaded onto the desalting column for desalting and buffer exchange. The collected protein was stored at -20°C for following concentration procedures.

2.3.4 Concentration and sterile filtration of the purified protein samples

Desalting and buffer exchange to DPBS (BE17-512F, Lonza, Switzerland) on the Äkta Purifier system caused a dilution of the protein sample, therefore the next purification step also needed to increase the protein concentration. For this purpose the ultrafiltration units Vivaspin 20

(VS2001, Sartorius, Germany) were used. These filtration units have a molecular weight cut-off of 10 kDa, therefore no decorin or nidogen-1 could be lost through the filter. Additional to the concentration function, the protein sample was also washed several times with DPBS on the filter to make sure the buffer exchange to DPBS was complete. The protein solution was concentrated to 3-5 ml, sterile filtered with a flip filter (SCGP00525, Millipore, USA), aliquoted and stored at -80°C. At important steps of the purification process small samples were taken for ELISA in order to track the efficiency of the purification process and to measure the decorin or nidogen-1 concentration in the final concentrated protein solution.

2.3.5 SDS-PAGE and Western Blot

Sodium dodecyl sulfate polyacrylamide gel electrophoresis (SDS-PAGE) and Western Blot was conducted with the purified and concentrated decorin and nidogen-1 solutions to verify the identity and expected size of the proteins. The protein samples were mixed with 4x Roti-Load (K929.2, Carl Roth, Germany) and denatured during heating for 5 min at 90°C. The denatured decorin sample was run on a NuPAGE®Novex 4-12% Bis-Tris 1.0 mm 12 well gel (NP0322BOX, Life Technologies, USA) and nidogen-1 on a NuPAGE® Novex® 3-8% Tris-Acetate gel, 1.0 mm, 12 well (EA03752BOX, Life technologies) under denaturing conditions. According to the gel, different SDS running buffers were used. A MES SDS running buffer (950 ml ddH2O + 50 ml NuPage® MES SDS Running Buffer (20x) (NP0002, Life Technologies, USA)) on the 4-12% Bis-Tris gel or a Tris-Acetate running buffer (950 ml ddH2O + 50 ml NuPAGE® Tris-Acetate SDS Running Buffer (20X) (LA0041, Life Technologies, USA) on the Tris-Acetate gel. The SeeBlue® Plus2 Pre-Stained Standard (LC5925, Life Technologies, USA) was used on the 4-12% Bis-Tris gel and the HiMark™ Pre-Stained Protein Standard was used on the Tris-Acetate gel for easy band identification in the protein molecular weight analysis. After loading of the protein samples the SDS-PAGE run was started at 50 V for 20 min and was then increased to 150-190 V until the end of the run. The protein markers were used for orientation to stop the SDS-PAGE at the right time.

In a next step the proteins from the gel needed to be transferred to a nitrocellulose membrane (10402495, Whatman, UK). This was accomplished in an electrical field (30 V, 60 min) in the XCell II™ Blot Module (EI9051, Life Technologies, USA) fixed inside the XCell II™ Mini-Cell with the transfer buffer (50 ml NuPAGE Transfer Buffer (20x) (NP0006-1, Life Technologies, USA) + 100 ml methanol (4627.2, Carl Roth, Germany) + 850 ml ddH_2O).

For an unspecific protein staining the nitrocellulose membrane was incubated in a Ponceau-Red solution (P7170-1L, Sigma Aldrich, USA) for 5 min at room temperature. After pictures of the unspecific protein staining were taken with the Intas Gel Imager (Intas, Germany), the membrane was discolored in a 0.1 M NaOH solution and afterwards could be used for the specific protein immunodetection. Therefore the membrane was blocked for 20 min in a blocking buffer (5% skim milk powder (70166-500G, Sigma-Aldrich, USA) in 1x TBS-T (10x TBS-T: 150 mM NaCL + 20 mM Tris-HCL (T5941-1KG, Sigma-Aldrich, USA) in 1 l ddH_2O)) and then incubated with the primary antibody overnight at 4°C while shaking. The primary antibody was diluted in 5 ml blocking buffer: decorin antibody (1:2000, rabbit, GTX 101250, Genetex, USA) and nidogen-1 antibody (1:400, rabbit, SC-33141, Santa Cruz, USA). After overnight incubation with the primary antibody the membrane was washed with TBS-T for an hour at 4°C with several changes of fresh TBS-T. Incubation with the secondary antibody (goat anti-rabbit IgG H&L (HRP), ab6721, Abcam, UK) occurred in a 1:4000 dilution in 5% skim milk powder in 1x TBS-T for 1h at 4°C. The membrane was washed again with 1x TBS-T for 1 h and then the SuperSignal West Dura Extended Duration Substrate (34075, Thermo Scientific, USA) was applied onto the membrane, drained off after few seconds and the developed chemiluminescence was detected in the Luminescent Image Analyzer LAS-1000 plus (FujiFilm, Japan).

2.3.6 Protein deglycosylation

Deglycosylation of the purified decorin and nidogen-1 with a protein deglycosylation enzyme mix (P6039S, New England Biolabs, USA) was conducted under denaturing conditions to enzymatically remove N-linked as well as O-linked oligosaccharides. The glycoprotein (100 µg in 18 µl H_2O) was mixed with 2 µl of 10x glycoprotein denaturing buffer for a 20 µl total reaction volume. This reaction mix was heated at 100°C for 10 minutes to denature the glycoprotein for better accessibility to the glycosylated amino acids. After chilling the denatured glycoprotein on ice and centrifugation for 10 seconds, 5 µl 10x G7 reaction buffer, 5 µl 10% NP40 and 15 µl H_2O were added. 5 µl of the deglycosylation enzyme cocktail, containing PNGase F, O-Glycosidase, Neuraminidase, β1-4 Galactosidase and β-N-acetylglucosaminidase, were added to the reaction mix and gently agitated. According to the manufacturer's description the reaction was incubated at 37°C for 4 hours. Additionally an identical reaction mix was incubated at 37°C for 20 hours. The control sample was treated accordingly, except for the addition of the deglycosylation enzymes, and incubated at 37°C for 4 hours. Subsequently the success and extend of the

deglycosylation was analyzed by the mobility shift of the decorin or nidogen-1 band to a lower protein size on a SDS-PAGE gel.

2.3.7 Co-Immunoprecipitation (Co-IP)

For the Co-IP experiment a protocol described in Mann et al. [54] was modified to confirm the TGF-β1 binding activity of decorin and the laminin γ1 chain binding activity of nidogen-1. Human TGF-β1 from platelets (T1654-1UG, Sigma Aldrich, USA) as well as human recombinant Laminin 511 (LN511-02, BioLamina, Sweden) were purchased. The interaction partners decorin (0.5 µg) + TGF-β1 (0.225 µg) as well as nidogen-1 (1 µg) + laminin 511 (0.5 µg) were mixed in 500 µl of the dilution and washing buffer described in Mann et al. (0.1 M NaCl, 0.05 M Tris/HCl pH 7.4 containing 0.04% Tween-20 and 1 % BSA) and were agitated gently on a rotisserie mixer overnight. The antibodies against decorin (10 µg = 10 µl, GTX 101250, Genetex, USA) or against laminins (6 µg = 11.11 µl, ab11575, Abcam, UK) were added to the protein mix and incubated for 24 h for Co-IP. These antibodies were not added in the negative control (unspecific background control). Protein A magnetic beads (LSKMAGA02, Millipore, USA) were added and gently agitated on a rotisserie mixer with the protein ± antibody complexes for 2.5 h in the fridge and another 30 min at room temperature. After washing of the magnetic beads with the washing buffer on a magnetic stand (LSKMAGS08, Millipore, USA), the protein complexes were eluted from the beads and denatured in 30 µl of 1x Roti-Load (K929.2, Carl Roth, Germany) via heating for 10 min at 90°C. Detection of the specific protein bands occurred after SDS-PAGE and Western Blotting with primary antibodies against decorin (1:200, mouse, sc-73896, Santa Cruz, USA), TGF-β1 (1:1000, rabbit, ab66043, Abcam, UK), nidogen-1 (1:400, rabbit, SC-33141, Santa Cruz, USA) and laminin (1:500, rabbit, ab11575, Abcam, UK). As the secondary antibody a HRP-labelled goat anti-rabbit IgG H&L antibody (ab6721, Abcam, UK) in the dilution 1:4000 or a HRP-labelled goat anti-mouse IgG1 antibody (ab97240, Abcam, UK) in the dilution 1:1000 was used.

2.3.8 Dermal equivalent contraction assay

For the construction of 3 dermal equivalents 2.4 x 10^6 human dermal fibroblasts were resuspended in 4 ml of gel neutralization solution (pH 8.5), composed of 232.5 ml 2x concentrated DMEM medium (41965-039, Life Technologies, USA), 7.5 ml 3 M HEPES solution

(H4034, Sigma Aldrich, USA), 1.25 ml chondroitin-4-sulfate solution, 1.25 ml chondroitin-6-sulfate solution and 7.5 ml sterile FBS. Subsequently the suspension was mixed with 8 ml of a collagen solution and dispensed into 3 6-well inserts (Cellstar®, Greiner bio-one, Austria/Germany). For the collagen solution, collagen was isolated from rat tails and adjusted to a concentration of 6 mg/ml in 0.1% acetic acid. An acellular collagen gel was constructed in the same way but without the dermal fibroblasts. The dermal equivalents were incubated 5 – 10 min at 37°C to allow polymerization and gel formation, subsequently 4 ml of culture media were added per well (DMEM (41965-039, Life Technologies, USA), 10% FBS, 1% Pen/Strep (15070, Gibco, Life Technologies, USA)). For a decorin treatment, a concentrated recombinant decorin solution was used to reach a 50 µg/ml or 150 µg/ml decorin in the dermal equivalent as well as in the initial culture media. 5 ng/ml TGF-β1 were added to the initial culture media only. The dermal equivalents were cultured in the initial culture media with the possible addition of decorin or TGF-β1 for 24 h. Then the initial media was removed and exchanged to the culture media without the addition of decorin or TGF-β1. This media was exchanged every 3-4 days. Pictures were taken of each dermal equivalent together with a ruler for circumference calculation at day 1 and day 16, as well as at several time points in between. The circumference was determined using the ImageJ software.

2.3.9 Immunological assays

For endotoxin detection the LAL Chromogenic Endotoxin Quantitation Kit (88282, Thermo Scientific, USA) was used according to the manufacturer's instructions. In the presence of endotoxin, factor C of the LAL is activated to a protease, which hydrolyses the chromogenic substrate and releases p-nitroaniline visible as yellow color that can be measured by the absorbance at 405 nm.

The cellular endotoxin assay is based on TNFα release of human PBMCs, isolated from buffy coat or whole blood using Ficoll density gradient centrifugation. 15 ml Ficoll reagent in a 50 ml falcon tube were covered with 30 ml diluted blood (1:2 dilution with PBS at RT) and centrifuged for 30 min at 800 g. The PBMC-containing layer was removed, washed three times in cool PBS and subsequently incubated with 50 µg/ml or 100 µg/ml decorin or nidogen-1 as well as 10 ng/ml or 100 ng/ml LPS as a control for 24 h. In the presence of endotoxins TNF-α release from activated macrophages and monocytes was triggered. This was detected with the human TNF-α ELISA Max Deluxe Set (430205, Biolegend GmbH, Germany).

To test the effect of decorin and nidogen-1 with and without anti-CD3 co-stimulus (Janssen-CILAG GmbH, Germany) on immune cell proliferation and activation, 96-wells were coated overnight at 4°C with 50 µl of a 0.05 µg/ml concentrated anti-CD3 solution. Decorin and nidogen-1 coating occurred after washing with PBS, using 100 µl of these proteins in the concentrations 50, 250 and 500 µg/ml for 6 h incubation at RT. Subsequently all wells were washed three times with PBS. 3 x 10^5 carboxyfluorescein succinimidyl ester (CFSE)-marked PMBCs were dispensed per well and incubated in a cell culture incubator for 5 days. At day 5 the cells were harvested and FACS analyses were conducted to detect proliferation and late activation status (HLA-DR) of monocytes, natural killer cells, B- and T-cells (**Table 6**). Furthermore early and intermediate activation markers (CD69, CD25) on natural killer, B- and T-cells were analyzed.

Table 6: Fluorescence-marked antibodies for FACS analyses.

Antibody	clone	Company
CD19-PE	LT19	BD Biosciences, USA
CD14-PerCP/Cy5.5	M5E2	BioLegend GmbH, Germany
CD56-PE/Cy7	HCD56	BioLegend GmbH, Germany
HLA-DR-APC	L243	BioLegend GmbH, Germany
CD3-APC/Cy7	HIT3a	BioLegend GmbH, Germany
LIVE/DEAD ® Fixable Dead Cell stain Kit		Life Technologies, USA
CD69-PerCP/Cy5.5	FN50	BioLegend GmbH, Germany
CD25-APC	BC96	BioLegend GmbH, Germany

2.4 In vitro and in vivo test of the cardio-inductive effect of decorin and nidogen-1

2.4.1 In vitro test of cardio-inductive effect

To test the cardio-inductive effect of the purified decorin and nidogen-1, EBs were generated and cultured in the cardiovascular differentiation protocol as described before (2.1.1 and 2.1.2) with one modification. On day 4 of differentiation the floating EBs were transferred to 6-well plates with different coatings, including 0.1% gelatin + 50 µg/ml decorin, 0.1% gelatin + 50 µg/ml nidogen-1, 0.1% gelatin + 50 µg/ml decorin + 50 µg/ml nidogen-1 or control coatings with 0.1% gelatin. On day 10 of differentiation the whole well was harvested for intracellular FACS analysis

as previously described. For detection of differentiation efficiency to cardiomyocytes on the different coatings a primary antibody against the cardimyocyte marker cTnT was added to the cells in the dilution 1:200 (anti-cardiac Troponin T antibody, monoclonal, mouse IgG1, ab8295, Abcam, UK). The secondary antibody (goat polyclonal secondary antibody to mouse IgG - H&L, Alexa Fluor® 488, ab150113, Abcam, UK) was used in the dilution 1:250. Cell analysis was conducted using the BD LSR II cell analyzer (BD Biosciences, USA) and cTnT-positive cells were detected with Alexa Fluor 488.

2.4.2 In vivo mouse MI/R and ECM injection

A mouse model for myocardial infarction at the UCLA was used to identify the effect of myocardial injections with decorin and nidogen-1 post MI. The experiments were conducted in cooperation with MD. Ali Nsair. Animal care and surgeries were performed in compliance with the University of California, Los Angeles Animal Research Committee under the protocols 2011-042 and 2013-057. Eight week old, female C57BL/6J mice, strain DLAMb6, were anesthetized using 2.0% isoflurane (Butler Schein, UK), placed on a heated surgical board and given flunixin (Flunixin Meglumine, Schering-Plough Animal Health, USA) 2.5 mg/kg subcutaneously. Under a dissecting microscope a midline cervical incision was made to expose the trachea for intubation with a PE-90 plastic catheter (Stoelting Company, USA). The catheter was connected to a Harvard minivent (Harvard Apparatus, Germany) supplying oxygen with a tide volume of 225 - 250 µl and a respiratory rate of 130 strokes/min. Surgical plane anesthesia was subsequently maintained with 1 - 1.5% isoflurane. A lateral incision was made in the fourth intercostal space. The heart was exposed and the left coronary artery was ligated intramurally 2 mm from its origin with a 9-0 nylon suture (Ethicon, USA). The suture was tied around a small piece of plastic tubing (PE-10) to occlude the coronary artery while allowing an easier and safer relief of the occlusion. This occlusion occurred for 45 minutes. During this time, a moist gauze pad was placed over the incision to maintain a sterile atmosphere. Ischemia was verified by the regional paleness of the myocardium that was no longer supplied with blood by the left coronary artery. Reperfusion was allowed by cutting the knot on the PE-10 tube and could be verified by the appearance of hyperaemia in the previously pale region. Due to reperfusion the infarcted region changed into a normal pinkish red color. This MI/R procedure was conducted on 15 mice.

After confirming that there was no bleeding, the animals received injections in the myocardial infarction border zone. The hydrogel and ECM injections were prepared as described in 2.4.3. Five animals in the control group were injected with a total of 50 µl of HyStem® Hydrogel

(Glycosan BioSystems, USA) + PBS per animal. In the decorin + nidogen-1 treatment group five animals received injections of HyStem® Hydrogel + PBS + 50 µg/ml decorin + 50 µg/ml nidogen-1 and in the nidogen-1 treatment group five further animals received injections of HyStem® Hydrogel + PBS + 50 µg/ml nidogen-1 each of a total of 50 µl per animal. For each mouse the 50 µl total injection volume was divided into 10 µl injections at 5 sites in the LV myocardial infarction border zone.

The mice chests were closed in two layers. The ribs (inner layer) were closed with 6-0 coated vicryl sutures (Ethicon, USA) in an interrupted pattern. The skin was closed using 6-0 nylon or silk sutures (Covidien, UK) in a subcuticular manner. The anesthesia was stopped and the mice were allowed to recover for several minutes before the endotracheal tube was removed. For alleviation of pain the mice received intraperitoneal injections of Banamine (2.5 mg/kg) post-surgery.

2.4.3 Hydrogel and ECM preparation for post MI/R injections

All procedures for hydrogel + ECM injections were conducted under sterile conditions. The hydrogel consists of two components HyStem® and Extralink (Glycosan BioSystems, USA), which were prepared by dissolving the lyophilized solids in DG water according to the manufacturer's instructions and by mixing HyStem and Extralink in a 1:4 volume ratio. Upon mixing of these two components gelation of the HyStem® Hydrogel occurred within 20 minutes. For each mouse a total of 50 µl of HyStem® Hydrogel + PBS ± ECM protein were needed. Therefore due to possible residues in the preparation tube or in the syringe 70 µl were prepared per mouse. For 70 µl of the injectable mix 8.4 µl consisted of the HyStem and Extralink mix. In the control group the remaining 61.6 µl were sterile PBS. In the decorin + nidogen-1 treatment group appropriate amounts of purified recombinant decorin and nidgen-1 were added to make up the total concentration of 50 µg/ml decorin + 50 µg/ml nidogen-1 in the 70 µl injectable mix. In the nidogen-1 treatment group nidogen-1 was added for a total concentration of 50 µg/ml nidogen-1 accordingly.

2.4.4 Echocardiography and Vevo strain analysis

Conscious echocardiography was conducted on four different time points. A baseline echocardiography measurement was conducted on each mouse prior to the MI/R procedure. In

serial nature further echocardiography measurements were conducted two days as well as two weeks and four weeks after the MI/R and myocardial injection procedure to track cardiac function.

For echocardiographic imaging the high-frequency ultrasound imaging system Vevo 2100 (VisualSonics, Canada) was applied for non-invasively microimaging conscious mice in vivo with the MS400 transducer 18-38 MHz. Echocardiography was performed on conscious mice, as anesthesia can influence the heartbeat and thereby the experimental results. Myocardial performance was assessed via the Vevo LAB software, which enables regional and global wall motion tracing and offers the quantification of the strain.

Prior to the conscious echocardiography hair was removed from the mice's chest using a depilatory cream 3 - 5 min (Nair, Church & Dwight, USA). The animals were restrained on a platform and the echocardiogram was performed rapidly to minimize distress. Also the animals were released from the restraints if they showed signs of pain. The performed protocol was approved with the Chancellor's Animal Research Committee (ARC-OARO). The mice were sacrificed after the 4 week echocardiography and their hearts were explanted for histological investigation.

2.4.5 Histological and immunofluorescence staining of mouse hearts

Histological staining (hematoxylin & eosin (H&E staining) as well as Russell-Movat Pentachrome staining) and immunofluorescence staining was performed on explanted mouse hearts 4 weeks post MI/R. The paraffin-embedded tissue sections were deparaffinized in xylene and hydrated in baths of decreasing ethanol concentrations.

H&E staining: Deparaffinized and hydrated sections were stained in hematoxylin (1.09249.2500, Merck, USA) for 8 minutes, washed in ddH_2O, differentiated in HCL-ethanol (HCl, 1090571000, Merck, USA) and washed in ddH_2O before blueing for 5 min in lukewarm tap water. Sections were stained in eosin (Dr. K. Hollborn & Söhne) for 1 min, washed in ddH_2O, differentiated in 70% ethanol and dehydrated in rising concentrations of ethanol until 2x 5 min incubation in isopropanol. Isomount (055 47535, Labonord, France) was used as mounting media. H&E stain nuclei (purple/blue), cytoplasm (light pink), muscle (red) and other tissue components (shades of pink and red).

Russell-Movat Pentachrome staining: Deparaffinized and hydrated sections were stained as previously described [124, 125]. This staining visualizes mature elastin-containing elastic fibers

(black), nuclei (dark red), collagens (yellow), muscle tissue (red) and proteoglycans (blue-green). The chemicals applied for Russell-Movat Pentachrome staining are listed in **Table 7**.

Table 7: Chemicals for Russel-Movat Pentachrome staining.

Chemical	Company and order information	Lot #
2-propanol	AnalaR Normapur, VWR Chemicals, USA, 20842.330, 2.5 L	13K210507
Alcian blue 8GX	Waldeck, Germany, 1A-288, 5 g	222726
Brilliantcrocein R	Waldeck, Germany, 1B108, 25 g	341719
Acetic acid 100%	Carl Roth, Germany, 3738.1, 1 L	K38877863 825
Ethanol	AnaloR Normapur, VWR Chemicals, USA, 20821.330, 2.5 L,	14B180530
Hematoxylin	Fisher Scientific, UK, BP2424-25, 25 g	107681
Iodine	Fisher Scientific, UK, 1/0500/48, 100 g	1288322
Iron(III)chloride anhydrous	Fisher Scientific, UK, 1/1035/53, 500 g	1285433
Isomount 2000	Labonord, France, 05547536, 1 L	SM00002777
Sodium thiosulphate	Fisher Scientific, UK, 5/7250/53, 500 g	1138921
Phosphotungstic acid 44-hydrate	Acros Organics, Belgium, 417931000, 25 g	A0309796
Potassium iodide, puriss. p.a.	Sigma-Aldrich, USA, 60400, 100 g	126086440306005
Safran du Gatinais	Waldeck, Germany, 5A-394, 25 g	301629
Acid Fuchsin calcium salt	Sigma-Aldrich, USA, 857408-25g, 25 g	MKBG4043V
Xylene	AnaloR Normapur, VWR Chemicals, USA, 28975.325, 2.5 L	13C140513

Bright field images of H&E and Russell-Movat Pentachrome staining were acquired using the Zeiss Axio Observer Z1 (Carl Zeiss AG, Germany).

Immunofluorescence staining on the explanted mouse hearts 4 weeks post MI/R was performed as previously described (2.1.5.), utilizing a cTnT antibody (1:3000, HPA015774, Sigma Aldrich, USA) and a DAPI solution (10236276001, 5 mg/ml in PBS, Roche, Germany). Fluorescent images were acquired using the laser scanning microscope (LSM710 Meta, Carl Zeiss AG, Germany). The acquired images were processed with Adobe Photoshop CS3 (Adobe System Inc., USA).

3 Results

3.1 Identification of hESC-derived cardiovascular ECM proteins

3.1.1 Characterization of EB cardiovascular differentiation

A modification of the spin EB method [85, 126] was used for the aggregation of a defined cell number of hESCs, line H9, by centrifugation in conical 96-wells. While other EB approaches mechanically disrupt adherent hESC colonies and thereby generate irregularly shaped cell aggregates [127], the method used in this work reproducibly generated EBs with uniform size and shape. Spin EBs formed based on aggregation of the cells, without the need of supplementation of extrinsic ECM proteins, which was a pre-requisite in previous studies [61] in order to obtain proper EB formation from hESCs. MEF-contamination was less than 2% (1.63% ± 0.15%) as identified by FACS analysis for the mouse marker CD29. Interestingly, we also tested this method for EB generation of other hESC lines such as Hes2 (ES Cell International, Singapore), H1 [62] and UCLA line 4, and we found that H1 and UCLA line 4 cells, probably due to a lower potential to aggregate, formed loosely packed EBs that disintegrated on days 1 to 4 of differentiation due to cell death. Very gentle handling of the newly formed H9 EBs prevented any disruption and supported the integrity and health of the cell spheroids. The modified cardiac differentiation protocol described schematically in **Figure 6** shared many characteristics with two previously described protocols [64, 92]. Main differences are the EB size, shape and generation method but especially the attachment of whole EBs on 0.1% gelatin-coated plates on day 4 of differentiation. This modified protocol generated first beating EBs on day 7 of cardiovascular differentiation, 3 days after attachment of the EBs to the 0.1% gelatin-coated 6-well dish. On day 10 of differentiation beating and non-beating EBs were counted and a robust and reproducible generation of spontaneously beating EBs (85% ± 17.6%, n = 7) could be observed.

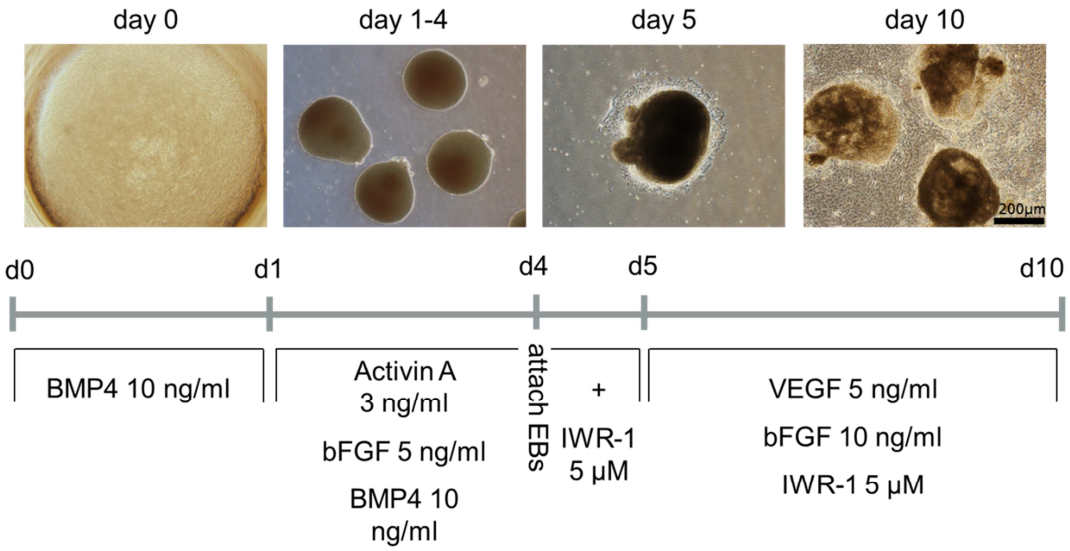

Figure 6: Bright field images of important steps of the cardiovascular differentiation protocol with hESC line H9 at day 0, day 1, day 5 and day 10 of differentiation. Additives to the mTeSR1 media (day 0) or StemPro-34 media (day 1-10) in the different stages are specified. The scale bar equals 200 µm.

To identify the numbers of cells differentiating towards the cardiac lineage, FACS analyses were performed five times (n = 5) on day 10 of differentiation for sarcomeric myosin, a muscle protein in early heart development, using the MF20 antibody. A representative analysis is shown in **Figure 7**. The dissection of the beating from the non-beating cells that grew out of the attached EBs is schematically described (**Fig. 7 D**). As expected, these two sample types showed significant differences in the FACS analyses for sarcomeric myosin with 49.4% ± 11.4% MF20-positive cells in the beating EBs and only 6.5% ± 2.3% MF20-positive cells in the non-beating outgrown cells. This result clearly shows that by employing the modified cell culture protocol, we were able to reproducibly differentiate high numbers of cells in the EBs towards the cardiac lineage, within only 10 days of differentiation.

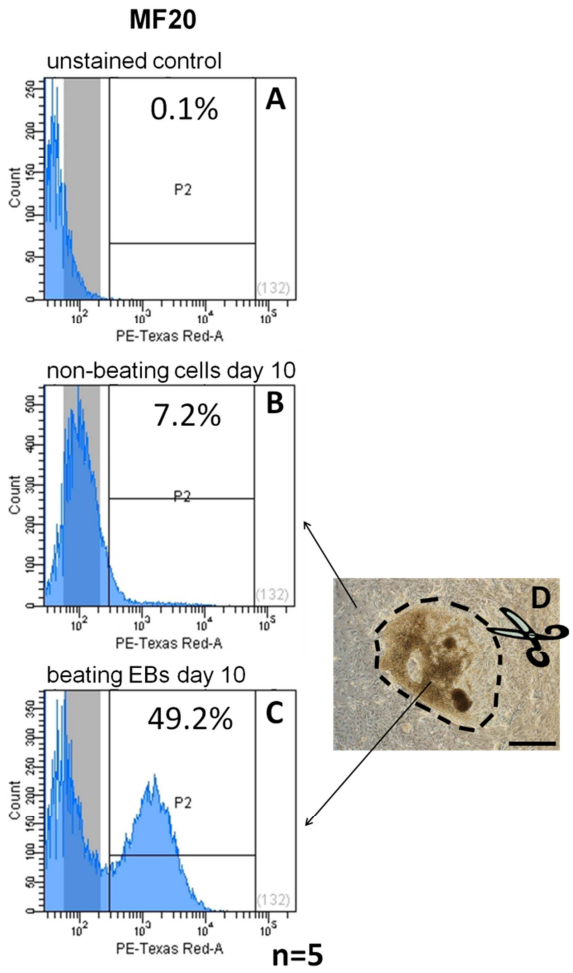

Figure 7: Representative FACS analysis of sarcomeric myosin (MF20 antibody) on day 10 of cardiovascular differentiation. **A**) Unstained control sample (0.1% MF20-positive cells), **B**) non-beating outgrown cells (7.2% MF20-positive cells) and **C**) dissected beating EBs (49.2% MF20-positive cells). A bright field image schematically shows the dissection of a beating EB from the surrounding non-beating cells **D**). Cells were analyzed using the BD LSRFortessa cell analyzer, MF20-positive cells were detected with Texas PE. The FACS analysis was conducted five times (n = 5). The scale bar equals 200 µm.

QPCR was performed on dissected beating EBs and non-beating cells to monitor the expression of the genes T-box transcription factor 5 (Tbx5) cardiac Troponin T (cTnT also TNNT2) and cardiac myosin alpha heavy chain (MYH6) on day 10 of differentiation (**Fig. 8**). The expression of these cardiac specific genes increased with a high significance (**p <0.01) in the beating EB samples compared to the non-beating samples, supporting the successful differentiation of the spin EBs in the cardiac lineage.

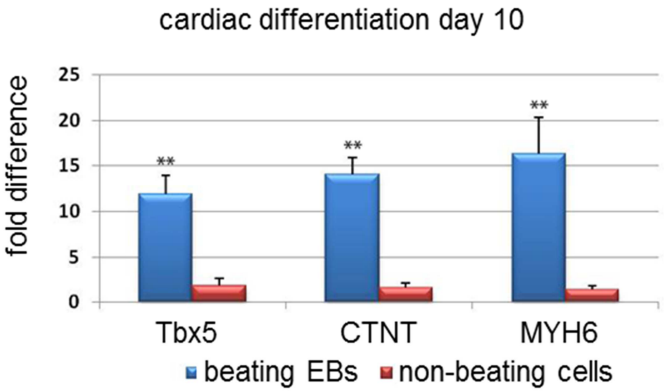

Figure 8: QPCR analyses of T-box transcription factor 5 (Tbx5), cardiac troponin T (cTnT) and cardiac myosin alpha heavy chain (MYH6) expression. The analyses show highly significant increase of the expression of the cardiac transcription factor Tbx5 and the cardiomyocyte markers cTnT and MYH6 in beating EBs compared to non-beating cells on day 10 of cardiac differentiation. Statistical results were assessed by one-way ANOVA, using statistical significance at a p-value **$p<0.01$.

IF co-staining for cTnT (green, 488 nm) and sarcomeric myosin (red, 594 nm) was performed on beating EBs on day 10 of differentiation and human fetal heart (17 weeks) (**Fig. 9**) to compare the maturation status of the myosin filaments in the beating EBs to the mature myosin filaments in the human fetal heart. The clear striated structure, high organization and complete co-expression of cTnT and sarcomeric myosin identify the mature myosin filaments in the fetal heart, while the myosin filaments in the beating EBs are still unorganized, with only incomplete co-expression of cTnT and sarcomeric myosin as well as only occasional striation. Due to these characteristics the beating EBs represent an early developmental stage.

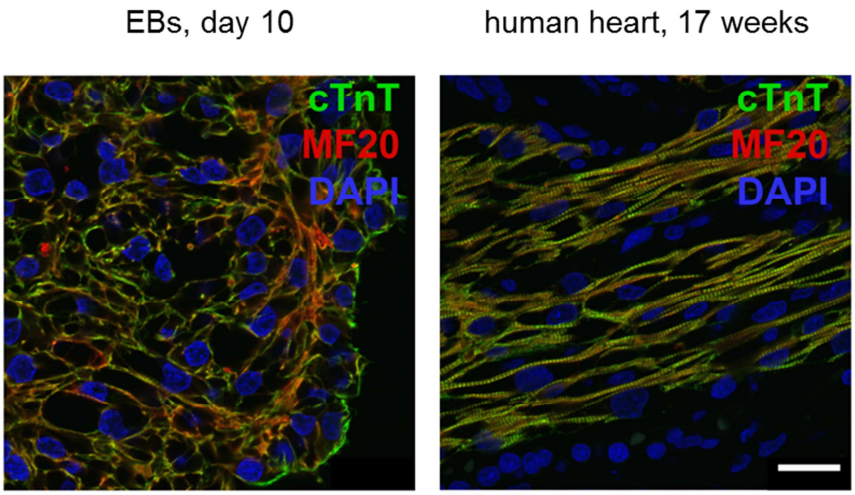

Figure 9: Immunofluorescence staining of paraffin-embedded tissue sections of beating EBs on day 10 of cardiac differentiation and human fetal heart (17 weeks). The staining of the cardiac marker cardiac troponin T (cTnT) (green) and sarcomeric myosin (MF20 antibody) (red) shows myosin filaments with a clear striated structure, high organization and complete co-expression of cTnT and sarcomeric myosin in the fetal heart, while the myosin filaments in the beating EBs are unorganized, with only incomplete co-expression of cTnT and sarcomeric myosin as well as only occasional striation. Cell nuclei are stained with DAPI (blue). The scale bar equals 20 µm.

With the above results we have confirmed that the modified cardiac differentiation protocol effectively and reproducibly generated beating EBs with significantly increased amounts of cardiomyocytes compared to the control (MF20 FACS results).

3.1.2 EB ECM protein expression

To analyze the cardiac ECM deposited by the beating EBs, we performed qPCR for several interesting ECM proteins on samples from three different time points during cardiovascular differentiation (undifferentiated hESCs (H9) = day 0, EBs on day 4 of differentiation (before attaching to the plate) and dissected beating EBs on day 10 of differentiation). Among the analyzed ECM proteins, the expression of the genes decorin and nidogen-1 was monitored (**Fig. 10 A, B**). The expression profile of both of these ECM proteins showed a stage- and culture condition-specific expression and a significant increase (*$p<0.05$) in the beating EB sample compared to the undifferentiated hESCs.

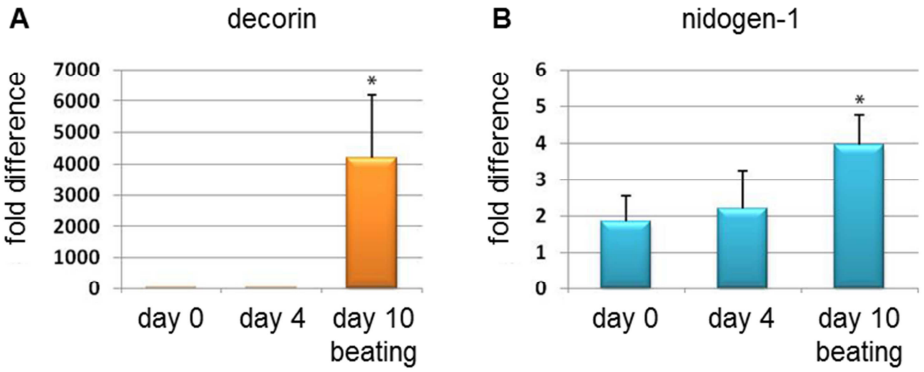

Figure 10: QPCR analyses of decorin (**A**) and nidogen-1 expression (**B**) on day 0, 4 and 10 of cardiovascular differentiation. The beating EB samples at day 10 show a statistically significant increase of decorin and nidogen-1 expression compared to day 0 samples (undifferentiated hESCs, line H9). Statistical results were assessed by one-way ANOVA, using statistical significance at a p-value *p<0.05.

3.1.3 EB and fetal heart ECM IF staining

IF co-staining of different ECM proteins with sarcomeric myosin (MF20 antibody) was performed on paraffin-embedded beating EBs on day 10 of differentiation and on human fetal heart (17 weeks). Staining was performed for decorin and nidogen-1, which were up-regulated during cardiovascular differentiation as identified by qPCR (**Fig. 10**), as well as for laminins and collagen type IV. IF co-staining showed positive staining for all these ECM proteins (green) in the beating EBs and the human fetal heart (**Fig**. **11 A**, **B**). Both of these tissues also expressed sarcomeric myosin (MF20, red). In general, the distribution of the analyzed ECM proteins as well as the sarcomeric myosin in the beating EB sections (**Fig. 11 A**) showed a lower degree of organization than in the human fetal heart (**Fig. 11 B**). In contrast to the human fetal heart, staining of laminins in the beating EBs did not show a clear basal lamina structure. Collagen type IV and nidogen-1 showed a less homogenous expression in the beating EB tissue than in the fetal heart and appeared patchy. Decorin in the fetal heart displayed a higher expression in the vasculature than in the actual myocardium. The beating EBs did not show such a compartmentalization, but a homogenous expression of decorin throughout the whole EB tissue. Also, striation of sarcomeric myosin was barely detectable in the EBs, while IF staining of human fetal heart demonstrated the expression of sarcomeric myosin with clear striation.

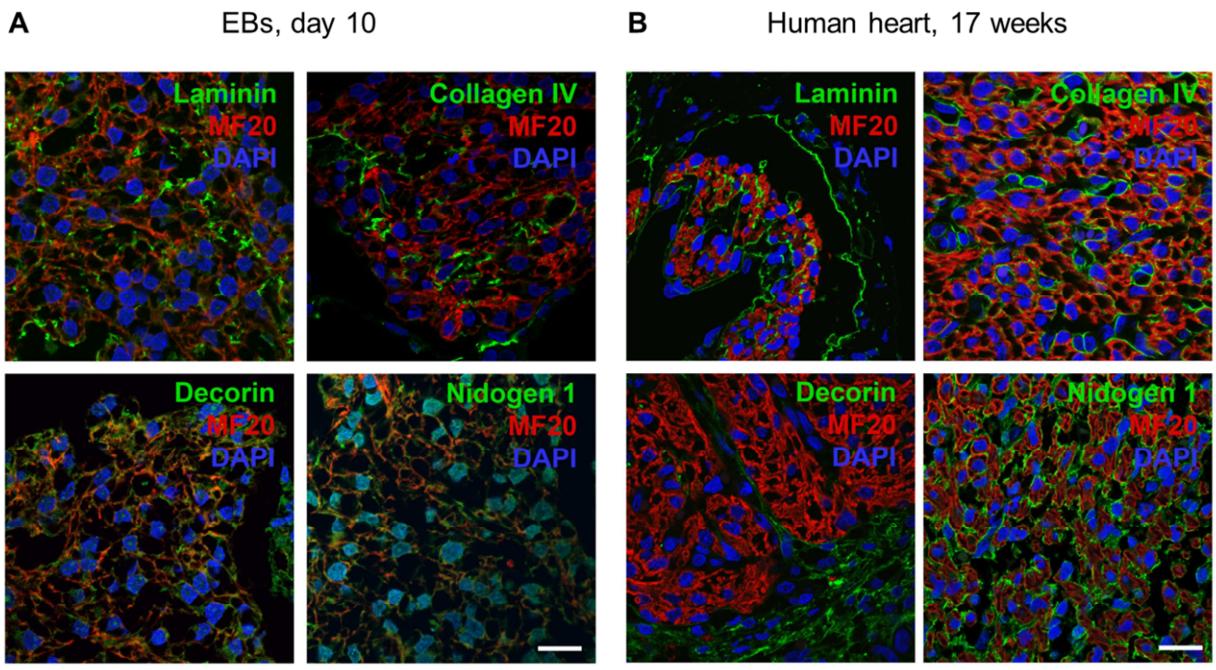

Figure 11: Immunofluorescence staining of paraffin-embedded tissue sections of beating EBs on day 10 of cardiovascular differentiation (**A**) and 17 week old human fetal heart (**B**). Sarcomeric myosin (MF20 antibody) is shown in red and the ECM proteins laminins, collagen type IV, decorin and nidogen-1 are all shown in green. Cell nuclei are stained with DAPI (blue). The scale bars equal 20 µm.

Semi-quantification analysis of ECM protein IF staining of beating EBs at day 10 of cardiac differentiation was conducted with focus on the ECM proteins decorin, nidogen-1, fibronectin, periostin, laminins, collagen type IV and collagen type I (**Fig. 12**). Normalized gray value intensities (GVI) of IF images were compared using the ImageJ software (n = 3). Statistical results were assessed by one-way ANOVA, using statistical significance at a p-value **$p<0.01$. This analysis revealed a significantly higher amount of decorin and nidogen-1 in the beating EBs compared to fibronectin, periostin, laminins and the collagens type IV and type I.

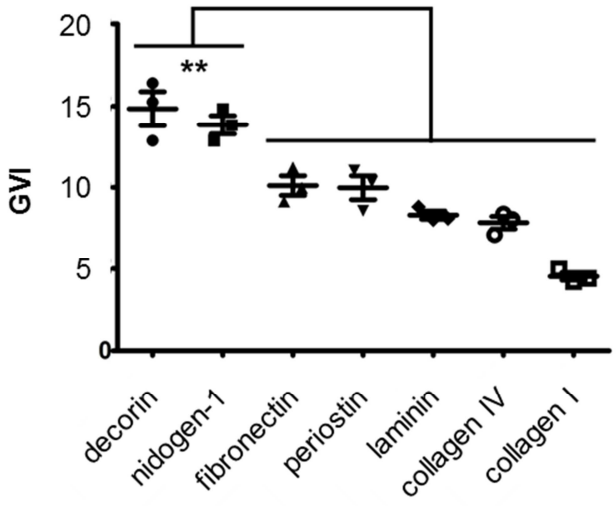

Figure 12: Semi-quantification of the IF staining. Gray value intensities (GVI) of IF images of beating EBs at day 10 of cardiovascular differentiation were compared with focus on the ECM proteins decorin, nidogen-1, fibronectin, periostin, laminins, collagen type IV and collagen type I. The analysis was conducted using the ImageJ software (n = 3). Statistical results were assessed by one-way ANOVA, with statistical significance at a p-value **p<0.01.

3.2 Generation of stable decorin and nidogen-1 production clones

3.2.1 DCN and NID1 production plasmid construction

The results of the EB experiments established decorin (DCN) and nidogen-1 (NID1) as potential cardio-inductive ECM proteins. The generation of stable production clones for these proteins of interest is described in the following section. Several sections of commercially available vectors were used for the construction of the inducible pTet and non-inducible pTD DCN and NID1 production plasmids. The main backbone of the inducible and non-inducible vector consisted of the pcDNA™3.1 vector from the pcDNA™3.1 Directional TOPO® Expression Kit. Expression of the wild type (wt) DHFR gene was controlled by the TK promoter from pGL4.74(hRluc/TK). The inducible promoter for the expression of decorin or nidogen-1 in the inducible expression system was excised from pTRE3G. The inducible expression system required a CHO clone that stably expressed the activator protein for activation of the TRE promoter. This CHO clone (acCHO) was generated by transfecting CHO DHFR-negative mutant cells with the pCMV-Tet3G plasmid and selecting for G418 resistance. Codon-optimized DCN and NID1 sequences were prepared

from GeneArt. A scheme of the inducible or non-inducible production plasmids is shown in **Figure 13**.

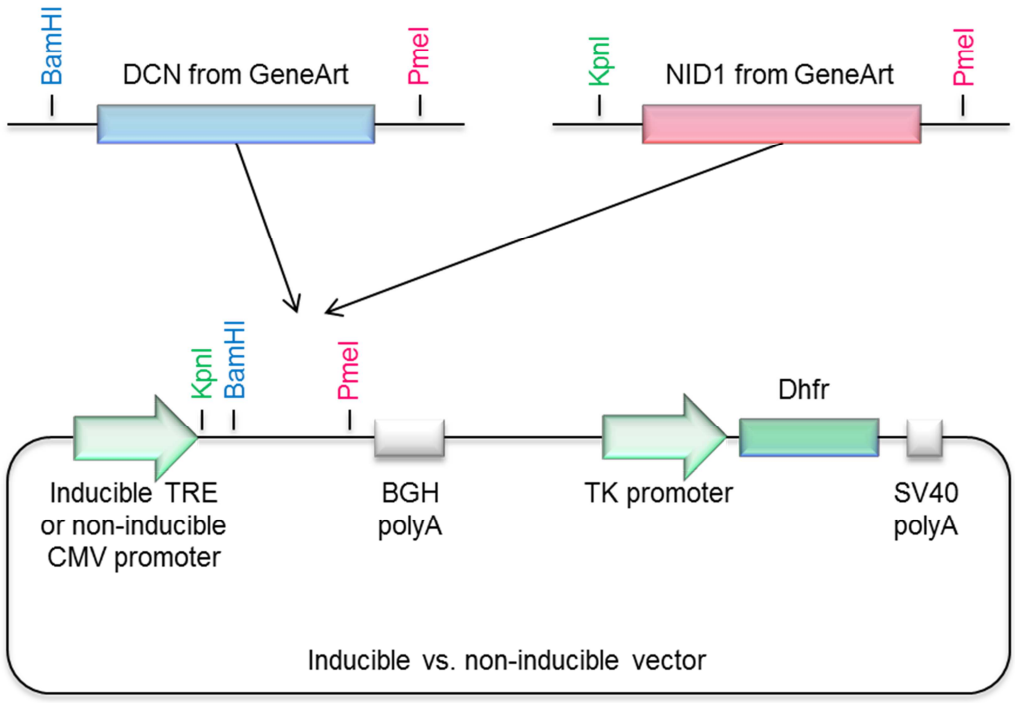

Figure 13: Schematic of the codon-optimized DCN or NID1 sequence synthesized from GeneArt and the inducible or non-inducible vector and indication of the directed insertion site.

A PCR amplification of GFP (798 bps), using 25 ng of the pEGFP-C1 plasmid was conducted using the primers GFPfor and GFPrev (**Fig. 14 A**). The PCR amplification of the CHO wt DHFR was done with cDNA from non-mutated (DHFR-positive) CHO cells, using the primers CgDhfrHind3For and CgDhfrSpeIRev (**Fig. 14 A**). The primers had been designed to include specific restriction sites for the restriction enzymes HindIII and SpeI to enable further cloning steps. The hamster DHFR gene has a size of 564 bps, according to accession # M19869, CRUDHFRA. TOPO cloning of the pcDNA3.1 plasmid and the PCR amplified GFP fragment with the pcDNA™3.1 Directional TOPO® Expression Kit incorporated GFP into this plasmid. The product of this ligation (pcDNA3.1D-GFP) was the main backbone of the inducible and non-inducible expression plasmids. Transformation of Top10 cells, plating and picking of colonies transformed with the pcDNA3.1D-GFP ligation followed.

A PCR cleanup of the DHFR PCR and digestions with the restriction enzymes HindIII and SpeI were prepared in order to be cloned into the pGL4.74 (hRluc/TK) plasmid between HindIII and XbaI restriction sites. 25 ng of the gel purified DHFR PCR digest was ligated with 100 ng of the

pGL4.74 (hRluc/TK) digest. No gel picture was taken to minimize the exposure to UV and damage to DNA. The region containing the TK promoter, DHFR gene, and SV40 polyA of the ligation product was PCR amplified using the primers TKPromDra3For and SV40Rev (**Fig. 14 B**). Unlike CMV, the weaker TK promoter was chosen for the transcription of the wt DHFR gene. This is a more effective strategy for the selection of genomic amplification events as a greater amount of amplification would be required to produce more DHFR on the protein level with a weak promoter. Minipreps of pcDNA3.1D-GFP were digested with the restriction enzymes BamHI and XbaI to screen for the correct plasmid size (**Fig. 14 C**).

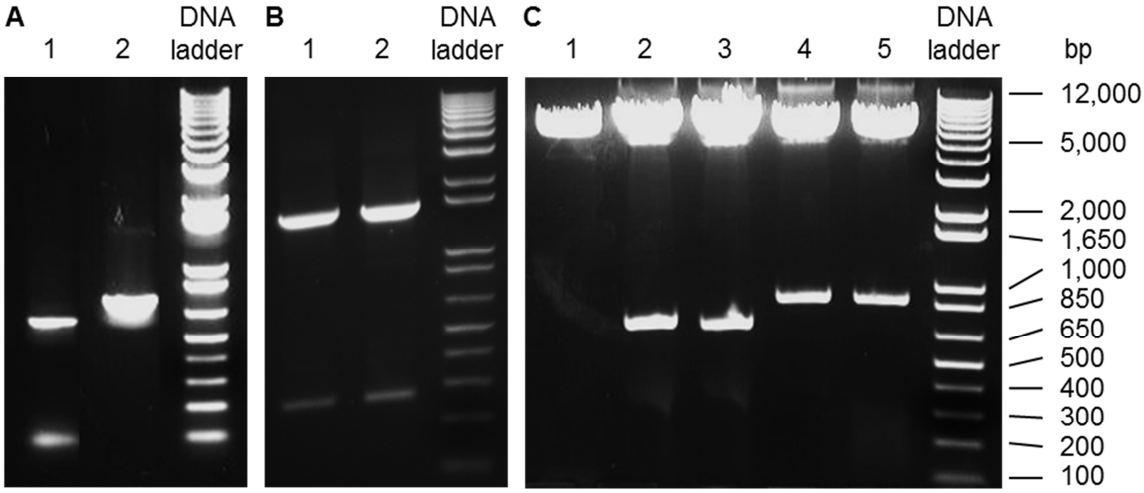

Figure 14: Agarose gel pictures of the (**A**) PCR amplification of (lane 1) the wild type CHO dihydrofolate reductase (DHFR, 564 bps) and (lane 2) GFP (798 bps). (**B**) PCR amplification products of the TK-DHFR-SV40 polyA cassette (1540 bps, lane 1 and 2). (**C**) BamHI and XbaI digests of five pcDNA3.1D-GFP Minipreps (lane 1-5). Minipreps 2 and 3 show correct fragment sizes (798 bps). The 1 Kb Plus DNA ladder was used for DNA fragment size estimation.

Codon-adapted sequences of human DCN (1080 bp) and human NID1 (5406 bp) with a histidine/ asparagine tag at the C-terminus (synthesized from GeneArt) were the template for several PCRs that sequentially attached the wt DCN or wt NID1 secretion peptide to the N-terminus of the DCN or NID1 sequence (**Fig. 15 A, B**). Two primer pairs were sufficient to attach the shorter wt DCN secretion peptide (46 base pairs), while three primer pairs were necessary to attach the longer wt NID1 secretion peptide (84 base pairs).

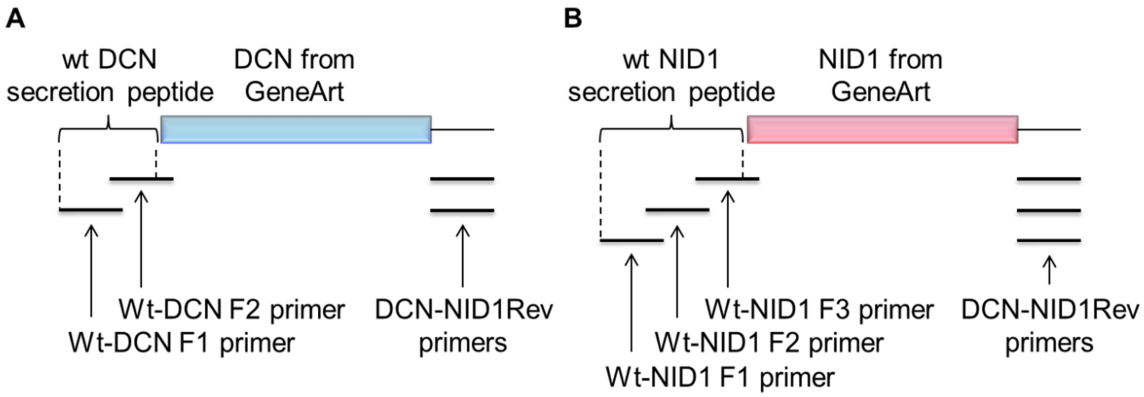

Figure 15: Schematic of the sequential attachment of the DCN and NID1 secretion peptide. **A**) the 46 base pairs wt DCN or **B**) 84 base pairs wt NID1 secretion peptide were attached via PCR to the N-terminus of the DCN or NID1 sequence that has been synthesized from GeneArt.

For the attachment of the DCN and NID-1 secretion peptide using sequential PCRs, the same reverse primer (DCN-NID1Rev) could be used. The different forward primers were Wt-DCN F2 for the first round of DCN PCRs (**Fig. 16 A**) or Wt-NID1 F3 for the first round of NID1 PCRs (**Fig. 16 B**). The Wt-DCN F2 PCR was used to prime the second round of PCR for wt DCN with the primer Wt-DCN F1. The Wt-NID1 F3 PCR was used to prime the second round of PCR for wt NID1 with the primer Wt-NID1 F2. The Wt-NID1 F2 PCR was used to prime the third round of PCR for wt NID1 with the primer Wt-NID1 F1.

Minipreps number 2 and 3 of pcDNA3.1D-GFP (**Fig. 14 C**) showed the correct fraction sizes. Miniprep 2 was chosen and digested with the restriction enzyme SmaI. A PCR cleanup was done before a second digestion with DraIII followed. To prepare the ligation with pcDNA3.1D-GFP, a PCR cleanup of TK-DHFR-SV40pA and digestion with DraIII was prepared. This ligation brought the TK promoter with DHFR into the pcDNA3.1D-GFP vector backbone. 100 ng gel purified pcDNA3.1D-GFP vector backbone were ligated with 25 ng TK-DHFR-SV40 PCR digest. A transformation of competent bacteria, plating and picking of colonies transformed with the ligation product followed. Minipreps of pcDNA3.1D-GFP + TK-DHFR-SV40 were prepared and digested with the restriction enzyme HindIII (**Fig. 16 B**). Lanes 2 – 5 contain correct fragment sizes of pcDNA-GFP + TK-DHFR-SV40pA (2260 bps + 5040 bps for a total of 7300 bps) hereinafter referred to as pTD. One of the correct pTD Minipreps was digested with BamHI & PmeI or with KpnI & PmeI and subsequently gel purified.

A PCR cleanup of wt DCN and digestion with BamHI & PmeI as well as a PCR cleanup of wt NID1 and digest with KpnI & PmeI were prepared. Ligations of 100 ng digested pTD with 25 ng of the digested wt DCN or 75 ng of the digested wt NID1 were set up. Competent bacteria were

transformed with these ligation products and plated. Colonies from the bacteria that had been transformed with the pTD ligations were picked. Minipreps were prepared and pTD-GFP as well as pTD-DCN clones were digested with BamHI & PmeI (**Fig. 16 C**) while pTD-NID1 clones were digested with KpnI & PmeI (**Fig. 16 D**). Overnight cultures and Maxipreps of desired pTD clones were prepared.

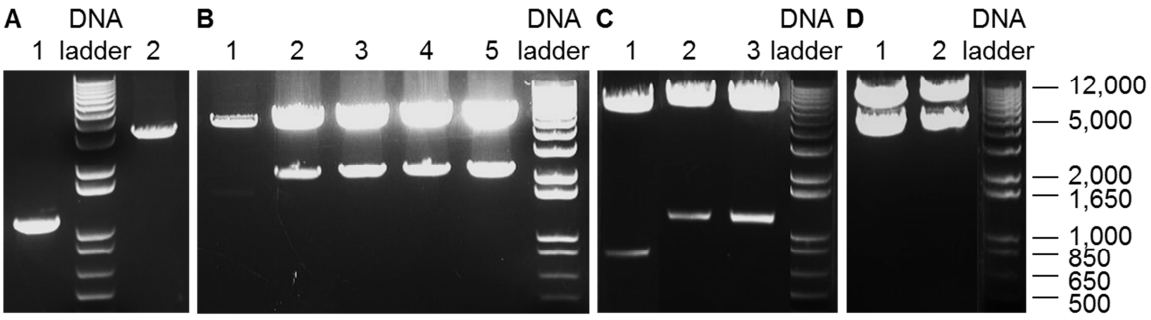

Figure 16: Agarose gel pictures of (**A**) the PCR product Wt-DCN F2 (1160 bps, lane 1) and the PCR product of Wt-Nid1 F3 (3420 bps, lane 2). (**B**) Minipreps A – E (lanes 1-5) of pcDNA-GFP + TK-DHFR-SV40pA. Lanes 2 – 5 contain correct fragment sizes (2260 bps + 5040 bps) hereinafter referred to as pTD. (**C**) BamHI & PmeI digests of pTD GFP (798 bps + 7300 bps, lane 1) and pTD DCN (1160 bps + 7300 bps, lanes 2 + 3). (**D**) KpnI & PmeI digests of pTD NID-1 (3420 bps + 7300 bps, lane 1 + 2). In all agarose gels the 1 Kb Plus DNA ladder was used for DNA fragment size estimation.

For the inducible protein expression system the Tet inducible promoter of the pTRE3G Tet-On 3G Inducible Expression System Bicistronic was amplified in a PCR with the primers TRE3Gfor2 and TRE3Grev2 (**Fig. 17 A**). The Tet inducible promoter was gel purified and digested with BamHI & KpnI. The pTD-B plasmid was digested with BglII & KpnI (sequentially, to remove the CMV promoter. After gel purification the pTD plasmid (without CMV promoter) and the Tet inducible promoter were ligated. Transformation of competent bacteria, plating and picking of colonies transformed with the pTD+TRE3G ligation followed. Minipreps of these clones were digested with BamHI & XhoI (**Fig. 17 B**). The correct clone is hereinafter referred to as pTet-GFP. The pTet-GFP vector was digested with BamHI & PmeI or with KpnI & PmeI. The vector backbone was gel purified and ligated with human DCN and NID-1 previously digested with BamHI & PmeI and KpnI & PmeI. Gel purification, tansformation of competent bacteria, plating and picking of clones followed. Minipreps of pTet clones were prepared and digestions of the pTet-GFP and pTet-DCN clones with BamHI & PmeI (**Fig. 17 C**) and pTet-NID1 clones with KpnI

& PmeI (**Fig. 17 D**) were prepared. Overnight cultures and maxipreps of the pTet clones were prepared.

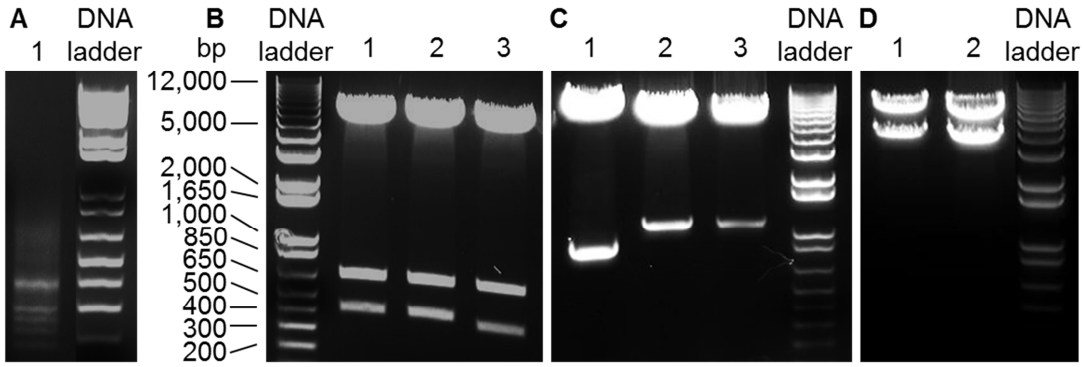

Figure 17: Agarose gel pictures of (**A**) the PCR amplification product of the Tet inducible promoter of the pTRE3G Tet-On 3G Inducible Expression System Bicistronic (322 bps, lane 1). (**B**) Lanes 1 - 3 contain BamHI & XhoI digested Minipreps of the ligation product of pTD+TRE3G (lanes 1 and 2 have the correct 322 bps band). (**C**) Lane 1 contains the BamHI & PmeI digested pTet-GFP Miniprep (798 bps +7030 bps). Lanes 2 and 3 contain BamHI & PmeI digested pTet-DCN Minipreps (1160 bps + 7030 bps). (**D**) Lanes 1 and 2 contain KpnI & PmeI digested pTet-NID1 Minipreps (3420 bps + 7030 bps). In all agarose gels the 1 Kb Plus DNA ladder was used for DNA fragment size estimation.

3.2.2 Generation of activator clones

For the activation of the TRE promoter that regulates DCN or NID1 expression in the inducible expression system, an activator protein was required. This activator protein undergoes a conformational change in the presence of doxycycline and then can induce DCN or NID1 expression. Therefore a stable clone was generated from the DHFR-negative CHO cells that produced the activator protein, which could be accomplished by transfecting these cells with the pCMV-Tet3G plasmid. After transfection and selection for G418 resistance for 3 - 4 weeks in selection media with 500 µg/ml G418, single activator clones were isolated. Prior to transfection of an activator clone with the pTet-DCN or pTet-NID1 plasmid, the best activator clone needed to be chosen. To identify the best activator-producing clone, all the activator clones (acCHO 1 – acCHO 7) were transfected with the pTet-GFP plasmid and as a control, one of the activator clones (acCHO 5) was additionally transfected with the pTD-GFP plasmid. The pTet-GFP plasmid only can express the GFP product in the presence of a sufficient amount of the activator

protein, produced by the activator clones, and after induction with Dox. 48 hours post transfection the activator clones were induced with 100 ng/ml Dox, after another 24 hours the GFP expression of the activator clones could be analyzed (**Fig. 18**). The pTD-GFP plasmid served as a positive control as GFP can be expressed from this plasmid independent of the presence of the activator protein or Dox. GFP expressing acCHO cells expressed a sufficient amount of the activator protein that also could support the expression of DCN or NID1 from the pTet-DCN and pTet-NID1 construct.

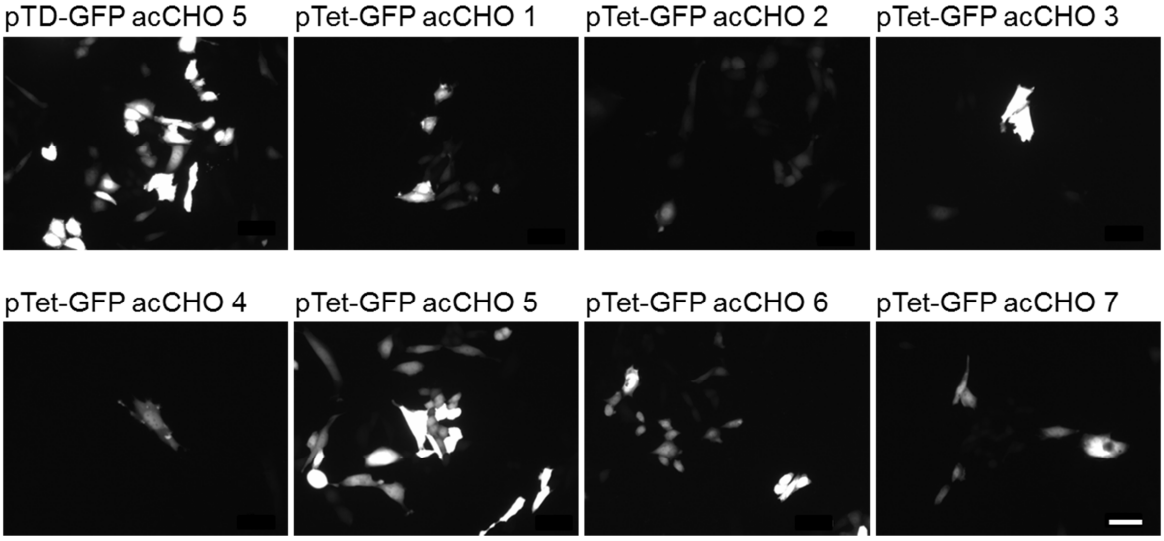

Figure 18: Fluorescence images of the activator clones acCHO 1 – acCHO 7, 72 hours post transfection with the pTet-GFP plasmid or the pTD-GFP plasmid as a positive control, and 24 hours after induction with 100 ng/ml Dox. GFP fluorescence is shown in white. The scale bar equals 50 µm.

The acCHO 5 clone shows a GFP expression after pTet-GFP transfection and Dox induction that is very similar to the positive control transfection with the pTD-GFP plasmid. This clone was chosen for the transfection with the pTet-DCN and pTet-NID1 plasmid for the inducible expression system.

3.2.3 DCN and Nid1 expression plasmid transfection and stable clone selection

The expression plasmids pTD-DCN or pTD-NID1 were introduced into CHO DHFR-negative mutant cells via lipofection for the permanent expression system. As shown above, for our

inducible expression system activator protein-producing acCHO cells were generated in order to support the expression of decorin or nidogen-1 in the inducible expression system. Therefore the pTet-DCN or pTet-NID1 plasmid was introduced into cells of the acCHO 5 clone for the inducible expression system. Selection of CHO cells that had successfully been transfected started 24 hours post transfection, when the media was switched to selection media that only supported growth of cells with a non-mutated DHFR gene. The complete wt DHFR gene was an important feature of all the different expression plasmids and therefore the active DHFR enzyme was present in successfully transfected CHO cells. The media change to selection media at first lead to a slower growth of the cultures. This was the case as transfection was not successful in every CHO cell, and non-transfected cells did not contribute to the proliferation in selection media. Culture in selection media was maintained for two weeks and frequent passaging of the cultures accelerated the loss of non-transfected cells. Proliferation in selection media was proof for the presence of the wt DHFR, but it did not automatically mean that these cells were additionally capable of decorin or nidogen-1 production. There was a possibility that the DCN or NID1 genes on the plasmids were lost or destroyed during plasmid integration into the genome of the CHO host. Formation of stable production cells due to plasmid integration was an important step in the permanent and inducible production system. But inherent to the non-directed integration was the risk, that host genes are destroyed at the site of integration. Therefore transfection of a cell line (CHO DHFR-negative or acCHO) and selection for stably transfected cells lead to a cell culture consisting of a mixture of genetically different cells. Only some of the cells in such a mixture have a high potential for protein production. Cells in the permanent expression system carry a metabolic burden of high decorin or nidogen-1 expression at any time and might grow slower than other cells in the mixture that have a lower decorin or nidogen-1 expression. Over time the productivity of such a mixed culture would therefore decrease. Single cell cloning is an efficient method that stops this negative development already at an early time point in the selection process. Although the cells in the inducible expression system should not have a comparable metabolic burden during selection, single cell cloning was conducted for the inducible cultures as well, as it is beneficial to choose the most potent cells for protein production. After sparse cell plating, spatially separated single cells were grown to cell foci. All the cells in a cell focus originated from the same cell and therefore share the same genomic information. These clonal cells were picked, replated into 12-wells and grown to 100% confluency. Samples of the media were collected to determine the decorin or nidogen-1 content in specific ELISA assays (in the inducible expression system sample collection occurred 48 h after induction with 100 ng/ml Dox). This first selection phase is schematically described in **Figure 19**. The clones with the

highest measured decorin or nidogen-1 levels were replated to undergo the next selection phase, MTX selection for genomic amplification.

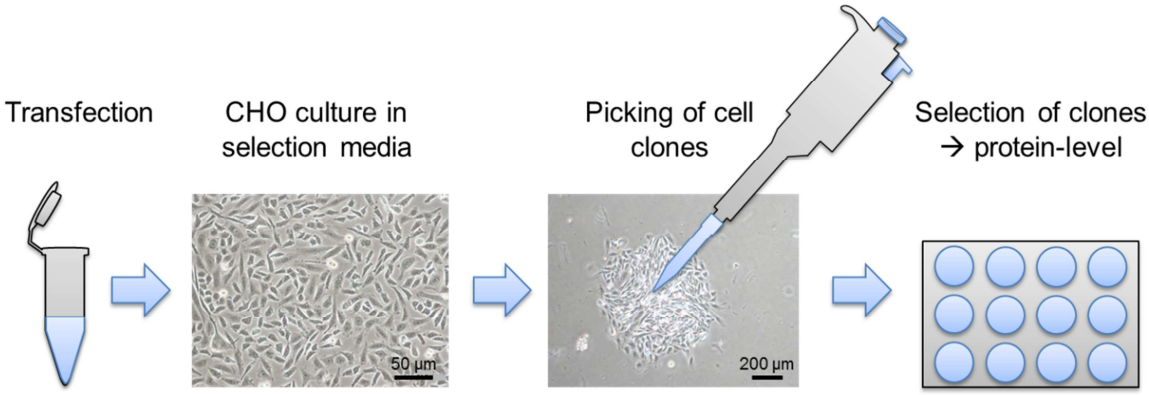

Figure 19: Schematic of the first selection phase after transfection of CHO DHFR-negative or acCHO cells with the DCN or NID1 expression plasmids. This phase included the culture in selection media after transfection, picking of clonal cell foci and selection of the best clones for decorin or nidogen-1 production based on ELISA measurements.

3.2.4 Genomic amplification

In a second selection phase the best clones for decorin or nidogen-1 production from the previous selection phase were exposed to 0.065 µM MTX in the selection media. MTX is a potent inhibitor of the DHFR enzyme and leads to growth arrest of clones with only one wt version of the DHFR gene in the genome. The addition of MTX to the media had varying degrees of impact on the different clones. Some did not show a change in their proliferation while others showed decreased proliferation or even growth arrest. The explanation for this behavior in the presence of MTX can be found in the genome of the different clones. In some of the clones, genomic amplification of the DHFR gene occurred. As these clones have several copies of the DHFR gene, they are also capable of higher production of the DHFR enzyme and a low concentration of MTX did not inhibit their proliferation. The clones that showed reduced proliferation or growth arrest did not amplify their DHFR gene or only to a lower extend. Thereby MTX exposure selects for clones that by chance amplified the wt DHFR gene. As this non-mutated DHFR gene originated from the expression plasmid and all the expression plasmids were designed to have the complete decorin or nidogen-1 expression cassette in close proximity to the wt DHFR cassette, there was a chance that these protein cassettes were co-amplified. In that case the cells should not only produce higher amounts of the DHFR mRNA and the DHFR enzyme but also of decorin or nidogen-1, which can be determined by ELISA measurements. A

scheme for the co-amplification of the DHFR cassette and the DCN or NID1 cassette in the genome as well as the effect on the mRNA and protein level is shown in **Figure 20**.

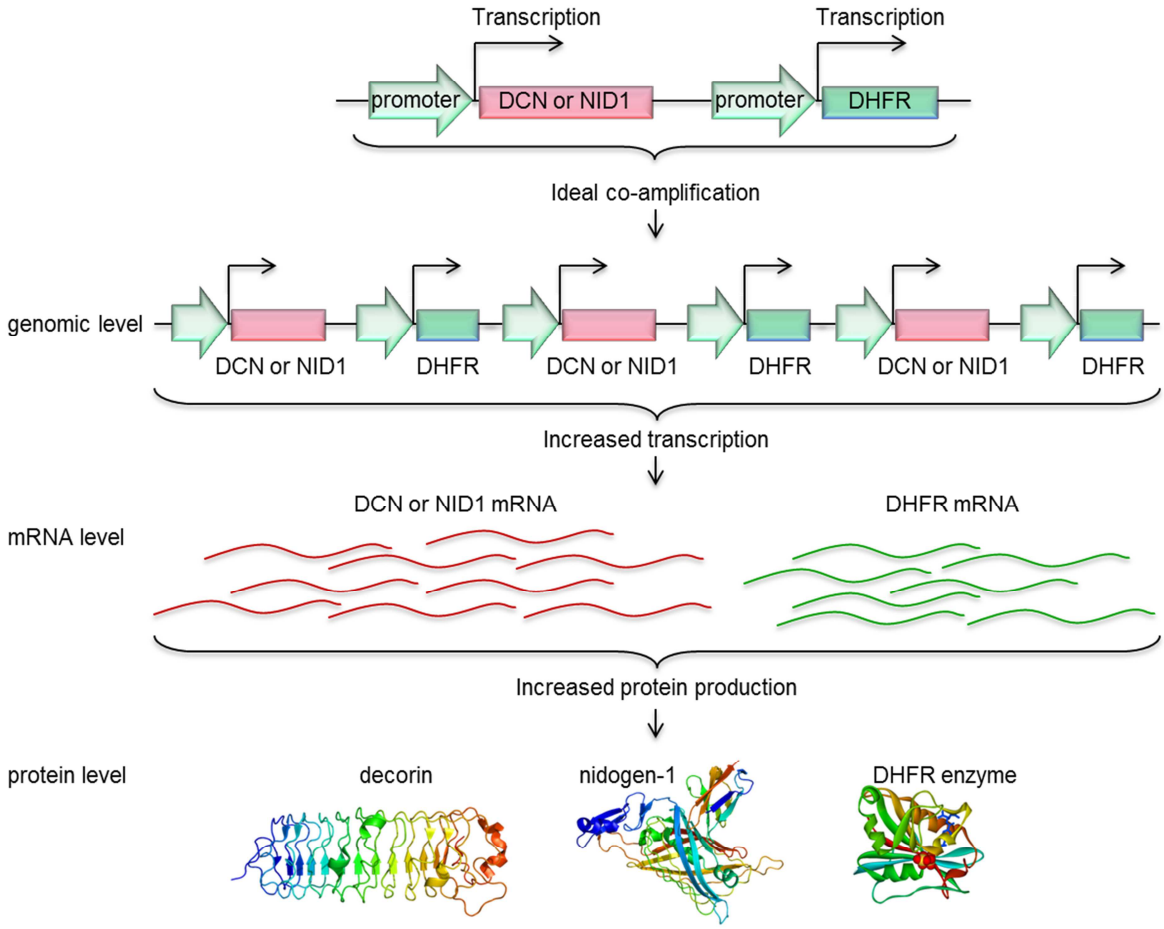

Figure 20: Schematic of an ideal co-amplification of the DHFR cassette and the DCN or NID1 cassette in the genome of CHO cells during MTX selection. As a consequence of the multiplication of these protein expression cassettes on the genomic level the transcription of these genes increases. This leads to an increased mRNA level and increased production of the DHFR enzyme as well as decorin or nidogen-1.

Similar to the first selection phase the selection pressure is maintained for 2 - 3 weeks, clonal cell foci were picked and cell clones were analyzed in order to choose the clones with the highest decorin or nidogen-1 production. In addition qPCR analysis on the genomic level as well as the mRNA level was conducted to verify the mechanistic background of the increase in protein production (for the DHFR enzyme as well as decorin or nidogen-1). The different analysis (ELISA (protein level), genomic qPCR and qPCR from mRNA) as well as growth

behavior and morphological abnormalities were considered to choose the clones for the next MTX selection round. Here clones were favored that co-amplified the decorin or nidogen-1 cassette together with the DHFR cassette in their genome, as these showed the highest decorin or nidogen-1 production. Serial rounds of selection for clones with genomic co-amplification events with increasing MTX concentrations were conducted in the second selection phase. A scheme of a MTX selection round is shown in **Figure 21**.

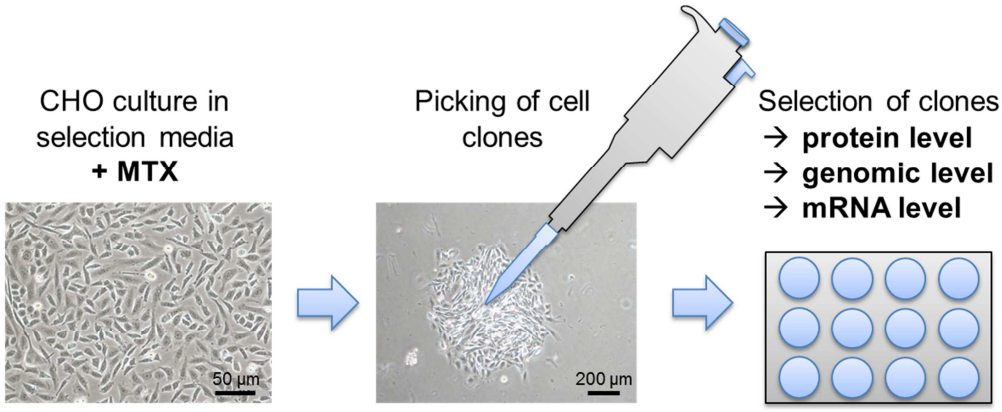

Figure 21: Schematic of one of the serial selection rounds in the second selection phase. Each round exposed the cell clones to higher concentrations of MTX (0.065 µM, 0.275 µM, 0.55 µM, 1.0 µM and 2.5 µM) to select for cells with amplified DHFR cassette for 2 - 3 weeks.

The MTX concentrations used in the serial selection rounds were 0.065 µM, 0.275 µM, 0.55 µM, 1.0 µM and 2.5 µM. But with most clones it was beneficial to leave out some of the intermediate steps. In order not to risk the loss of a clone due to complete growth arrest in a selection medium with too much MTX, a selection system with different MTX concentrations was used in parallel. For example after the first MTX selection round with 0.065 µM MTX the best production clones were selected with 0.275 µM MTX as well as 0.55 µM MTX in a second MTX selection round. The best clones for the next MTX selection round were again chosen after clonalization and clone analysis, while the other clones were discarded. QPCR analyses (genomic and from mRNA) for DHFR, DCN and NID1 are shown for samples of clones after the first selection phase (no MTX), and the first two selection rounds with MTX (**Fig. 22**). The genomic qPCR analysis and the qPCR analysis from mRNA showed an increase in the genomic copy numbers and the mRNA level of DHFR over the course of the MTX selection rounds for chosen clones. Therefore genomic amplification of the DHFR cassette occurred, and lead to an increase of DHFR expression. Genomic qPCR analysis of DCN and NID1 was conducted with two primer pairs each. One amplified a segment at the 5' and one at the 3' terminus of the gene. If the DHFR cassette would have been amplified with only a part of the DCN or NID1 cassette, typically the 3'

terminus, there should be no increase detectable with the 5’ DCN or 5’ NID1 primers. The genomic qPCR analysis in **Figure 22** show an increase of the DCN and NID1 gDNA level due to the MTX selection rounds in both primer pairs. Therefore a complete co-amplification of the DHFR cassette with the DCN or NID1 cassette occurred in these clones and also lead to an increased decorin or nidogen-1 expression, as shown with the 5’ and 3’ primer pairs in the qPCR analysis of the mRNA level. Again the two different primer pairs at the 5’ and 3’ terminus were used to prove that the DCN and NID1 mRNA was complete.

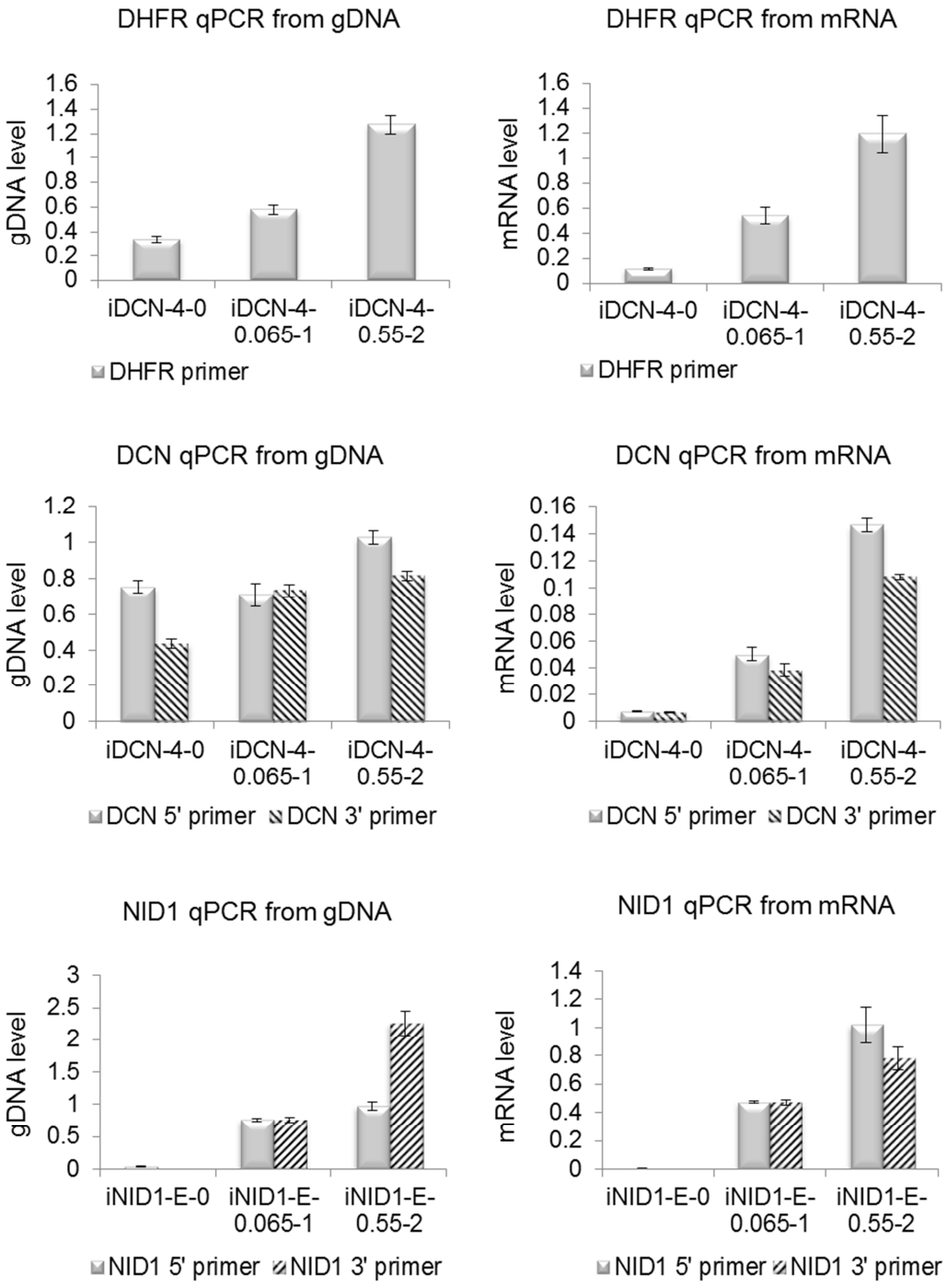

Figure 22: QPCR analyses of the genomic DNA level and mRNA level of the DHFR enzyme as well as DCN and NID1. The analyses were conducted for samples of CHO clones after the first selection phase (no MTX) as well as after the MTX selection rounds one and two. For DCN and NID1 two different primer pairs for the 5' terminus and 3' terminus were used.

An example and explanation of the nomenclature of the CHO clones is shown in **Figure 23**.

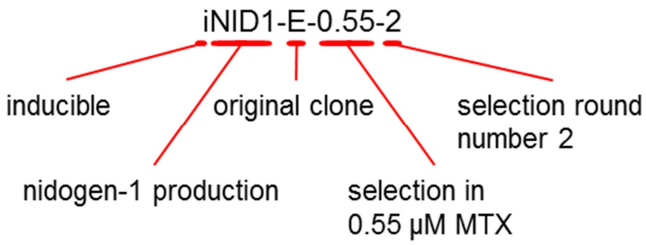

Figure 23: Clone nomenclature. In this example, iNID1-E-0.55-2 indicates that the protein production is inducible (i), which protein is produced (nidogen-1), the number or letter of the original clone after the first selection phase (E), the MTX concentration the clone is selected in (0.55 µM) and the number of MTX selection rounds the clone has already passed (2).

Examples of ELISA measurements that showed an increased production of decorin and nidogen-1 over the course of the MTX selection are shown in **Figure 24**. These measurements of decorin and nidogen-1 secretion to the cell culture media prove that the increase of the cellular mRNA level of these ECM proteins also caused an increased protein production.

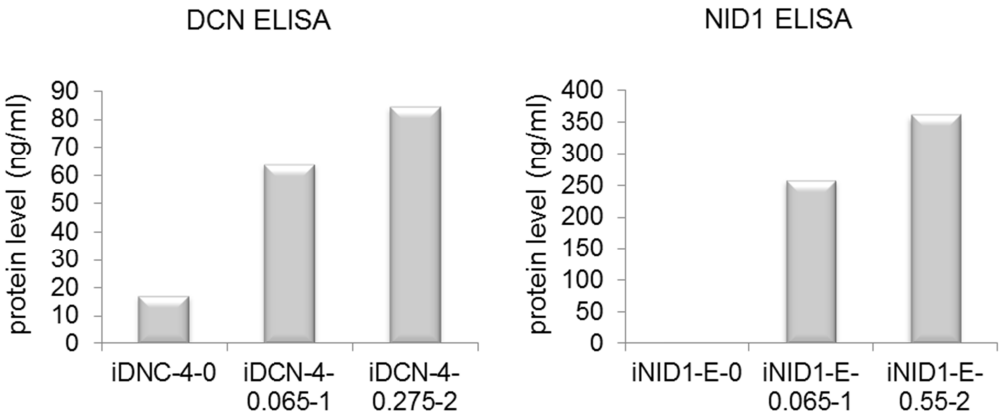

Figure 24: ELISA measurements of the decorin and nidogen-1 protein levels were conducted for samples of CHO clones after the first selection phase (no MTX) as well as after the MTX selection rounds one and two.

After the third selection round with MTX a production test over 4 days was conducted, to determine the best day to harvest the media (**Fig. 25**). The cell clones were grown in T175 flasks until confluency, the media (40 ml) was changed on day 0 and 200 µL of the media was

collected on each of the following 4 days for ELISA measurements of the secreted decorin or nidogen-1. The CHO clones that produced nidogen-1 in the permanent expression system showed only very low production in the MTX selection rounds and therefore the selection was only continued with the inducible nidogen-1 clones. For the three different clones, inducible and permanent decorin production as well as inducible nidogen-1 production, a steady increase in the protein concentration of the culture media could be detected. Even after several days of culture no negative effect on the secreted proteins was obvious in the ELISA measurements, for example due to proteolysis. The inducible DCN clones were clearly less productive than the clones that produced decorin in the permanent expression system. Therefore after the third MTX selection round decorin production was only continued with the non-inducible DCN clones.

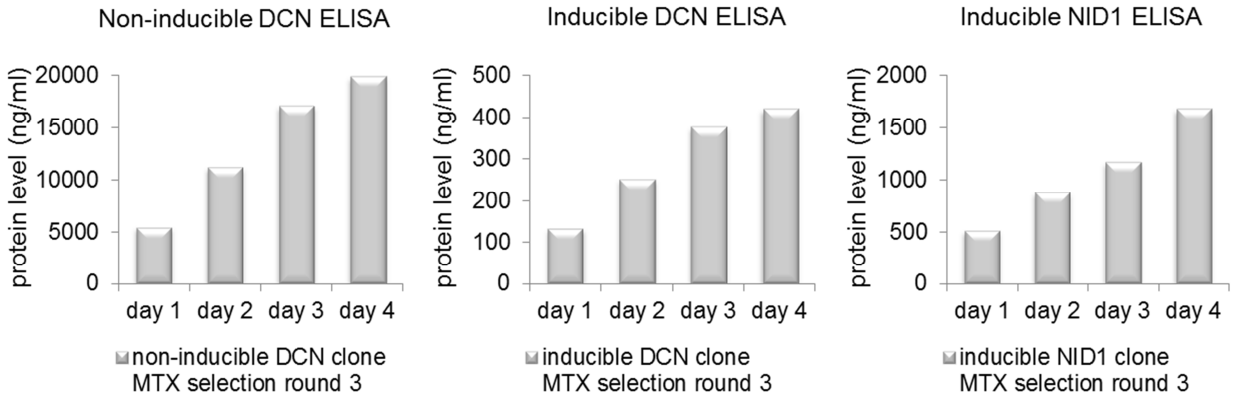

Figure 25: ELISA measurements of the decorin and nidogen-1 protein levels over a period of 4 days were conducted for samples of CHO clones after the third MTX selection round. Cell culture samples were collected daily over a period of 4 days after media change on day 0 as well as induction with 100 ng/ml Dox for the inducible clones.

3.2.5 Selection of the best production clones for suspension growth adaptation

Seven of the most promising CHO clones for decorin or nidogen-1 production were grown in 12-wells in parallel in order to determine the best two production clones for suspension growth adaptation. The CHO clones were renamed for convenience and their growth characteristics were monitored and rated, as this is an important criterion for efficient production (**Table 8**).

Table 8: CHO clone renaming and individual rating of cell growth in adaptation culture.

Old nomenclature	New nomenclature	cell growth
DCN-19-0.275A-2	DCN A1	medium
DCN-5-0.275-A-2	DCN A6	fast
DCN-19-1.1CB-3	DCN B4	slow
DCN-19-1.1CC-3	DCN B5	slow
DCN-19-1.1CD-3	DCN B6	medium
iDCN-4-0.55A-2	iDCN C1	slow
iDCN-4-0.55B-2	iDCN C2	medium
iNID1-E-0.55B-2	iNID1 E2	fast
iNID1-E-0.55H-2	iNID1 E7	fast
iNID1-E-1.0E-2	iNID1 F6	medium
iNID1-E-3.0B1-3	iNID1 G3	fast
iNID1-E-3.0H1-3	iNID1 H1	fast
iNID1-E-3.0F1-3	iNID1 I1	slow
iNID1-E-5.0I3-3	iNID1 I4	fast

Due to inconsistent growth behavior of the different clones the ELISA measurement has additionally been normalized to the cell number, thereby describing the specific decorin or nidogen-1 production (**Fig. 26**). For the decorin clones, the normalization to the cell number only caused slight changes to the overall readout of the ELISA. However the normalization to the cell numberchanged the ranking of the best nidogen-1 production clones. In this case, the specific production was estimated to be more reliable. The inducible decorin clones (iDCN C1 and iDCN C2) clearly showed a lower production than the non-inducible clones (DCN A1, DCN A6, DCN B4, DCN B5, DCN B6). The best two decorin production clones were DCN B4 and DCN B5 (according to the protein level in the media and the specific protein production). Despite this fact, the clones DCN A6 and DCN B4 were chosen for suspension growth adaptation as the clones DCN B4 and DCN B5 both came from the DCN-19-1.1C selection and therefore had a very similar genomic background. Furthermore, these clones are characterized by slow cell growth. In order to have a better chance to succeed in the suspension growth adaptation a greater diversity of the chosen clones was preferable. Therefore instead of the second best decorin-producing clone DCN B5, the third best clone DCN A6 was chosen for suspension growth adaptation, as this clone has a different genetic background and is characterized by fast cell growth. The DCN

A6 clone had been selected in two MTX selection rounds, while the DCN B4 clone has been selected in three MTX selection rounds.

The best two nidogen-1 producing clones were iNID1 H1 and iNID1 I4 (according to the protein level in the media and the specific protein production). These clones had a different genetic background and both showed fast cell growth. Therefore these inducible nidogen-1-producing clones were chosen for suspension growth adaptation. Both of these clones had been selected in three MTX selection rounds.

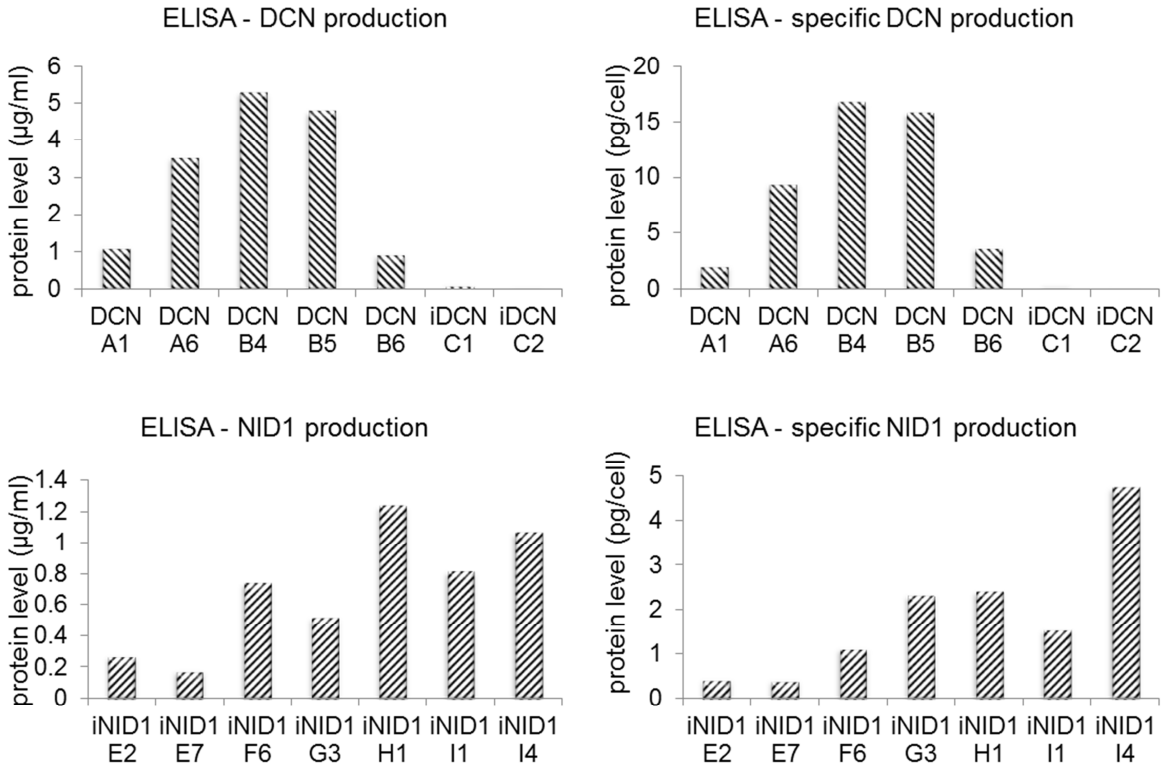

Figure 26: ELISA measurements of the decorin and nidogen-1 protein levels and specific protein production. Measurements were conducted for samples of seven CHO clones each after the second or third MTX selection round. The media was collected two days after a media change (and induction with 100 ng/ml Dox for the inducible production clones). Exact cell numbers were measured by the automated CASY cell counter and specific protein production (shown in pg/cell) was determined by dividing the protein amount per ml (µg/ml) by the cell number per ml (cells/ml).

3.2.6 Adaptation to suspension culture and serum depletion

Based on the highest protein production as well as growth behavior two non-inducible DCN clones (DCN B4 and DCN A6) and two inducible NID1 clones (iNID1 H1 and iNID1 I4) were selected for suspension culture adaptation. As described in the material and methods section 100 ml of suspension media in 250 ml Erlenmeyer flasks were inoculated with 10 x 10^6 cells of each of the selected four production clones. The cells were passaged every four to five days up to ten times in suspension media containing 10% FBS dialyzed for adaptation to suspension culture. Prior to adaptation to suspension culture some of the cells formed clumps or adhered to the wall of the Erlenmeyer flask. When adaptation to suspension culture was visible due to lower clump formation or adherence to the wall of the Erlenmeyer flask, the productivity of the cells was tested in ELISA measurements (**Fig. 27**). The clone DCN A6 showed a drastic decrease of decorin-production after adaptation to the suspension culture. These cells only produced 0.064 µg/ml in suspension culture compared to the 3.53 µg/ml in adherent culture (**Fig. 26**). Furthermore morphological changes of the DCN A6 clone during adaptation to suspension culture were observed, which can indicate a possible chromosomal instability. Such a chromosomal instability could be the explanation for the decreased decorin production. As the second suspension culture-adapted decorin production clone DCN B4 showed very high protein production (23.98 µg/ml), suspension culture of the DCN A6 clone was not continued. The inducible nidogen-1 production with nidogen-1 concentrations of 2.70 µg/ml (iNID1 H1 clone) and 1.26 µg/ml (iNID1 I4 clone) in the suspension media was considerably lower than the permanent decorin production by the DCN B4 clone.

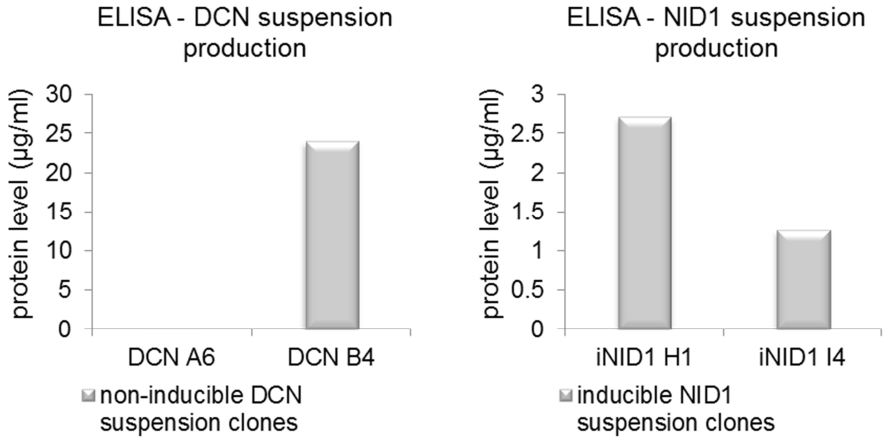

Figure 27: ELISA measurements of the decorin and nidogen-1 protein levels were conducted for DCN and iNID1 production clones after adaptation to suspension culture with 10% FBS dialyzed. The media was collected four days after a media change (and induction with 100 ng/ml Dox for the inducible iNID1 production clones).

After adaptation to suspension culture the three remaining clones were ready for adaptation to gradual serum reduction. Over a period of several months the cells could be adapted to suspension media culture with 5%, 3% and 1% FBS dialyzed. Prior to adaptation to media with reduced serum content the cells showed a decreased cell growth. In order to avoid growth arrest the DCN B4 clone needed additional intermediate steps of reduced serum content in the suspension media (4% and 2% FBS dialyzed). While the iNID1 H1 and I4 clones could be adapted to growth and protein production in 0.5% FBS dialyzed, this was not possible for the DCN B4 clone due to complete growth arrest. Therefore serum depletion of the B4 clone was stopped at 1% FBS dialyzed. In order to choose the best clone for nidogen-1 production the productivity of the two remaining inducible clones H1 and I4 after serum reduction to 0.5% was compared (**Fig. 28**).

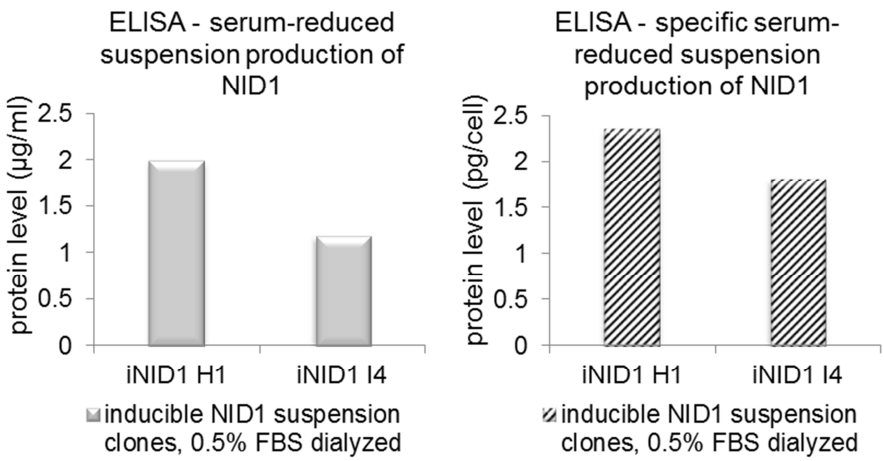

Figure 28: ELISA measurements of the nidogen-1 protein levels were conducted for the iNID1 production clones H1 and I4 after adaptation to suspension culture with 0.5% FBS dialyzed. The media was collected two days after induction with 100 ng/ml Dox. Exact cell numbers were determined by the automated CASY cell counter and specific protein production (shown in pg/cell) was determined by dividing the protein amount per ml (µg/ml) by the cell number per ml (cells/ml).

After adaptation to suspension culture with reduced serum content the clone iNID1 I4 showed a considerably lower nidogen-1 production than the iNID1 H1 clone. This was true for the comparison of nidogen-1 concentration in the media (1.18 µg/ml compared to 1.99 µg/ml) as well as for specific nidogen-1 production of the two clones (1.81 pg/cell compared to 2.36 pg/cell). Therefore for subsequent up-scaling and protein production the suspension culture of the iNID1 I4 clone was not continued and the iNID1 H1 culture in the incubation shaker was expanded.

As shown in **Figure 25**, decorin and nidogen-1 concentration in the culture media continuously increased for the permanent and inducible production system. Therefore for maximum protein yields while ensuring adequate nutrient supply and pH buffering of the culture, the protein-containing culture medium from the decorin production clone B4 and nidogen-1-production clone H1 were harvested every 4-5 days. Thereby protein concentrations in the serum-reduced culture medium of up to 42.8 µg/ml decorin and 4.2 µg/ml nidogen-1 could be reached (**Fig. 29**).

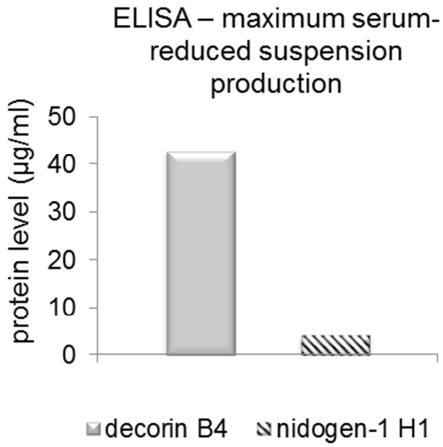

Figure 29: ELISA measurements of the decorin and nidogen-1 protein levels were conducted for the decorin B4 production clone after adaptation to suspension culture with 1% FBS dialyzed and the nidogen-1 H1 production clone after adaptation to suspension culture with 0.5% FBS dialyzed. The culture media was collected 4 days after media change and induction with 100 ng/ml Dox for the H1 clone.

3.3 Decorin and nidogen-1 protein production, purification and characterization

3.3.1 Protein purification with chromatography methods

The protein purification was conducted via IMAC as described in the material and methods. Several different equilibration, wash and binding buffers were tested to optimize the purification efficiency and selectivity. Buffer compositions at pH 7.4 with the best purification result are shown in **Table 5**. The FPLC system Äkta Explorer 10 controled the purification process and monitored and recorded different measurement data like flow rates, conductivity, pressure and absorption at 280 nm and 256 nm (**Fig. 30**). UV light absorption is characteristic for proteins and the absorption peaks for the wavelengths 280 nm and 256 nm (shown by the blue and red line) indicated the protein-rich elution fractions. It is characteristic for protein solutions that the absorption at the wavelength 280 nm (blue line) exceeds the absorption at 256 nm (red line).

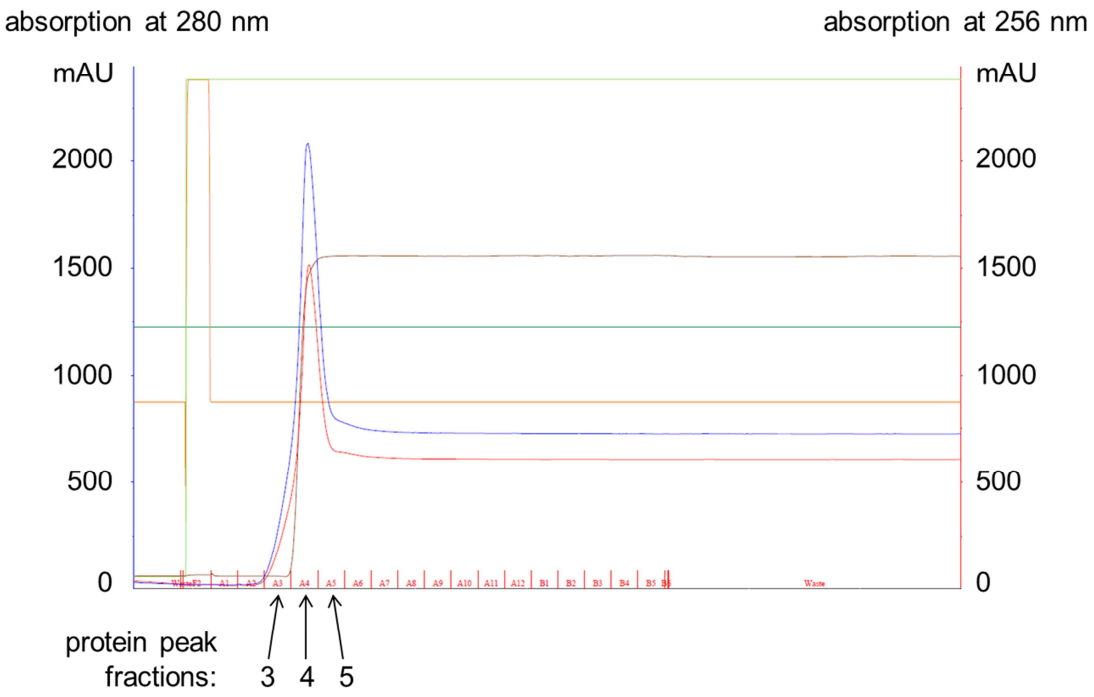

Figure 30: Elution phase in the IMAC purification with the HisPrep FF 16/10 20 ml column, controlled by the Äkta Explorer 10. Elution of histidine-tagged proteins occurred in elution fractions three, four and five. The blue line shows the absorption at the wavelength 280 nm and the red line shows the absorption at the wavelength 256 nm in milli absorbance units (mAU). Other colored lines show the conductivity, flow rates, pressure and buffer mix position in this elution phase.

Typically the elution fractions three, four and five contained the highest protein concentrations and were used for the subsequent desalting and buffer exchange to PBS on the Äkta Purifier 100 system with the 53 ml HiPrep™ 26/10 desalting column (17-5087-01, GE Healthcare, USA) (**Fig. 31**). Applying this chromatographic desalting method an additional dialysis step was rendered unnecessary. Desalting and buffer exchange are important as the elution buffer for protein elution from the affinity chromatography column contains high salt und imidazole concentrations that would interfere with any biological application.

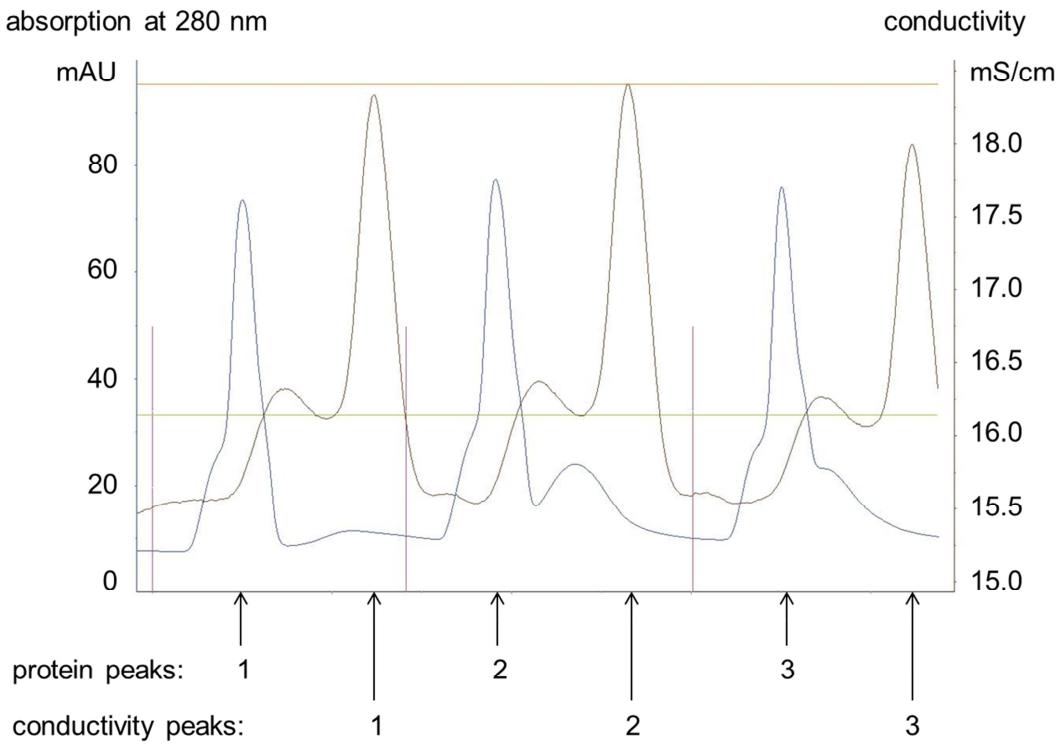

Figure 31: Desalting and buffer exchange of the elution fractions from the IMAC purification. Three protein-containing elution fractions (each 6 ml) were loaded sequentially onto the HiPrep™ 26/10 desalting column, controlled by the Äkta Purifier 100 system. The blue line shows the absorption at the wavelength 280 nm in mAU and the brown line shows the conductivity in mS/cm (milli Siemens per centimerter). The desalted protein was manually collected during three periods while the absorption peaks at 280 nm indicated high protein content.

Sequentially 3 x 6 ml of protein-containing elution fraction from the IMAC purification as well as DPBS for buffer exchange were loaded onto the desalting column. The diluted protein-containing solution was manually collected while the UV absorption reading at 280 nm peaked (3 protein peaks in **Fig. 31**). No sample was collected during high conductivity readings (3 conductivity peaks in **Fig. 31**). The desalting and buffer exchange procedure caused a dilution of the protein solution from the original 18 ml in the three IMAC purification fractions to around 100 ml manually collected protein solution after desalting.

In order to reach higher protein concentrations, complete the buffer exchange to DPBS, exert washing steps and reduce the volume for the protein stocks, protein concentration was conducted in the Vivaspin 20 ultrafiltration units. The protein solution was concentrated to a

volume of 3 - 5 ml. Further concentration to 1-2 ml would increase the protein concentration but cause a slight protein loss due to adsorption to the filter membranes. After concentration of the protein solution sterile filtration was conducted with a flip filter and the protein concentrate was aliquoted and stored at -80 °C.

ELISA measurements revealed the purification efficiency of decorin and nidogen-1-containing culture media (**Fig. 32**). 420 ml of suspension culture medium containing 42.8 µg/ml decorin were purified and concentrated with the methods described above. Out of the 18.0 mg decorin in these 420 ml B4 culture medium, 14.1 mg could be purified. This represents a purification efficiency of 78%. In a similar way, 363 ml of suspension culture medium containing 4.2 µg/ml nidogen-1 were purified and concentrated. Out of the 1.5 mg nidogen-1 in these 363 ml H1 culture medium, 1.1 mg could be purified. This represents a purification efficiency of 73%.

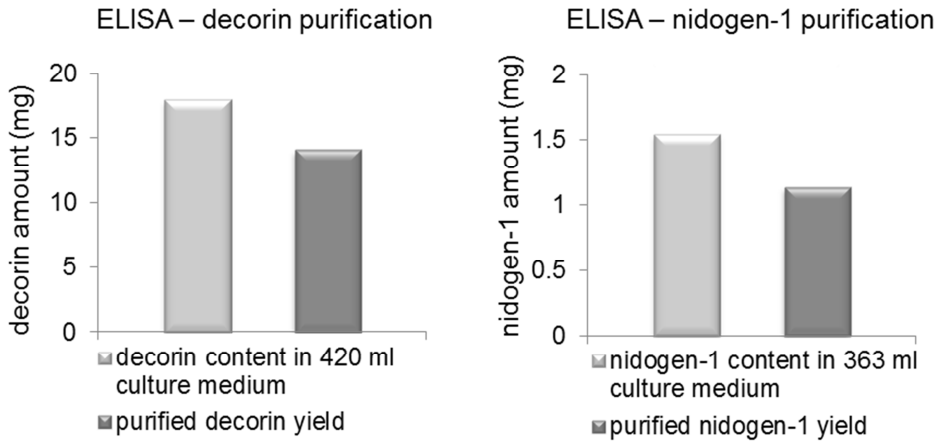

Figure 32: Decorin and nidogen-1 content before and after protein purification and concentration. Using ELISA measurements of the decorin and nidogen-1 protein concentrations in the B4 and H1 culture media and the purified and concentrated protein samples, the decorin and nidogen-1 protein contents and purification efficiencies were calculated.

3.3.2 Protein detection

For a first detection of the purified proteins after IMAC purification on the Äkta explorer 10 and an estimation of possibly remaining unspecific proteins, 2 µl of the decorin eluate and the nidogen-1 eluate were loaded onto a NuPAGE®Novex 4-12% Bis-Tris gel. Additionally a control IMAC purification of suspension media with 1% FBS dialyzed was conducted. As this media was not used for the CHO cell culture, it did not contain any human decorin or nidogen-1 and just

served as a control for possibly unspecific binding of FBS components to the HisPrep FF 16/10 affinity chromatography column. 10 µl of the control eluate (compared to the 2 µl from the decorin or nidogen-1 eluate) were utilized for SDS-PAGE in order to detect even lower amounts of possibly unspecifically purified proteins. After the SDS-PAGE, the proteins were blotted onto a nitrocellulose membrane, which was incubated in a Ponceau-Red solution for an unspecific protein staining (**Fig. 33 A, B**). The decorin eluate clearly contained protein, visible at about 47-65 kDa and accordingly the nidogen-1 eluate contained a protein band at about 130 – 145 kDa after Ponceau-Red staining. The Ponceau-Red staining did not show any unspecifically purified proteins in the control eluate. Therefore already in the first purification step (IMAC) FBS components of the production media could be specifically separated from the histidine-tagged human decorin and nidogen-1. After pictures of the unspecific Ponceau-Red protein staining were taken, the membrane was discolored to be used for specific protein immunodetection using antibodies against decorin or nidogen-1. The following detection via a HRP-labeled secondary antibody and the HRP substrate revealed the identity of the Ronceau-Red stained protein bands form **Figure 33 A** and **B** as decorin and nidogen-1 (**Fig. 33 C, D**).

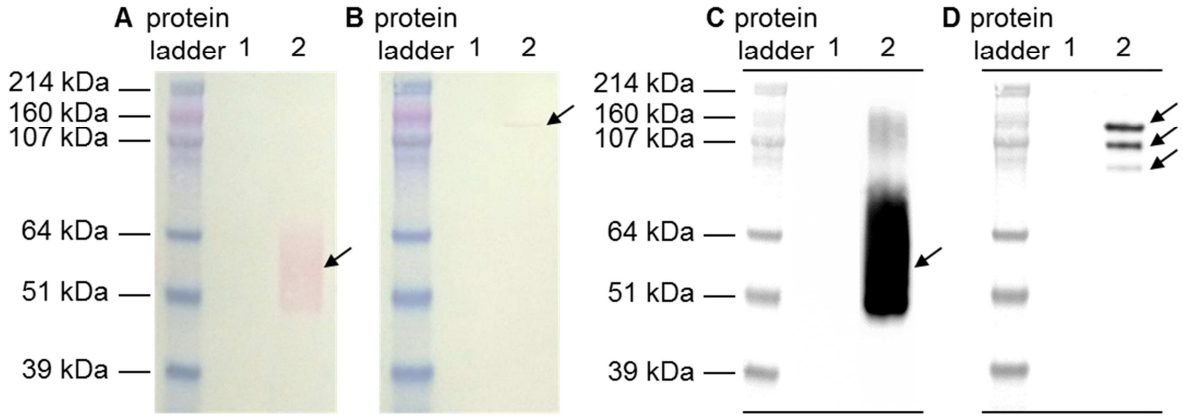

Figure 33: SDS-PAGE and Western Blot analyses. **A** and **B** show Ponceau-Red staining of nitrocellulose membranes. Lane 1 of both membranes contain the negative control (10 µl of a IMAC purification of suspension media with 1% FBS dialyzed). Lane 2 of membrane **A** and **B** contain 2 µl of the affinity chromatography purification of decorin-containing cell culture media with originally 1% FBS dialyzed (**A**) or the affinity chromatography purification of nidogen-1-containing cell culture media with originally 0.5 % FBS dialyzed (**B**). In both nitrocellulose membranes the HiMark Pre-stained protein standard was used for protein size estimation. **C** and **D** show the same membranes after discoloring and specific immunodetection of decorin (**C**) or nidogen-1 (**D**).

The SDS-PAGE and Western Blot analysis of purified decorin and nidogen-1 (**Fig. 33 C** and **D**) showed a wide decorin band at about 47- 80 kDa and the proteolysis-sensitive nidogen-1 in 3 characteristic protein bands at about 140 kDa, 110 kDa and 90 kDa.

3.3.3 Protein deglycosylation

Like many other ECM proteins both human decorin and nidogen-1 carry complex glycosylations. These have important functions in growth factor sequestering, cell-ECM interactions or ECM-ECM interactions. The CHO host cell line used for decorin or nidogen-1 production contains the required enzymes for post-translational modification like glycosylation of human proteins. To determine whether glycosylation of the human decorin and nidogen-1 occurred we used a deglycosylation enzyme mix consisting of both endoglycosidases and exoglycosidases to remove N-linked as well as O-linked oligosaccharides. The enzymatic reaction was stopped after 4 hours or 20 hours. Successful deglycosylation was detected in comparison with the control sample of decorin or nidogen-1 after SDS-PAGE and Western Blotting via a size-shift of the protein band to a lower protein size (**Fig. 34**). For decorin as well as nidogen-1 a protein size-shift was detectable (**Fig. 34 A, B)**. The lowest protein size of decorin after deglycosylation was about 42 kDa compared to the 48 kDa in the untreated decorin sample. The sizes of the characteristic nidogen-1 bands with 140 kDa (whole nidogen-1) and 110 kDa and 90 kDa (proteolysis fragments) also were shifted slightly after deglycosylation to approximately 130 kDa, 100 kDa and 89 kDa. No additional size shift could be detected for the prolonged enzymatic reaction time of 20 hours compared to the 4 hour deglycosylation.

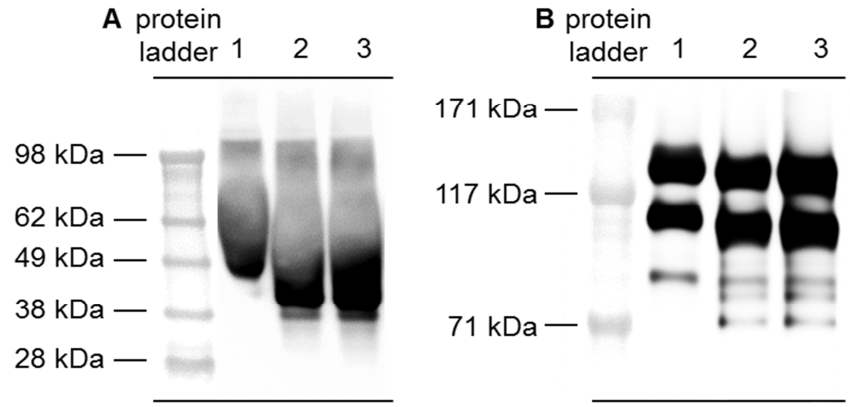

Figure 34: Deglycosylation of decorin and nidogen-1. **A** and **B** show specific immunodetection of decorin (**A**) or nidogen-1 (**B**) after SDS-PAGE and Western Blotting on a nitrocellulose membrane. (**A**) SDS-PAGE was conducted with a NuPAGE®Novex® 4-12% Bis-Tris gel. The untreated decorin control (10 µg) is shown on lane 1. The decorin sample that was deglycosylated for 4 hours is shown on lane 2 and for 20 hours on lane 3. On each lane 10 µg of protein were loaded. The SeeBlue® Plus2 Pre-Stained protein standard was used for protein size estimation. (**B**) SDS-PAGE was conducted with a NuPAGE® Novex® 3-8% Tris-Acetate gel. The untreated nidogen-1 control (10 µg) is shown on lane 1. The nidogen-1 sample that was denatured for 4 hours is shown on lane 2 and for 20 hours on lane 3. On each lane 10 µg of protein were loaded. The HiMark Pre-stained protein standard was used for protein size estimation.

3.3.4 Confirmation of characteristic protein interactions

Identity confirmation and characterization of decorin and nidogen-1 on the protein level so far was conducted via ELISA, and specific antibody detection of decorin and nidogen-1 bands with characteristic sizes after Western Blotting. Also the glycosylation of the purified decorin and nidogen-1 could be shown via enzymatic deglycosylation. In a further step important protein interactions and therefore the activity of decorin and nidogen-1 was analyzed.

A characteristic protein interaction occurs between decorin and TGF-β1. Decorin binds and inhibits the pro-fibrotic factor TGF-β1, and therefore has an important anti-fibrotic effect. Nidogen-1 binds the laminin and collagen type IV networks in the basement membrane, crosslinks these networks and thereby stabilizes the basement membrane. These important protein-binding activities were tested via Co-IP of decorin and TGF-β1 as well as nidogen-1 and laminin 511. A schematic of the protein complex that forms in the event of a protein interaction is shown in **Figure 35**.

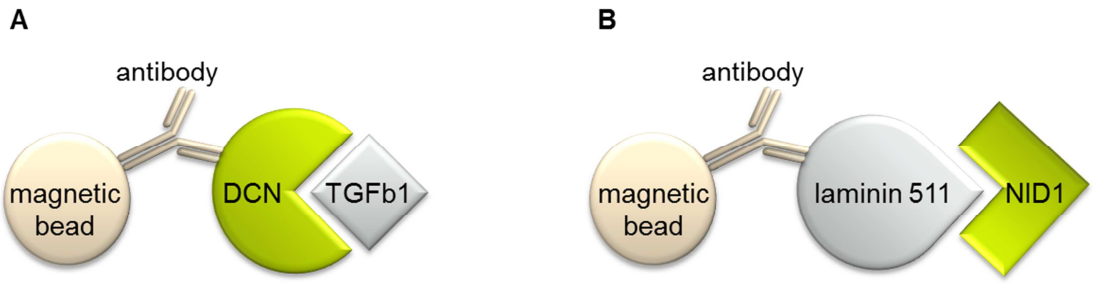

Figure 35: Schematics of Co-IPs for the protein interaction between decorin and TGF-β1 (**A**) and between nidogen-1 and laminin 511 (**B**).

Western blots of a representative Co-IP of decorin and TGF-β1 are shown in **Figure 36**. The Co-IP eluate contained decorin as well as TGF-β1 (**Fig. 36 A** and **B**, lanes 1). Decorin was present in the Co-IP eluate as it was bound to the magnetic bead via an antibody against decorin. TGF-β1 was present in the Co-IP eluate as it was bound to decorin. An unspecific binding of decorin or TGF-β1 to the magnetic beads can be excluded, as the unspecific binding control did not contain decorin or TGF-β1 (**Fig. 36 A** and **B**, lanes 2). Therefore the TGF-β1 binding activity and biofunctionality of the human decorin after recombinant production and chromatographic purification could be proven.

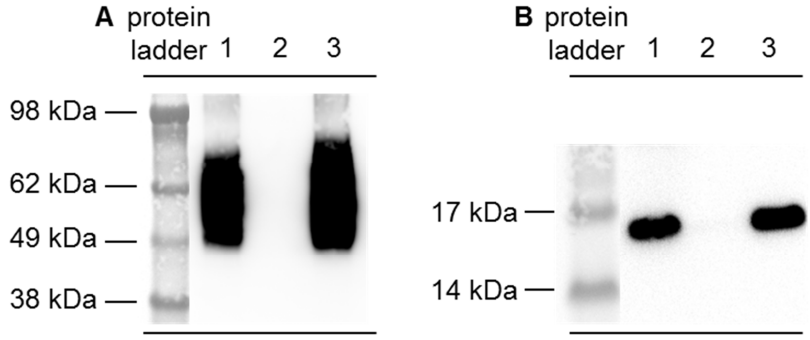

Figure 36: Specific immunodetection of human decorin (**A**) or TGF- β1 (**B**) after Co-IP, SDS-PAGE on a NuPAGE®Novex® 4-12% Bis-Tris gel and Western Blotting on a nitrocellulose membrane. Co-IP was conducted with purified decorin, TGF- β1 from human platelets, a primary antibody against human decorin and a suspension of protein A magnetic beads. The SeeBlue® Plus2 Pre-Stained protein standard was used for protein size estimation. **A**) The Co-IP eluate is shown on lane 1. An unspecific background control without the antibody against human decorin is shown on lane 2 and the positive control (250 ng decorin) on lane 3. **B**) The Co-IP eluate is shown on lane 1. An unspecific background control without the antibody against human decorin is shown on lane 2 and the positive control (100 ng TGF-β1) on lane 3.

Western blots of a representative Co-IP of nidogen-1 and laminin 511 are shown in **Figure 37**. The Co-IP eluate contained laminin 511 as well as nidogen-1 (**Fig. 37 A** and **B**, lanes 1). Laminin 511 was present in the Co-IP eluate as it was bound to the magnetic bead via an antibody against laminins. Nidogen-1 was present in the Co-IP eluate as it was bound to laminin 511. An unspecific binding of laminin 511 or nidogen-1 to the magnetic beads can be excluded, as the unspecific binding control does not contain laminin 511 or nidogen-1 (**Fig. 37 A** and **B**, lanes 2). Therefore the laminin-binding activity and biofunctionality of the human nidogen-1 after recombinant production and chromatographic purification could be proven.

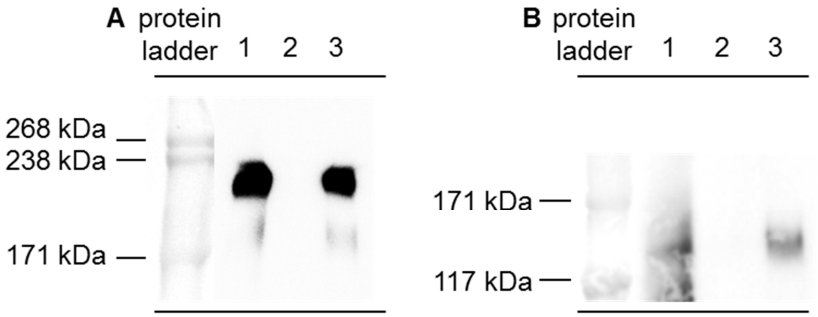

Figure 37: Specific immunodetection of human laminin 511 (**A**) or nidogen-1 (**B**) after Co-IP, SDS-PAGE on a NuPAGE® Novex® 3-8% Tris-Acetate gel and Western Blotting on a nitrocellulose membrane. Co-IP was conducted with laminin 511, purified nidogen-1, a primary antibody against laminins and a suspension of protein A magnetic beads. The HiMark™ Pre-Stained Protein Standard was used for protein size estimation. **A**) The Co-IP eluate is shown on lane 1. An unspecific background control without the antibody against laminins is shown on lane 2 and the positive control (100 ng laminin 511) on lane 3. **B**) The Co-IP eluate is shown on lane 1. An unspecific background control without the antibody against laminins is shown on lane 2 and the positive control (1 µg nidogen-1) on lane 3.

It has been described that biologically active decorin can reduce the TGF-β1-induced contraction of dermal equivalents [128]. Dermal equivalents composed of a collagen gel mixed with human fibroblasts isolated from a human skin biopsy contract due to transdifferentiation of fibroblasts to contracting myofibroblasts. TGF-β1 is one main inducer of transdifferentiation of fibroblasts to myofibroblasts. Dermal equivalents with fibroblasts from human skin were cultured initially for one day in DMEM (10% FBS) with 50 µg/ml or 150 µg/ml of the recombinant purified decorin, 5 ng/ml TGF-β1, 5 ng/ml TGF-β1 + 50 µg/ml decorin, 5 ng/ml TGF-β1 + 150 µg/ml decorin or as a control without any addition of decorin or TGF-β1 (**Fig. 38**). In the dermal equivalents, a significantly higher contraction was induced with the application of 5 ng/ml TGF-

β1, as identified by circumference reduction (56.72% ± 8.80% of original circumference) compared to the base level of contraction seen in the controls (69.65% ± 7.24%). This significant increase in dermal equivalent contraction was not observed when 50 µg/ml or 150 µg/ml decorin were utilized in addition to 5 ng/ml TGF-β1. A non-cellular collagen gel control was cultured as well and showed no signs of contraction after 16 days of culture.

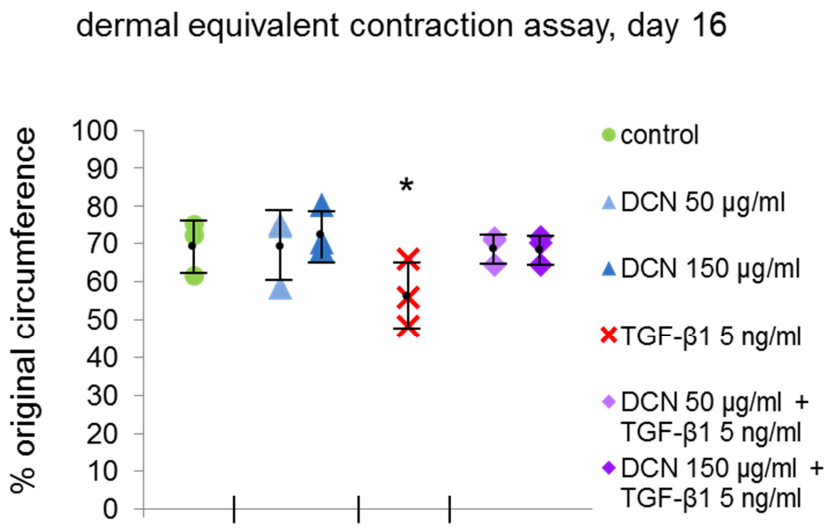

Figure 38: Dermal equivalent contraction assay. The percentage of original circumference of dermal equivalents composed of collagen gels with cells isolated from healthy human skin biopsies after 16 days of culture is shown. Circumference was measured from images using the ImageJ software on day 1 and day 16 of the dermal equivalent culture. Circumference values on day 16 were normalized to the circumference values on day 1 for each dermal equivalent. The experiment was conducted three times (n = 3). Results were assessed by one-way ANOVA using the Fisher LSD test with statistical significance at a p-value *p<0.05.

3.3.5 Effects of decorin and nidogen-1 on human immune reaction in vitro

Prior to in vivo experiments the influence of the recombinant human decorin and nidogen-1 on the human immune reaction was tested in vitro. In order to estimate eventual risks and to choose appropriate concentrations for decorin and nidogen-1 injections in in vivo experiments, potential endotoxin contaminations were tested and the influence of the proteins on human immune cells with and without co-stimulation with anti-CD3 were identified (Katrin Sudrow: “Einfluss der EZM-Komponenten Decorin und Nidogen-1 auf die humane Immunantwort in vitro”,

study project). To test whether the concentrated protein solutions contain endotoxins, a quantitative analysis of endotoxin content was conducted using the limulus amebocyte lysate (LAL) test [129, 130]. Also the proteins were tested in a cell assay, in which tumor necrosis factor alpha (TNF-α)-release of human peripheral blood mononuclear cells (PBMCs) is correlated with endotoxin content. The results of these analyses revealed a considerable endotoxin burden of the purified recombinant decorin sample, while the endotoxin content of the nidogen-1 sample was negligible. Proliferation of PBMCs (containing T- and B-cells) as previously described [53, 131] could not be induced with decorin and with the co-stimulus anti-CD3 50 µg/ml decorin even significantly reduced the induction of T- and B-cell proliferation, which means that decorin has an immunosuppressive effect in this concentration. Although no negative effects of decorin on immune cell proliferation and activation could be shown, in consideration of the results of the endotoxin tests, high concentrations of decorin should be avoided in in vivo applications. The immunosuppressive effect of decorin in the concentration 50 µg/ml supports its safe application and good tolerability in vivo.

In combination with the co-stimulus anti-CD3, nidogen-1 showed a tendency to induce immune cell proliferation with rising nidogen-1 concentrations as well as T-cell activation. Even without the co-stimulus, nidogen-1 could induce the proliferation of natural killer cells (nk cells). Therefore the influence of nidogen-1 on human immune cells leads to a similar conclusion as for decorin: for an application of nidogen-1 in vivo preferably a concentration of 50 µg/ml should be tested in order to prevent an adverse immune reaction.

3.4 In vitro and in vivo test of the cardio-inductive effect of decorin and nidogen-1

3.4.1 Test of cardio-inductive effect in vitro

The human proteins decorin and nidogen-1 were active after recombinant production and FPLC-controlled purification. They bound characteristic protein interaction partners as shown by Co-IPs. To test our hypothesis that decorin and nidogen-1 are potentially cardio-inductive proteins, we conducted in vitro differentiation experiments of hESC-derived EBs on different coatings (**Fig. 39**) (Anne Knopf: “Influence of human extracellular matrix proteins on cardiovascular differentiation of human embryonic stem cells and cardiac function post myocardial infarction in a small animal model”, master thesis). The same differentiation protocol was used as displayed in **Figure 6**. In this experiment on day 4 of the cardiovascular differentiation, the EBs were

seeded onto 6-wells coated with 0.1% gelatin + 50 µg/ml decorin, 0.1% gelatin + 50 µg/ml nidogen-1, 0.1% gelatin + 50 µg/ml decorin + 50 µg/ml nidogen-1 or as a control with 0.1% gelatin. On day 10 of cardiovascular differentiation, the cells of the whole well were collected and intracellular FACS analysis using an antibody against the cardiac marker protein cTnT was conducted. The percentage of cTnT-positive cells on day 10 of differentiation on the different coatings is shown in **Figure 39**.

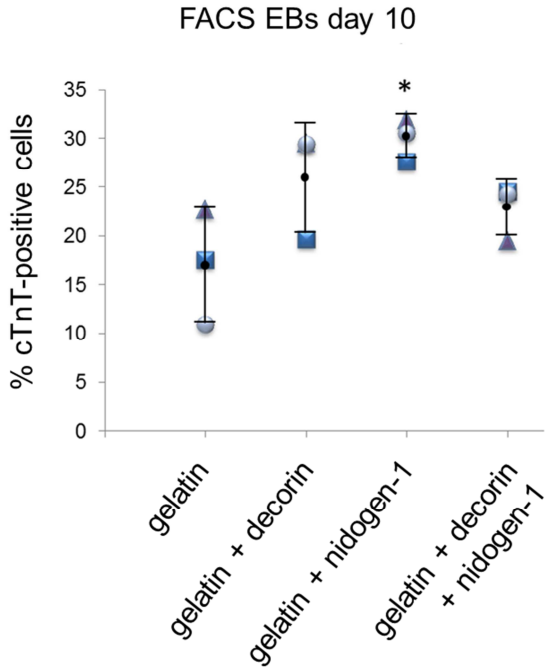

Figure 39: In vitro test of cardio-inductive effect of decorin and nidogen-1. Cardiovascular differentiation efficiency on different coatings (0.1% gelatin + 50 µg/ml decorin, 0.1% gelatin + 50 µg/ml nidogen-1, 0.1% gelatin + 50 µg/ml decorin + 50 µg/ml nidogen-1 or 0.1% gelatin as a control) was detected on day 10 of EB differentiation via intracellular FACS analysis. A primary antibody against the cardimyocyte marker cTnT was used. Cell analysis was conducted with the BD LSR II cell analyzer and cTnT-positive cells were detected with Alexa Fluor 488. The experiment was conducted three times (n = 3). Results were assessed by one-way ANOVA using the Tukey test with statistical significance at a p-value *p<0.05.

A significant increase (*p<0.05) of cTnT-positive cells was seen on the coating with 0.1% gelatin + 50 µg/ml nidogen-1 compared to the control coating with 0.1% gelatin. The mean percentage of cTnT-positive cells on the coating with 0.1% gelatin + 50 µg/ml nidogen-1 was 30.1%. The cardiovascular differentiation of hESC-derived EBs on this coating with nidogen-1 was

considerably increased compared to the 17.1% of mean cTnT-positive cells on the control coating. This result demonstrated that nidogen-1 has a cardio-inductive effect that increases the differentiation efficiency of hESCs to cardiomyocytes. In the three conducted tests the mean percentage of cTnT-positive cells on the coatings with 0.1% gelatin + 50 µg/ml decorin or 0.1% gelatin + 50 µg/ml decorin + 50 µg/ml nidogen-1 were also increased when compared to the mean percentage of cTnT-positive cells on the control coating. But due to high biological variability this was not considered a significant difference.

3.4.2 In vivo mouse MI/R and ECM injection

The cardio-inductive nidogen-1 was used alone or in combination with the TGF-β1-inhibiting anti-fibrotic decorin to test our hypothesis that these two human ECM proteins can support the regeneration of the heart after a MI (Anne Knopf: “Influence of human extracellular matrix proteins on cardiovascular differentiation of human embryonic stem cells and cardiac function post myocardial infarction in a small animal model”, master thesis). MI/R experiments were conducted with eight-week old female C57BL/6J mice (strain DLAMb6). The left coronary artery of the mice was ligated and after 45 min reperfusion was allowed. Subsequently the mice received injections in the MI border zone. Five mice in each of the two treatment groups received injections with HyStem® Hydrogel + PBS + 50 µg/ml decorin + 50 µg/ml nidogen-1 or HyStem® Hydrogel + PBS + 50 µg/ml nidogen-1 while the five mice in the control group were injected with HyStem® Hydrogel + PBS without the ECM proteins. Conscious echocardiography was conducted on the mice prior to the MI/R experiment to evaluate a baseline of the ejection fraction (EF) percentage and on three different time points after the MI/R (**Fig. 40**). The EF is an important characteristic for the performance of the heart. Baseline EF had mean values of 84.9% ± 4.7% and 85.7% ± 8.6% for the mice in the nidogen-1 treatment group and the decorin + nidogen-1 treatment group and a comparably high mean value of 89.5% ± 3.1% for the mice in the control group. One mouse in the nidogen-1 treatment group died of arrhythmia directly after surgery and conscious echocardiography of 2 out of the 5 mice in the control group revealed that the MI/R experiment did not cause a robust infarction due to incomplete ischemia. Therefore these mice were excluded. For the remaining mice conscious echocardiography 2 days post MI showed the high initial impact of the MI in a drop of the EF from the value in the baseline measurement to only 42.4% ± 0.8% in the nidogen-1 treatment group, 45.5% ± 2.3% in the decorin + nidogen-1 treatment group and 46.4% ± 2.9, in the control group. These EF values 2 days post MI do not show significant differences between the three groups. Echocardiography at

the time point 2 weeks post MI showed no significant change in the nidogen-1 treatment group (43.7% ± 0.6% EF) or the decorin + nidogen-1 treatment group (43.3% ± 5.6% EF) compared to 2 days post MI. Two weeks post MI a significant decrease to 28.9% ± 5.1% EF in the control group in comparison to the time point 2 days post MI (46.4 % ± 2.9 % EF) could be seen. The mice in the nidogen-1 and decorin + nidogen-1 treatment groups had a significantly higher EF 2 weeks post MI than the mice in the control group. At this time point the mean difference to the control group was 14.8% EF for the nidogen-1 treatment group and 14.4% EF for the decorin + nidogen-1 treatment group. Four weeks post MI echocardiography revealed that the EF of the mice in the nidogen-1 treatment group was significantly higher than the EF of the mice in the control group. At this time point the mean difference between the nidogen-1 treatment group and the control group was 14.5% EF and therefore almost as high as the difference between these two groups at the time point 2 weeks post MI. Four weeks post MI no significant decrease in the EF can be seen in the nidogen-1 treatment group (44.6% ± 1.6% EF) or the decorin + nidogen-1 treatment group (38.6% ± 5.3% EF) compared to the echocardiography results of the same groups 2 days post MI. Again echocardiography revealed a significant decrease to 30.2% ± 4.3% EF in the control group in comparison to the time point 2 days post MI (46.4% ± 2.9% EF).
While the echocardiography of the control group 2 weeks and 4 weeks post MI revealed significantly decreased EF compared to the time point 2 days post MI, this is not the case for the decorin + nidogen-1 treatment group and the nidogen-1 treatment group. The mean EF values of the nidogen-1 treatment group even show a slight but continuous increase from 42.4% ± 0.8% EF in the echocardiography 2 days post MI to 43.7% ± 0.6% EF 2 weeks post MI and 44.6% ± 1.6% EF 4 weeks post MI. This is not considered a significant increase by One Way ANOVA using the Fisher LSD or Tukey test with statistical significance at a p-value *$p<0.05$ when all the groups are analyzed. But if only the development of the EF of the nidogen-1 treatment group is analyzed over time, both tests consider the increase in the EF of the time point 4 weeks post MI compared to 2 days post MI significant.

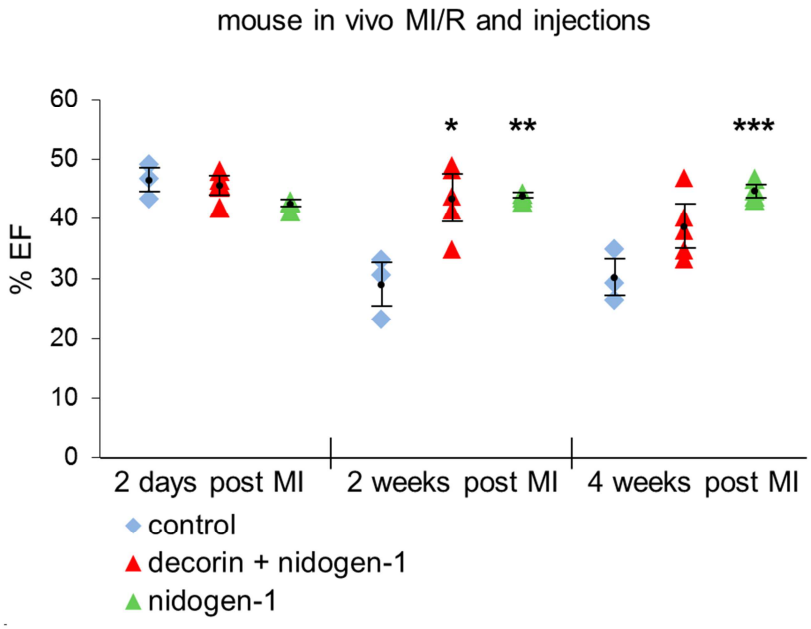

Figure 40: Echocardiography analysis of the EF after in vivo intra-cardiac injections of decorin and nidogen-1 in a mouse MI/R model. In an established model of eight week old, female C57BL/6J mice for myocardial infarction at the UCLA the animals' hearts were exposed and the left coronary artery was occluded for 45 minutes. Subsequently reperfusion was allowed and the animals received injections of HyStem® Hydrogel + PBS + 50 µg/ml decorin + 50 µg/ml nidogen-1 or HyStem® Hydrogel + PBS + 50 µg/ml nidogen-1 in the MI border zone. In the control group the animals were injected with HyStem® Hydrogel + PBS. For each mouse the 50 µl total injection volume was divided into 10 µl injections at 5 sites in the LV myocardial infarction border zone. The MI/R procedure as well as intra-cardiac injections were conducted on 15 mice (five per group). Conscious echocardiography was conducted on three different time points to analyze the EF two days as well as two weeks and four weeks after the MI/R and myocardial injection procedure. Results were assessed by one-way ANOVA using the Fisher LSD test with statistical significance at a p-value $p<0.05$ (* = decorin + nidogen-1 versus 2 week control; ** = nidogen-1 versus 2 week control; *** = nidogen-1 versus 4 week control).

3.4.3 Histological H&E and Russel-Movat Pentachrome staining and immunofluorescence staining of mouse hearts

Histological staining (H&E and Russel-Movat Pentachrome) as well as immunofluorescence staining of the cardiomyocyte marker protein cTnT was performed on comparable sections of mouse hearts 4 weeks after MI/R and injections of 50 µg/ml nidogen-1 or control injections in the

peri-infarct zone (**Fig. 41**). Qualitative differences due to nidogen-1 or control injections can be seen in all of the conducted staining methods. In the H&E staining, the infarct zone is identified by a high density of cell nuclei and a lighter red tissue staining compared to the surrounding cardiac muscle. This infarct zone appears smaller in the mouse hearts that received nidogen-1 injections (**Fig. 41 D, E, F**) compared to the control injections (**Fig. 41 A, B, C**). Russel-Movat Pentachrome staining was conducted to visualize the impact of the infarct and the subsequent injections with nidogen-1 or control injections on the ECM of the cardiac tissue. This staining clearly distinguishes between the ECM-rich infarct zone (blue-green and yellow colors) and the surrounding tissue with intact cardiac muscle (red). The blue-green colors in the Russel-Movat Pentachrome staining indicate proteoglycans, while yellow indicates collagen-rich ECM deposition in the infarct zone. The Russel-Movat Pentachrome staining supports the result of the H&E staining and identifies a lower degree of pathological remodeling in the hearts that received nidogen-1 injections (**Fig. 41 J, K, L**) compared to the control hearts (**Fig. 41 G, H, I**). Collagen deposition in the nidogen-1-treated hearts appears more evenly distributed, whereas spatial accumulation of collagen deposits can be found in the control hearts. The IF staining of the cardiomyocyte marker protein cTnT (in red), shows a clear distinction of the infarct zone and the non-infarcted surrounding cardiac tissue with cTnT-positive cardiomyocytes. In accordance with the results of the H&E and Russel-Movat Pentachrome staining, the qualitative analysis of the cTnT IF staining identifies a smaller area that lacks the functional contractile cardiomyocytes in the nidogen-1-treated mouse hearts (**Fig. 41 P, Q, R**) compared to the control treatment (**Fig. 41 M, N, O**). Therefore, qualitative analysis of these histological staining methods revealed that the nidogen-1 treatment enabled a better preservation of the cardiac morphology compared to the control hearts. Furthermore, the extent of pathological remodeling is lower in the hearts that received nidogen-1 injections compared to the control injections.

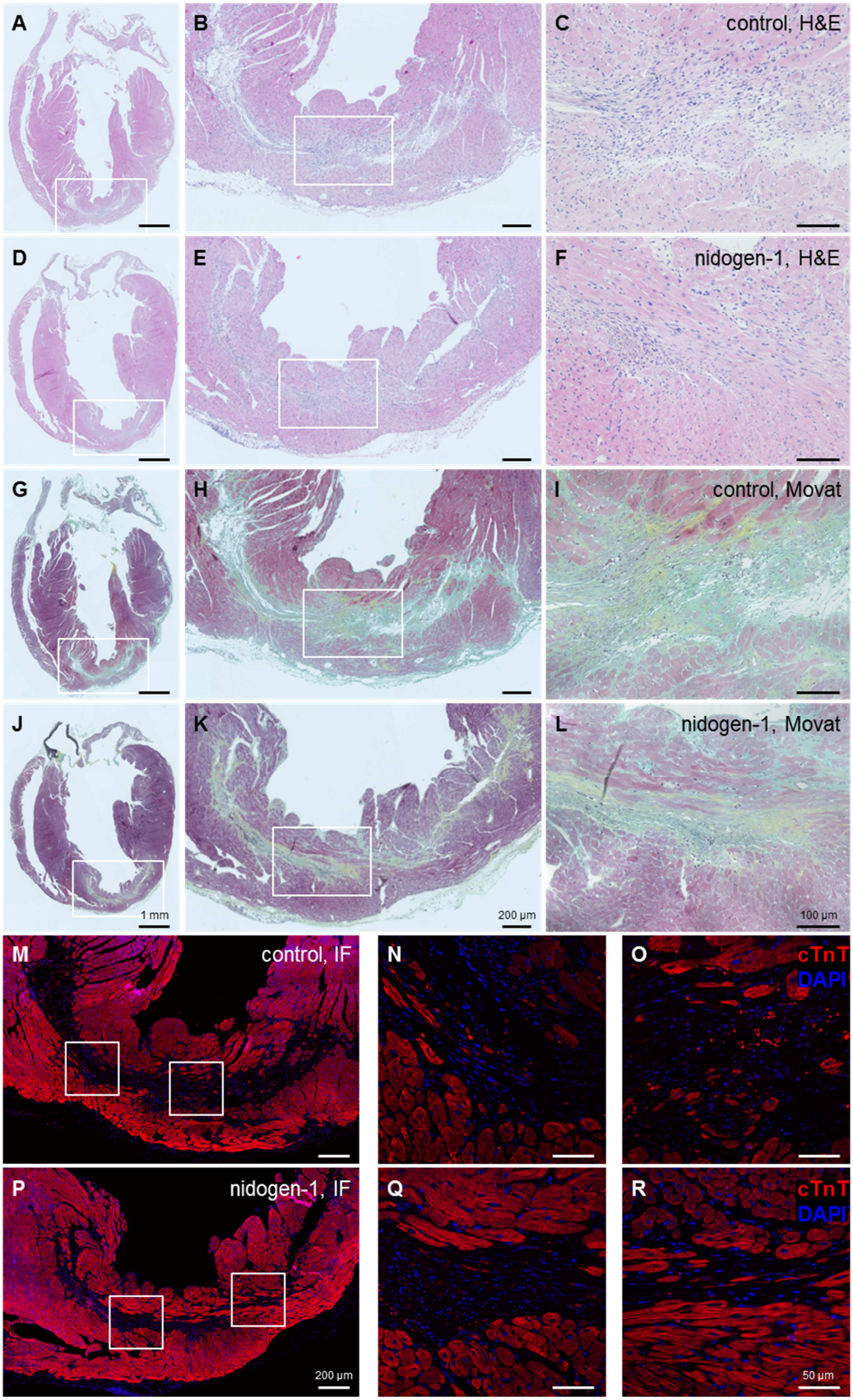
A
B
C
control, H&E
D
E
F
nidogen-1, H&E
G
H
I
control, Movat
J
K
L
nidogen-1, Movat
1 mm
200 µm
100 µm
M
control, IF
N
O
cTnT
DAPI
P
nidogen-1, IF
Q
R
cTnT
DAPI
200 µm
50 µm

Figure 41: Bright field images (H&E staining and Russel-Movat Pentachrome staining) and IF images of paraffin-embedded tissue sections of mouse hearts that received nidogen-1 injections or control injections after MI/R. White rectangles indicate the section that is shown in more detail in the image to the right. **A**, **B**, **C**) H&E staining of a mouse heart that received control injections. **D**, **E**, **F**) H&E staining of a mouse heart that received nidogen-1 injections. **G**, **H**, **I**) Russel-Movat Pentachrome staining of a mouse heart that received control injections. **J**, **K**, **L**) Russel-Movat Pentachrome staining of a mouse heart that received nidogen-1 injections. **M**, **N**, **O**) Immunofluorescence staining of cTnT (in red) and cell nuclei (DAPI, in blue) of a mouse heart that received control injections. **P**, **Q**, **R**) Immunofluorescence staining of cTnT (in red) and cell nuclei (DAPI, in blue) of a mouse heart that received nidogen-1 injections.

4 Discussion

With significant advances in the field of cardiology and cardiac surgery, increasing numbers of patients survive MI. Unfortunately, due to the impact of this cardiac event that can cause the loss of cardiomyocytes in the range of one billion [132], and the very limited regenerative capacity of the myocardium, the heart's contractile force and the patient's quality of life are drastically and permanently impaired. In contrast to appropriate functional tissue repair, MI remodeling creates a dense collagenous scar which leads to continuing pathological remodeling and promotes the further development of heart failure. The five-year survival rate for heart failure patients of 50% [133], which explains the urgent need for new therapies that prevent pathological remodeling and restore heart function in order to avert the development of heart failure. Several experimental approaches have been developed that aim to replenish the number of cardiomyocytes in the diseased heart. Cell therapies focused on the transplantation of exogenous cells from varying sources, especially skeletal muscle-derived cells [34, 35, 134-136], bone marrow mesenchymal stem cells [37, 137], and cardiac progenitor cells (CPCs) [138-141]. While a therapeutic effect due to true regeneration of cardiomyocytes in these studies is questionable and controversially discussed, substantial evidence indicates that transplantation of these and various other cell types (including cardiomyocytes [142-144], smooth muscle cells [145], fibroblasts [146], endothelial progenitors [147], hematopoietic stem cells [148] and embryonic stem cells [149] can provide functional improvement of the infarcted heart to a certain extent. This effect is probably due to mechanisms distinct from true regeneration [132], including the modulation of the infarct tissue's passive mechanical properties due to cell transplantation [136] or paracrine effects from the transplanted cells [147].

To increase the restricted therapeutic effectiveness of cell-based therapies to date, scientists are aiming for true regeneration of functional cardiomyocytes. Approaches have been investigated that have the potential to support cell therapies to overcome some of their main hurdles: inefficient cell delivery as well as low retention, survival, engraftment and differentiation of transplanted cells in the hostile and pathologically remodeled microenvironment of the heart post MI [47-49]. Scientists attempted to accomplish this by utilizing biomaterials (biologically derived, synthetic or hybrid materials) for example in tissue-engineered epicardial patches or in in situ-gelling injectable hydrogels. While epicardial patches have the disadvantage of requiring thoracotomy for patch placement, injectable biomaterials can potentially be used in minimally invasive procedures as delivery vehicle for cells or therapeutic agents like growth factors [150-153] and could be shown to improve the retention and viability of transplanted cells [151]. A

variety of biomaterials were tested for MI treatment in vivo with or without additional cells including fibrin [154-158], alginate [159-163], Matrigel [164, 165], and several decellularized tissue preparations including myocardium [55, 166-170]. These experiments provided evidence that the injection of biomaterials alone could improve functional parameters of the heart. The use of natural ECM preparations for MI treatment is intriguing, since it would provide a complex microenvironment, rich in biological signals that have the potential to support cell delivery, adhesion, survival and directed differentiation. However, the source materials and decellularization method as well as further preparation processes are considerable limitations that question the reproducibility, safety and effectiveness of these products for clinical applications. Matrigel, derived from the murine Engelbreth-Holm-Swarm (EHS) sarcoma, and other decellularized xenogeneic tissue preparations can cause immunological rejection. For any clinical application, product standardization is critical, but due to the natural tissue sources and discrepancies in the decellularization process, the composition of these decellularized ECM preparations vary from lot to lot and therefore are unlikely to have reproducible defined effects. Biologically important proteoglycans (such as decorin) or glycoproteins (such as nidogen-1) are lost in the detergent-based decellularization process [171, 172]. Also, in order to generate an injectable product, the matrix proteins are lyophilized and partially digested with pepsin [55, 169], further compromising the biological activity of the injectable product. Therefore the aim of this study was to identify the key cardio-inductive ECM proteins at the onset of human cardiogenesis utilizing EBs, generated from hESCs. Recombinant production and purification of cardio-inductive human ECM proteins in their biologically active state and their combination with a bio-inert hyaluronan-based HyStem® Hydrogel allows the generation of a defined, biologically active human ECM product for MI treatment, omitting decellularization-related limitations.

4.1 Cardiovascular differentiation

Based on a combination of two cardiovascular differentiation protocols [67, 69], important further modifications were made for the efficient directed cardiovascular differentiation of whole EBs (**Fig. 6**). These modifications, amongst others, include the EB generation with the spin EB method, the use of the basal media mTeSR1 and a defined high number of hESC cells for EB generation. Utilization of the spin EB method as well as improved health of the EBs due to the mTeSR1 media supported the formation of EBs with uniform size, round shape and smooth surface, which indicate good cell aggregation and survival. Experience in hESC culture techniques, the right timing and delicate handling of sensitive hESCs are not only a prerequisite

for hESC health and pluripotency maintainance, they are also essential to achieve highly efficient cardiovascular differentiation. Furthermore, we found a high impact of the initial method of EB generation and EB handling on the EB health and differentiation efficiency. The uniformity of the spin EBs benefited a regulated differentiation of hESCs. H9 EBs generated in this modified protocol did not disintegrate on the following days of floating EB differentiation and could attach to a 0.1% gelatin-coated 6-well plate on day 4 of differentiation.

The attachment of whole EBs on day 4 of differentiation was the most important modification to the differentiation protocols described by Yang et al. and Willems et al. Without EB attachment the same differentiation protocol only generated very low beating efficiencies below 10% compared to the reproducible efficient generation of spontaneously beating EBs (85% ± 17.6%), with the EB attachment. The drastic increase in cardiovascular differentiation efficiency upon EB attachment could be due to the changed mechanical properties of the EB's microenvironment. When EBs attach to a coated surface they can exert forces on this surface, in contrast to a suspension culture of floating EBs that are only in contact with the media. This difference in the mechanical properties of their microenvironment can be perceived by the EBs and it might influence their differentiation fate. With advances in molecular biology and the elucidation of signaling pathways in the cell, for many years scientists concentrated on these biological and chemical cues to explain tissue and organ genesis. Just recently interdisciplinary approaches started to focus on the interplay between physicality and developmental control and found fundamental links between mechanical forces, molecular biochemistry and gene expression [173]. The importance of the mechanical properties of a cell's or tissue's microenvironment has been recognized by many scientists especially in the field of tissue engineering [174-178]. As a result elaborate systems have been developed to culture cells and tissues in an environment with defined mechanical properties of surface rigidity, stretch and strain. In this case the attachment of whole EBs on gelatin-coated 6-well plates potentially provided the right environment that exerted a positive influence on the cell's cardiovascular fate decision.

Another explanation for increased cardiovascular differentiation efficiency of attached EBs could be found in the cells that outgrew the EBs and spreaded on the culture plate. These cells did not start beating and intracellular FACS analysis of sarcomeric myosin using the MF20 antibody confirmed that the cardiovascular differentiation of these cells was much lower (6.5% ± 2.3% MF20-positive cells) than of the cells from beating attached EBs (49.4% ± 11.4% MF20-positive cells) (**Fig. 7**). Importantly, a changed protein expression profile of the outgrown cells compared to the beating EB cells also could be detected in the qPCR analysis of ECM proteins. The outgrown cells showed a significantly higher expression of nidogen-1, laminins and fibronectin.

Therefore the outgrown 2D cell layer secreted an own ECM that was different from the ECM of the beating EBs. The EBs and their outgrown cell layer represent a simple form of tissue organization that can also be found at the onset of organogenesis. Benefits of comparably simple organization forms are used for pluripotency maintenance of ESC colonies on an ECM secreting supporting MEF feeder layer [58, 62, 66]. According to the same principle, the ECM as well as soluble factors secreted by the outgrow cell layer could influence EB cell fate decision and support cardiovascular differentiation.

The EBs were attached to the gelatin-coated culture plate on day 4 of differentiation and therefore at a time point when the cells were already committed to the mesoderm lineage. Only three days after EB attachment, on day 7 of differentiation, the EBs started beating. Therefore the modified differentiation protocol supported rapid induction of cardiovascular differentiation. After only 10 days of cardiovascular differentiation in the modified protocol, a high percentage of spontaneously beating EBs could be obtained (85% ± 17.6%, n = 7). Also a reproducibly high percentage of MF20-positive cells within these beating EBs (49.4% ± 11.4% MF20-positive cells) (**Fig. 7**) and their significantly increased expression of the cardiac transcription factor Tbx5 and the cardiomyocyte markers cTnT and MYH6 (**Fig. 8**) confirmed the high efficiency of the modified differentiation protocol.

The beating EBs represent an early stage in human fetal cardiovascular differentiation with unorganized myosin filaments and only occasional cardiomyocyte striation (**Fig. 9**). During fetal development the ECM microenvironment as well as soluble factors drive cardiovascular differentiation and define the high regenerative potential after wounding. Therefore, to identify the potentially cardio-inductive key ECM proteins, the ECM expression of beating EBs during cardiovascular differentiation was analyzed. To what extent the ECM deposition in EBs during in vitro cardiovascular differentiation resembles the same process during human fetal development is unclear. Divergences between the natural developmental process and the model have to be expected, considering the differences in complexity, regulation and microenvironment. While this is true for most biological models, they still serve a very important purpose providing a simplified version of the original process in a well-controlled reproducible manner. Even if deviations of the hESC-derived differentiation model to the natural developmental process cannot be excluded, these do not prevent cardiovascular differentiation as the model successfully and reproducibly generates cardiomyocytes. It is doubtful that the ECM deposition during cardiovascular differentiation does not support and reflect this efficient in vitro differentiation process. Therefore increased gene expression of ECM proteins during cardiovascular differentiation can indicate

cardio-inductive key ECM proteins. Monitoring of cardiac-specific ECM by qPCR on day 0, day 4 and day 10 of the modified differentiation protocol allowed the identification of a significantly increased expression pattern of decorin and nidogen-1 during the differentiation of pluripotent stem cells towards the cardiovascular lineage (**Fig. 10 A, B**). Additionally at the protein level, semi-quantitative analysis of IF images of beating EBs at day 10 of differentiation revealed a significantly higher amount of decorin and nidogen-1 compared to fibronectin, periostin, laminins, collagen type IV and collagen type I (**Fig. 12**).

Both on the gene expression level as well as on the protein level the results suggest an important role of the non-fibrillar ECM proteins decorin and nidogen-1 in early cardiac development. Further background information on the functions of decorin and nidogen-1 and their role during normal human development of organs and tissues support the hypothesis that these ECM proteins might have a positive effect on the regeneration potential post MI. In the healthy myocardium, the small leucine-rich proteoglycan (SLRP) decorin and the glycoprotein nidogen-1 contribute to the complex ECM of the interstitial space [5]. It has been reported that these two proteins also have an impact on human embryonic stem cell development and assembly [61, 179]. Their importance for regenerative medicine is just starting to be explored [53, 180, 181].

4.2 Decorin

The SLRP decorin (also PG40) consists of a 40 kDa core protein with approximately twelve leucine-rich repeats (LRRs) and either one single covalently linked chondroitin sulfate or dermatan sulfate GAG side chain [182, 183]. It could be previously shown that decorin plays an important role in ECM assembly [184, 185] as well as tissue development and remodeling [186-188]. The highly negatively charged GAG chains have a central function in maintaining the structural integrity and viscosity of the ECM [189, 190]. Decorin has been shown to mainly impact neural development [191], bone formation [192], functioning eye tissue (sclera) [193] as well as lung development [194]. It is a ubiquitous proteoglycan within the ECM of connective tissues and the major sulfated product of fibroblasts.

What makes decorin an ideal tool for an approach to reduce adverse remodeling post MI is that it directly interacts with two central players in adverse cardiac remodeling. Decorin inhibits the pro-fibrotic growth factor TGF-β1 [195, 196] and it binds collagen type I. Unbound as well as

collagen-bound decorin is a natural inhibitor of TGF-β1 bioactivity. The interaction between decorin and TGF-β1 predominantly occurs through the core protein of decorin [197, 198]. Furthermore, decorin is a negative modulator of TGF-β1 synthesis [199, 200]. Due to the important role of TGF-β1 for the transdifferentiation of cells to myofibroblasts post MI and increased TGF-β1 production in the pathophysiology of fibrosis, TGF-β1 inhibition has an anti-fibrotic effect [201]. Various models of pathological processes connected to scarring including pulmonary fibrosis [202], liver cirrhosis [203], fibrotic bladder [204] and hypertrophic scarring [205] proved that the expression and synthesis of decorin as well as another member of the SLRP family, biglycan, are pathologically altered. Biglycan is up-regulated, while decorin is down-regulated. Border at al. reported 1992 that the administration of decorin in an *in vivo* experimental glomerulonephritis rat model antagonizes TGF-β1-associated production of ECM and prevents scarring [195]. They also suggested decorin for the treatment of other conditions associated with TGF-β1 overproduction. One of these is the development of post-injury blindness due to corneal scarring or haze. Here, comparable to post MI remodeling, TGF-β1 plays an adverse role by facilitating the stepwise transdifferentiation of corneal keratinocytes and fibroblasts to myofibroblasts that show an increased expression of α-smooth muscle actin and deposition of disorganized ECM proteins [13, 206-210]. When disarranged collagen fibrils in the cornea accumulate, it is no longer transparent but hazy. Interestingly this condition also can be caused by a mutation in the decorin gene, as the defective protein cannot ensure the formation of uniformly sized and regularly spaced collagen fibrils, which is essential for corneal transparency. Mohan et al. [211] showed that decorin gene transfer can be used against TGF-β1-induced formation of myofibroblasts and fibrosis in the cornea and accordingly it could be shown to prevent fibrosis in other tissues, including the myocardium [199, 212-214].
The collagen-binding and organizing activity of decorin is another reason why this proteoglycan is especially attractive for an application post MI. Decorin binds to fibrils of collagen type I, II and IV in vivo in a characteristic “decorative” manner, leading to its naming. Decorin binding to type I collagen near their cell-binding site, inhibits the cell attachment-promoting activity of collagen and affects fibril formation. It promotes the formation of fibers that have a higher stability and it changes their solubility [215, 216]. The important role of decorin in promoting tensile strength by regulating the orderly assembly and uniform diameter of collagen fibrils became apparent in the abnormal fusion of collagen bundles and increased skin fragility in decorin-deficient mice [217].

The role of decorin in collagen fibrillogenesis, myofibroblast inhibition and reduction of myofibroblast-mediated unorganized fibrosis and scarring, could make it an ideal tool to prevent

cardiac stiffness, while supporting the heart's architectural integrity and the formation of stabile collagen fibers to prevent LV dilatation or rapture post MI. Therefore decorin occupies a unique position with a high potential for anti-remodeling strategies as well as for an increased ECM order and stability in the injured heart. It is of particular interest that decorin has the ability to act as immune-inert or even immune-suppressive protein, as shown by Hinderer et al. for bovine decorin [53] and confirmed for low doses of the recombinant human decorin used in this work (Katrin Sudrow: "Einfluss der EZM-Komponenten Decorin und Nidogen-1 auf die humane Immunantwort in vitro", study project).

4.3 Nidogen-1

The glycoprotein nidogen-1 (also entactin) is a 150 kDA secreted sulfated and glycosylated monomeric protein that consists of three globular domains (G1 - G3) linked by a link region between G1 and G2 and a longer rod-like region between G2 and G3. It is one of the ubiquitous proteins in basement membranes and has been reported to play an important role for cell adhesion, as it establishes contacts with various cellular integrins via its several L-arginine – glycine – L-aspartic acid (RGD) tripeptide sequences. Furthermore, it has a wide range of ECM binding partners as it is known to bind perlecan, collagen I and IV, fibulin-1 and -2 and to form stable complexes with laminins. Nidogen-1 serves as a major linking and stabilizing component of basement membranes which are extracellular matrices in close molecular and functional contact to a large variety of cells. These sheet-like supramolecular assemblies that are produced by epithelial cells, endothelial cells and many mesenchymal cells, appear early in development and surround cardiomyocytes. Basement membranes don't only serve as support for cells and cell layers, they also have important regulatory functions as they regulate cell attachment, growth and differentiation [218]. Nidogen-1 is widely expressed in basement membranes during human organogenesis [219]. As it binds laminins with its G2 domain and collagen type IV with its G3 domain [220], it connects these two networks, which are the most abundant components of basement membranes, forming a scaffold that plays a role in the control of migration, differentiation and proliferation of cardiac cells [221].

The transcription of nidogen-1 and its isomer nidogen-2 in various adult human tissues revealed similar patterns in most tissues. But there are striking differences for the two isoforms in heart and skeletal muscle tissue sections, with considerably stronger nidogen-1 staining in BMs surrounding cardiomyocytes and myotubes [222], which might indicate a unique function of nidogen-1 in heart and muscle.

Due to their similarities, scientists used extracts from the murine EHS sarcoma that has a unique architechture [223] in order to study the interactions within basement membranes. Commonly, Matrigel was utilized, a gelatinous ECM preparation containing nidogen-1, which is secreted by the murine EHS sarcoma cells. Matrigel is commercially available from BD Biosciences and has several interesting properties. When it is added to a single-cell suspension of MEF-free hESCs, it induces robust cell aggregation with complete EB formation after 24 hours in culture. Furthermore, in a recent publication, Matrigel was used to instruct human pluripotent stem cells to undergo epithelial-to-mesenchymal transition (EMT) [78]. This is an important event in early cardiac development, and in combination with known growth factors robust cardiac differentiation was achieved. Further experiments with Matrigel demonstrate that this complex ECM mixture supports EB formation as well as differentiation to cardiomyocytes [224, 225]. While these functions are of particular interest for the cardiovascular field, they could not be assigned to one or several effective components of Matrigel yet. Matrigel contains laminins, collagen type IV, heparan sulfate proteoglycans, and nidogen-1 [226], as well as small amounts of other proteins and a variety of growth factors, but its exact composition can vary from lot to lot.

While Matrigel is an interesting tool in a laboratory setting, its derivation from the murine EHS sarcoma and undefined exact composition represent a risk for any clinical application. In order to use an interesting biological function of a complex ECM mixture like Matrigel that is limited for a direct use in clinical applications, it is necessary to identify the key proteins that exert this function. Accordingly, Funanage et al. assigned a role in myogenesis to nidogen-1 due to its adhesion-promoting function as well as long-term maintenance and maturation of contractile skeletal myotubes on a diluted Matrigel substrate [227]. The same restriction is true for the complex ECM that is deposited during cardiovascular differentiation of hESCs. Therefore we identified decorin and nidogen-1 in EB differentiation experiments as potentially cardio-inductive ECM proteins.

4.4 Strategies for high-quality and high-yield recombinant protein production

To prove our hypothesis, the cardio-inductive effect and the influence on cardiac regeneration post MI of pure human decorin and nidogen-1 products needed to be tested in vitro and in vivo. However, most of the currently for research and development available proteins have either non-human identity or they are manufactured under non-GMP translatable conditions. Common

examples are commercially available protein extracts from animal tissues or cell cultures. As already described, these production methods are associated with serious risks and limitations for a potential application in clinic, which requires the compliance with GMP standards. Due to harsh extraction and purification methods [97] commercially available protein products can have impaired biological activities. The same is true for some commercially available recombinantly produced proteins. Also when recombinant proteins with human identity are produced in cell lines that cannot support proper folding and complicated post translational modification forms like glycosylation [102, 103], they cannot ensure biological functionality of the human proteins. This must be particularly considered, as both decorin and nidogen-1 carry complex glycosylation. Experimental tests with partially inactive decorin and nidogen-1 due to incomplete folding or post translational modification could lead to false-negative results.

To meet the demands of high quality human protein production we chose to produce decorin and nidogen-1 recombinantly under GMP-translatable conditions in order to retain the possibility of a future GMP compliant production and utilization of the GMP-grade proteins in clinical applications. The careful selection of the host cell line [101, 106], transfection and selection method is based on the requirements for recombinant human glycosylated protein production under GMP translatable conditions. The chromatographic purification procedure is not detergent-based and does not include harsh high salt-containing buffers and therefore prevents irreversible protein denaturation. Choosing a mutant CHO DHFR-negative host cell line that can enable proper protein folding and synthesis of the complicated human protein glycoforms, additionally a potent selection and gene-amplification method to increase protein production was provided [101, 107-109]. Mammalian host cells possess the enzyme machinery required for appropriate post-translational modification and therefore are favorable for the recombinant production of human proteins, as described above. Unfortunately recombinant protein yields of mammalian cell lines including CHO cells are clearly inferior to bacterial cultures like E. coli [228]. In order to reduce this disadvantage, several strategies to increase mammalian recombinant protein yields have been successfully applied in this work. Many of these strategies already need to be considered in the production plasmid design, such as the utilization of strong promoters and secretion peptides in the decorin or nidogen-1 transcription cassette, codon adaptation of the genomic decorin and nidogen-1 sequence to avoid predictable bottlenecks in t-RNA availability or the installation of an additional inducible production system. The strategy with the biggest impact on recombinant protein yield was the utilization of a DHFR-negative mutant CHO cell line for genomic co-amplification of the human decorin and nidogen-1 gene with the wt DHFR gene

that was provided on the production plasmid. In this work, genomic co-amplification was achieved via several MTX selection rounds and resulted in highly increased transcription of the decorin and nidogen-1 gene to mRNA, as identified by qPCR analyses of the genomic DNA level and mRNA level of decorin and nidogen-1 as well as DHFR in samples of CHO clones in the course of MTX selection (**Fig. 22**). This proved that the production plasmids designed and constructed for CHO transfection contained the necessary elements in correct orientation and in appropriate proximity on the plasmid to enable the process of co-amplification. As expected [229], genomic co-amplification and increased transcription of the decorin and nidogen-1 genes resulted in a highly increased decorin and nidogen-1 protein yield, as indicated in **Figure 24**. With protein concentrations of up to 42.8 µg/ml decorin and 4.2 µg/ml nidogen-1 in the production media (**Fig. 29**), protein yields are appropriate for elevated mammalian recombinant protein production and sufficient for future applications. The approximately 10-fold lower nidogen-1 production despite the use of the same host cell line and the same amount of MTX selection rounds for genomic co-amplification might be due to several reasons. A possible explanation is provided by the inducible production system of the nidogen-1-producing H1 clone. In contrast to the permanent production system of the decorin-producing B4 clone, the inducible nidogen-1 production system might have reached a limit in the amount of permanently produced activator protein available for the activation of the inducible TRE-promoter, which is responsible for induction of nidogen-1 transcription. While the amount of the nidogen-1 gene and its inducible promoter was highly increased due to genomic co-amplification in MTX selection rounds, this was not the case for the activator protein cassette. The host cells were transfected with the activator protein cassette on a separate plasmid prior to production plasmid transfection and therefore it is likely that these two plasmids integrated in two distant regions of the host genome, which excludes co-amplification of the activator gene with the DHFR gene. If this is the reason why inducible nidogen-1 production could not reach the high level of permanent decorin production, another transfection of the nidogen-1 production clone with the activator protein plasmid could increase the amount of the activator protein that is permanently available to a necessary level in order to reach the full potential of nidogen-1 production in the H1 clone. As current nidogen-1 production levels are sufficient for the foreseeable experimental approaches, and transfection of the production clone would cause the need to repeat clonal selection, and subsequently re-adaptation to suspension growth, this is not planned for the near future. Furthermore, repeated transfection might cause genomic instability of the production clone. While limitation of the inducible production system is a realistic theory that explains lower nidogen-1 production, it might not be suitable in this case, since there are further explanations

for this phenomenon. Nidogen-1 is approximately 3-times the size of decorin, possibly causing a higher burden for the host cell's metabolism and energy balance and reducing its productivity [113]. Also, the process of genomic co-amplification very likely does not always happen ideally with respect to the amplified sequence, which means that instead of the complete decorin or nidogen-1 cassette incomplete sections of these cassettes or other regions downstream of the DHFR cassette might be co-amplified. Each of these not ideal co-amplification events increase the probability of further not ideal co-amplifications and therefore could explain how additional MTX selection rounds do not increase production of the protein of interest. As genomic co-amplification is a statistical event it is likely to lead to different outcomes for protein production in the decorin and the nidogen-1 production clone.

4.5 Protein production and purification

In order to upscale protein production and to enable efficient selective purification of the secreted histidine-tagged decorin and nidogen-1, the production clones needed to be adapted to suspension culture and subsequently to reduced serum content. Adaptation to suspension growth with 10% serum was achieved for the different decorin and nidogen-1 production clones within several weeks with comparable efficiency, but after suspension adaptation ELISA measurements revealed a drop in protein production of the decorin-producing A6 clone, which subsequently was not cultured any more (**Fig. 27**). This clone also showed apparent morphological changes, which indicate that genomic instability could have caused the drop in decorin production. Genomic instability can result from plasmid integration in unstable sites of the host genome, thereby generating continuously unstable recombinational hotspots that undergo genomic amplification of both the integrated plasmid sequence and the adjacent host cell DNA [230]. In combination with the induction of genomic co-amplification due to MTX selection, the risk of a broad genomic instability is increased.

In the subsequent adaptation of the remaining cell clones to production media with reduced serum content, the decorin-producing clone B4 reacted to drastic serum reduction with reduced cell proliferation, while still maintaining high specific productivity. Despite modification of the adaptation protocol for this clone to a finer graduation of serum reduction, the reduction of proliferation could only be mitigated with this approach. Furthermore, to prevent complete irreversible growth arrest of the B4 clone, serum depletion was stopped at 1% serum content, while the nidogen-1-producing H1 clone that did not show reduced proliferation, could be adapted to a final serum content of 0.5%. Further serum reduction beyond these values was not

desirable as it compromised specific productivity. One possible explanation for the problematic adaptation of the decorin-producing B4 clone to reduced serum contents is its permanent decorin production system. Permanent high specific productivity of this proteoglycan can present a challenge, especially if the favorable energy source FBS is strongly reduced. When the burden due to excessive recombinant protein production is too high, serum reduction can cause a disadvantage for cell proliferation [106]. Also, considering that decorin is highly conserved among species, this biologically active human protein can exert effects on the hamster host. This is confirmed by a report from Yamaguchi and Ruoslahti, who observed how recombinant production of human decorin by a stably transfected CHO cell line negatively influences cell proliferation and that this effect increases with rising decorin production [114]. The knowledge of this report based the decision to design an inducible recombinant protein production system additional to the permanent one. With an inducible system, proliferation inhibition due to decorin could have been avoided by culturing the cells until a desired cell density is reached and then inducing decorin production. Unfortunately the selected clones for inducible decorin production were clearly inferior to the permanent production clones (**Fig. 25**, **26**). In contrast to an industrial setting where thousands of clones can be selected and analyzed, this was not possible within the scope of this work. Therefore permanent decorin production in the slow-growing production clone B4 with 1% serum was the best option, as this clone provides high yields of biologically active decorin.

A control affinity chromatography of media with 1% FBS dialyzed was conducted to test if serum proteins show an affinity to the nickel ions in the IMAC column and therefore might be unspecifically purified with the histidine-tagged decorin or nidogen-1. Although the volume of this control purification loaded onto the SDS-gel was five times the amount of a comparable purification of decorin or nidogen-1-containing media, no unspecific protein purification could be detected after SDS-PAGE, Western Blotting and Ponceau Red staining (**Fig. 33 A**). Therefore, with the chosen chromatographic purification methods, unspecific purification of serum proteins could be excluded and a further adaptation of the production clones to lower serum contents is not necessary under this aspect. To retain the biological activity of decorin and nidogen-1 the methods applied for protein purification, namely affinity chromatography, desalting, buffer exchange as well as washing, concentration and sterile filtration, are chosen to comply with this condition. Furthermore, optimal combination of these methods reduces freezing and thawing events to a minimum in order to decrease this negative impact on protein activity.

4.6 Protein activity tests

The identity of the human decorin and nidogen-1 could be verified via qPCR on the genomic and mRNA level as well as specific ELISA and immunoblot detection on the protein level. While the host cell line, production and purification method was chosen to provide high-quality active human recombinant protein products, the biological activity of these proteins needed to be demonstrated for well-described protein interactions first, before the proteins were used to test the hypothesis of this work. For this purpose Co-IPs were conducted that could prove that the recombinant human decorin binds human TGF-β1 (**Fig. 36**) and the recombinant human nidogen-1 binds laminin 511 (**Fig. 37**). As the TGF-β1-inhibiting activity of decorin already has been discussed to prevent scarring in conditions associated with TGF-β1 overproduction, including cardiac fibrosis [214], this activity was especially interesting for an application of decorin to increase cardiac regeneration post MI. Zhang et al. showed that TGF-β1 leads to an increased contraction of a dermal equivalent contraction model [128], which can be explained with the underlying mechanism of transdifferentiation of the human dermal fibroblasts to contracting myofibroblasts. In their study, Zhang et al. used decorin to bind and inhibit TGF-β1 so that it could not exert its function as a trigger for myofibroblast transdifferentiation. In a similar approach the TGF-β1-inhibiting effect of decorin was tested in a dermal equivalent contraction model in this work (**Fig. 38**). While acellular collagen gels do not show any signs of contraction after 16 days of culture, dermal equivalents, which are collagen gels seeded with human fibroblasts isolated from skin biopsies, contract during this culture time, as shown by a reduction to 69.65% ± 7.24% of their original circumference. This base level of dermal equivalent contraction due to transdifferentiation to myofibroblasts cannot be significantly reduced with the addition of 50 µg/ml or 150 µg/ml recombinant decorin, although the higher decorin concentration does show a positive tendency. The base contraction could be due to the exposure of the skin fibroblasts to stress, an important trigger for transdifferentiation to myofibroblasts, during their isolation from the biopsy or freezing and thawing procedure prior to their use in the dermal equivalents. In this case transdifferentiation to myofibroblasts of a portion of the cells is predetermined and cannot be significantly inhibited by decorin-addition to the dermal equivalents. In this model, the addition of 5 ng/ml TGF-β1 caused a significantly increased contraction of the dermal equivalents seeded with human fibroblasts (56.72% ± 8.80% of original circumference), compared to the controls, which were cultured without TGF-β1. No significantly increased contraction compared to the base level of dermal equivalent contraction in the controls could be observed when 5 ng/ml TGF-β1 was used in combination with 50 µg/ml or

150 µg/ml recombinant decorin. The dermal equivalent contraction experiment was conducted three times (n = 3) and showed a tendency of reduced contraction in the equivalents treated with the combination of 5 ng/ml TGF-β1 and decorin (50 µg/ml or 150 µg/ml) compared to the equivalents treated with 5 ng/ml TGF-β1. However, if the TGF-β1-inhibitory effect of decorin is significant and relevant needs to be further investigated.

4.7 In vitro cardio-inductive potential

Utilization of decorin and nidogen-1 in coatings to test their cardio-inductive potential (**Fig. 39**) rather than as a soluble media supplement allowed the hESC-derived EBs to interact with these recombinant proteins via attachment to the 6-well, which resembles the way cells interact with these proteins in their natural ECM environment. Although the control coating with 0.1% gelatin without further ECM protein additions did not change the cardiovascular differentiation protocol described in **Figure 6**, the cardiovascular differentiation efficiencies measured with FACS analysis in **Figure 7** and **39** were inconsistent. This can be partly due to the utilization of different protein markers for cardiovascular differentiation (sarcomeric myosin using the MF20 antibody or cTnT) and partly due to the analysis of dissected beating EBs in contrast to the analysis of the whole well, which also includes the non-beating outgrown cells. In the analysis shown in **Figure 7** the beating EBs were dissected from the non-beating outgrown cells and the FACS analysis using the MF20 antibody revealed 49.4% ± 11.4% MF20-positive cells in the beating EB sample compared to 6.5% ± 2.3% MF20-positive cells in the non-beating outgrown cell sample. The FACS analysis evaluated for **Figure 39** was conducted using an antibody against cTnT, here the whole control wells were analyzed. They contained 17.1% ± 5.9% cTnT-positive cells. Due to the differences in the analysis of the experiment, it was expected that the FACS analysis shown in **Figure 39** results in lower values than the analysis shown in **Figure 7**. It needs to be considered that the beating EBs made up only approximately half of the total cells in the well, while the non-beating and outgrown cells made up the rest. Assuming this 1:1 proportion for the samples analyzed in **Figure 7**, the analysis of a whole well would have resulted in a percentage of ~ 27.9% MF20-positive cells. Furthermore, while cardiomyocytes express both sarcomeric myosin and cTnT, the latter is a marker for more mature cardiomyocytes. After only 10 days of cardiovascular differentiation there can be a discrepancy between the cardiomyocytes detected with the MF20 antibody and the cTnT antibody, resulting in a lower percentage of cTnT-positive cells compared to MF20-positive cells. These factors need to be considered when interpreting the FACS analysis data as they explain why the

experiments described in **Figure 7** and **Figure 39** both promote robust cardiovascular differentiation.

Nevertheless these considerations, **Figure 39** clearly shows a cardio-inductive effect of the recombinant nidogen-1, which has not been described before. EBs plated onto a coating of 0.1% gelatin containing 50 µg/ml nidogen-1 differentiated significantly more effective into cTnT-positive cardiomyocytes (30.1% ± 2.2%) than the control on a 0.1% gelatin coating (17.1% ± 5.9%). Therefore the hypothesis of this work that key ECM proteins in the early healthy cardiovascular development hold cardio-inductive signals is correct for nidogen-1. While neither the decorin-containing coating (0.1% gelatin + 50 µg/ml decorin) nor the coating containing both decorin and niogen-1 (0.1% gelatin + 50 µg/ml decorin + 50 µg/ml nidogen-1) show a significant increase in the cardiovascular differentiation of the EBs, they both show a positive tendency compared to the control when considering the mean values (26.3% ± 5.7% and 22.8% ± 2.9% cTnT-positive cells compared to 17.1% ± 5.9% cTnT-positive cells). High standard deviations due to biological variances in cardiovascular differentiation of the sensitive hESC-derived EBs contribute to this fact. It is remarkable that the lowest value of cTnT-positive cells apart from the control coating can be found with the combination of both 50 µg/ml decorin and 50 µg/ml nidogen-1. While a direct interaction and possible inhibition of nidogen-1 by decorin has not been reported, this finding could be due to secondary effects of decorin, which reduce the cells positive reaction to nidogen-1, as further described in **4.8**.

Limitations of this in vitro study to test the cardio-inductive potential of decorin and nidogen-1 include the expandable number of biological replicates (n = 3) and the lack of sarcomeric myosin or cTnT IF staining to support the FACS result. While the amount of conducted experiments is sufficient to determine a significant cardio-inductive effect of nidogen-1, more biological replicates could reaffirm this result and might furthermore lead to an assessment of the cardio-inductive effect of decorin alone or in a mix with nidogen-1 as significantly higher than the control.

4.8 In vivo mouse MI/R experiments

In a final experiment, the hypothesis of this work was tested, which says that the injection of cardio-inductive key ECM proteins after myocardial wounding including ischemia improves cardiac function due to higher regeneration. In vivo mouse MI/R and intra-cardiac injections of the recombinant cardio-inductive nidogen-1 in the infarct border zone were conducted to test this hypothesis. Although a cardio-inductive effect of decorin could not be shown in vitro (**Fig. 39**),

decorin has other effects that make it an interesting candidate for an ECM-comprising therapy post MI [196, 214, 217]. Therefore we chose to additionally test a combination of the cardio-inductive nidogen-1 and decorin, due to its role in scar-reduction and collagen fibrillogenesis. To our knowledge up to this point in vivo experiments to test the effect of decorin after a myocardial infarction have only been described once before by Li et al. [214]. In their study, Li et al. could show that post MI decorin gene therapy via local adenovirus-mediated transduction of the decorin gene in mouse hindlimb muscles inhibited the activation of downstream mediators of TGF-β signaling. Preventing cardiac fibrosis, decorin could be shown to mitigate pathological cardiac remodeling and dysfunction. While this study confirms the great potential of decorin for a post MI treatment, the administration of decorin via virus-mediated gene transfer excludes a safe application in clinic. While adenoviruses are one of the most effective gene delivery vectors, ethical concerns towards adenoviral gene therapy exist at the latest since the death of the first patient in a gene therapy trial, who died directly due to the adenoviral therapy itself [231]. Furthermore, gene therapy leads to a continuous production and release of decorin into the circulation, which means the protein does not only reach the heart, but could have undesirable and in high doses potentially harmful systemic effects.

When designing an effective but ideally negligibly traumatic method for a local application of decorin and nidogen-1 to the heart of a patient post MI, minimally invasive methods are preferable. Modern intramyocardial injection catheter systems like the Myostar™ system (Biologics Delivery Systems, Diamond Bar, CA, USA), allow access to the LV myocardial infarct area and surrounding border zone from within the left ventricular chamber by crossing the aortic valve, like in a routine catheterization of the left ventricle [232]. From this position they can repeatedly inject therapeutic solutions and even cell suspensions for a cell therapy approach. The peri-infarct zone as the injection site can be detected using electromechanical mapping systems, such as the NOGA-XP® system with the Myostar™ catheter [233]. With such a mapping system, myocardial wall motion as well as state of viability can be assessed. While this minimally invasive procedure is clearly preferable, the necessary technology is available for human patients or large animal studies, but not for mice. Therefore, for the mouse MI/R and protein injection experiments, the mouse chests were surgically opened and myocardial injections were applied directly.

In vitro, the cardio-inductive effect of nidogen-1 on hESCs was seen for a concentration of 50 µg/ml (**Fig. 39**) and the same concentration of decorin showed a tendency to reduce TGF-β1-induced contraction of dermal equivalents (**Fig. 38**). Furthermore, the analysis of the effect on

human immune reaction suggested the use of these products in a concentration of 50 µg/ml in order to prevent adverse immune reactions. Therefore, for the in vivo experiments, a concentration of 50 µg/ml decorin and 50 µg/ml nidogen-1 in the combined approach or 50 µg/ml nidogen-1 in the individual approach was chosen. In order to retain the proteins at the injection sites and minimize leakage instantly after injection, the proteins were mixed with a bio-inert hyaluronan-based hydrogel to increase the viscosity of the injection mix. Furthermore, the total injection volume of 50 µl per mouse was divided into five separate injections, each of a small volume of 10 µl, for supplying the entire infarct border zone with the proteins and reducing leakage at the individual injection sites. In case small amounts of decorin or nidogen-1 enter the circulation, no negative systemic effect is expected. Also, circulating proteins are often trapped by the liver and cleared from the circulation within minutes, as already shown for decorin [234]. Out of the 15 mice used in the in vivo MI/R and ECM injection experiment, only one died after the operation and two needed to be excluded due to incomplete ischemia. These rare events taken into account, the experimental setup and methodology is robust and provides reliable data even with small groups of animals.

The best results of cardiac function 2 and 4 weeks post MI, as identified by EF, could be seen in the nidogen-1 treatment group. The mean EF of the decorin + nidogen-1 treatment group (43.36% ± % 5.68% EF) and the nidogen-1 treatment group (43.75% ± 0.62% EF) at the time point 2 weeks post MI were nearly identical, which would suggest that nidogen-1 alone is critical for the significantly higher EF in comparison to the control group at the same time point. Histological analysis of the hearts treated with the mix of decorin and nidgen-1 have to be conducted to better understand why the decorin treatment did not fulfil the high expectations it had raised. Possibly the concentration of 50 µg/ml decorin was not sufficient to adequately inhibit TGF-β1 levels in vivo or influence collagen fibrillogenesis in a major infarct. Also a continuous supply with decorin or repetitive administration might have been more efficient.
At the time point 4 weeks post MI, again the nidogen-1 treatment lead to a significantly higher EF compared to the control group, but at this time point there was also a significant difference to the decorin + nidogen-1 treatment. This would suggest that the administration of 50 µg/ml decorin did not only bring no additional benefit to the nidogen-1 treatment, but even significantly reduced its positive effect. The in vitro experiment to test the cardio-inductive potential of decorin and nidogen-1 showed similar tendencies. As already discussed briefly in the previous paragraph, no direct interaction between decorin and nidogen-1 is known to date, but as decorin has been implied in various biological processes, a secondary effect of decorin might be

responsible for reduced nidogen-1 functionality, both in the in vitro (**Fig. 39**) and in vivo experiments (**Fig. 40**). Decorin increases migration [235] and inhibits cell attachment [236-239], possibly challenging the adhesion-promoting function of nidogen-1. In an early phase of tissue regeneration, attraction and adhesion promotion of circulating cells or heart-specific progenitor cells to the wounded area are essential, and can dictate the mid- and long-term outcome of a healing process. Furthermore, the endotoxin load of the decorin sample, which probably originated from the FBS used for culture, might be responsible for the adverse performance in vivo. Although the concentration applied in vivo was tested in immunological assays, where it did not cause an induction of immune cell proliferation or activation but immunosuppression, it is possible that the application of this sample in an immunologically active infarct lead to a different outcome. Also the immunological assays were conducted with human PMBCs and are therefore a better model for human than murine immune reaction. A combination of both decorin and nidogen-1 was not investigated with the human immune reaction assays in vitro. Therefore this combination might have undesired immune effects that were not detected in the analysis of the individual proteins.

Qualitative histological analysis of the mouse hearts 4 weeks post MI showed that the nidogen-1 treatment enabled a better preservation of the cardiac morphology and a lower extent of pathological remodeling compared to the control hearts (**Fig. 41**). This analysis supports the result of the conscious echocardiography that revealed a significant positive effect of the nidogen-1 treatment on cardiac function. While we could show the cardio-inductive effect of nidogen-1 in vitro (**Fig. 39**), it is unclear if this effect enabled the nidogen-1-mediated significant increase of cardiac EF compared to the controls in vivo. In order to verify the result of the qualitative analysis of the histological staining, a quantification of the whole pathologically remodeled area and the preserved cardiac tissue in the nidogen-1-treated as well as the control hearts need to be performed. IF staining of special cell phenotype markers like Ki-67 can be utilized to determine if true cardiac regeneration occurred due to cardiomyocyte proliferation or the attraction and subsequent directed differentiation of potent circulating cells or residing CPCs to the site of injury. Other explanations for the better preservation of cardiac morphology due to nidogen-1 treatment could be an increased cardiomyocyte survival or the initiation of cardiomyocyte-ingrowth from intact myocardium surrounding the infarct. The Russel-Movat Pentachrome staining showed qualitative differences in ECM deposition in the pathologically remodeled areas, especially when focusing on collagen (**Fig. 41**). IF staining of important ECM components like collagen type I and collagen type III as well as IV, laminins, fibronectin, decorin

and nidogen-1 will enable a quantitative comparison of these ECM components in the pathologically remodeled areas or in remote areas of hearts that received nidogen-1 or control injections.

Contrary to ideal fetal wound healing that enables true regeneration of functional tissue [50, 51], the corresponding process in adults is limited to wound closure and contraction. Evolutionary, the wound healing process mainly developed for a rapid closure and stabilization of small or medium-sized skin wounds in order to prevent infection and death. CVD came into focus in the past few hundred years as increased life expectancy and industrialization drastically increased their prevalence, but this time span is not nearly enough to enable an evolutionary adaptation. Also mayor myocardial infarcts do not have a strong impact on the evolutionary development of natural wound healing strategies, as they mainly affect people beyond their reproductive age. Considering the strongly impaired cardiac functionality and ongoing adverse remodeling post MI, the natural wound healing process is obviously less than ideal. Compared to the outcome with control treatment, nidogen-1 injection improved murine cardiac function by 14.8% EF two weeks post MI and maintained a comparably high therapeutic effect at least for four weeks (improvement of 14.5%). This exceeds the therapeutic effect of various other biomaterials tested in vivo that were reported to significantly increase cardiac EF post MI, including fibrin in rat [155, 157], Matrigel in rat [164, 165] or calcium hydroxyapatite in sheep [240, 241]. Although the increase in EF shown in this work is not the highest reported with a biomaterial-only treatment [55, 242, 243], it has the potential to be further increased when combined with a cell therapy, as already shown for several other biomaterials [155, 157, 165, 242]. A combined treatment with the cardio-inductive nidogen-1 and a large number of potent cells like CPCs is intriguing; unfortunately within this work it was not possible to test such a combined approach in the established murine MI model due to an insufficient amount of flow cytometrically-sorted CPCs. Still, if the high therapeutic effect of the nidogen-1 treatment alone could be achieved for a human patient, this would mean a substantial improvement of the patient's life quality as well as life expectancy. Learning from the fetal blueprint for tissue repair, in this work a novel regenerative medicine approach was presented that utilized the cardio-inductive glycoprotein nidogen-1 to support cardiac regeneration post MI. The possibility to transfer the production of this human ECM protein to a cGMP-banked CHO cell line in order to comply with GMP requirements allows the generation of a reproducibly safe treatment with defined composition that is not limited by the disadvantages of decellularized ECM products.

5 Conclusion

CVD has a significant impact on our ageing society. It is one of the leading causes of death in the world, and generates exceedingly high costs for healthcare systems while simultaneously reducing the economic output of CVD sufferers. New therapies need to be developed to treat the diseased heart and prevent the progression to heart failure. Ongoing pathological changes of the cardiac ECM are a main cause of this devastating development. It has been hypothesized that introducing ECM proteins could be the key to successful treatment, potentially supporting a higher regenerative capacity of the heart or overcoming limitations of cell therapy approaches. For such an application, cardio-inductive components of the ECM microenvironment during fetal development may be of particular promise as they potentially hold the key unlocking the unique regenerative capacity of the fetus and scar-free fetal wound healing.

In this thesis, potential key ECM proteins involved in human cardiogenesis were identified using hESCs. Recombinant nidogen-1 production enabled the generation of a defined and biologically active human protein product for in vitro experiments and MI treatment, omitting limitations of undefined ECM generated by decellularization methods. For the first time, a cardio-inductive effect of nidogen-1 was shown performing in vitro hESC differentiation experiments. The in vivo application of nidogen-1 in a murine MI/R model significantly improved heart function four weeks post MI compared to the controls, due to an improved preservation of cardiac morphology and a lower degree of pathological remodeling, as shown by qualitative histological analyses. A combined application of the nidogen-1 treatment and an additional cell therapy could further increase the positive effect on heart function, which is the focus of ongoing experiments that are beyond the scope of this thesis.

While further studies need to be performed to analyze nidogen-1 function post-MI in more detail, the in vivo results provided in this work are promising and create a basis for the development of an early-stage therapy to prevent heart failure.

6 Outlook

In this work the treatment with recombinant human nidogen-1 post MI resulted in a significantly increased cardiac function compared to controls. The histological and immunohistological analysis of the mouse MI/R experiment will be finalized utilizing sections of the murine hearts that have been explanted 4 weeks post MI/R in order to understand the therapeutic basis of the nidogen-1-mediated effect. The analysis will focus on quantification of the pathologically remodeled area, infarct wall width, LV ECM composition as well as cardiomyocyte and overall cell density in the infarct area and surrounding border zone. Proliferation markers like Ki-67 will be utilized to determine if true regeneration of functional cardiomyocytes occurred, or if other mechanisms are responsible for the therapeutic effect of the nidogen-1 treatment. Nidogen-1 injection could be shown to maintain a significant increase of murine cardiac functionality for at least 4 weeks post-MI compared to the controls. Further investigation will have to prove how much longer this effect lasts, or if it is retained in long-term. The exact signaling pathways activated or inhibited by nidogen-1 to enable its cardio-inductive effect should be elucidated. Further ECM proteins or small molecules involved in the same signaling pathways could be detected, which might support and enhance the therapeutic effect of nidogen-1.

In the near future, experiments will be conducted utilizing an immune-suppressed rat model, to test the nidogen-1 injections in combination with a human CPC transplantation approach post MI. In these experiments the previously described shortage of flow cytometrically-sorted CPCs that prevented a combined nidogen-1 and cell therapy approach will be overcome by utilizing an efficient protocol for the derivation of PDGFR-α-positive and CD31-positive CPCs from hESCs. In this combined approach, an improved microenvironment due to the cardio-inductive and cell attachment-promoting function of nidogen-1 might give the right signals to support the success of the cell therapy by increasing cell delivery, retention, survival, engraftment and directed differentiation to cardiomyocytes. The application of CPCs could provide the necessary cell number to replenish for cardiomyocytes that were lost in the MI. Additionally to preventing a significant decrease in EF in the weeks following the initial MI impact, as achieved by the nidogen-1 treatment alone, CPC transplantation could support a significant robust recovery of heart function with time.

Further plans include the application of the nidogen-1 treatment with or without additional hCPC cell therapy in a preclinical study with a large animal model for MI. Using a pig model, the in vivo

effects of the treatment will be more comparable to expected effects in the human system. With promising results of the large animal experiments, a complete transfer of the recombinant protein production system to comply GMP standards would be the next step towards the development of a nidogen-1-based therapy post MI. Transfection of a cGMP-banked CHO cell line and recombinant protein production in defined serum-free GMP-compliant culture media will solve the issues caused by endotoxin-contaminated serum for cell culture. If supported by the results of immunological tests, the GMP compliant proteins could be tested in higher concentrations, which might result not only in a better therapeutic effect of nidogen-1, but also in an additional supporting effect of decorin.

Acknowledging the importance of ECM in cell fate decision that could be unveiled so far, we believe that specific ECM components or mixtures could be used in a variety of applications in tissue regeneration strategies. With results of this work in the cardiovascular field, the following patents were filed: **Shannon Layland, Katja Schenke-Layland, Monika Holeiter**, Glycosylated protein of an extracellular matrix for use in a method of treating an ischemic heart of a human or animal subject, # EP 13178951.3-1456 patent pending and # PCT/EP2014/066497 patent pending.

7 Appendix

7.1 List of figures

7.2 List of tables

7.3 References

1. Sutton, M.G. and N. Sharpe, *Left ventricular remodeling after myocardial infarction: pathophysiology and therapy.* Circulation, 2000. **101**(25): p. 2981-8.
2. Volders, P.G., et al., *Interstitial collagen is increased in the non-infarcted human myocardium after myocardial infarction.* J Mol Cell Cardiol, 1993. **25**(11): p. 1317-23.
3. Lindsey, M.L., et al., *Extracellular matrix remodeling following myocardial injury.* Ann Med, 2003. **35**(5): p. 316-26.
4. van den Borne, S.W., et al., *Myocardial remodeling after infarction: the role of myofibroblasts.* Nat Rev Cardiol, 2010. **7**(1): p. 30-7.
5. Hein, S. and J. Schaper, *The extracellular matrix in normal and diseased myocardium.* J Nucl Cardiol, 2001. **8**(2): p. 188-96.
6. Czubryt, M.P., *Common threads in cardiac fibrosis, infarct scar formation, and wound healing.* Fibrogenesis Tissue Repair, 2012. **5**(1): p. 19.
7. Espira, L. and M.P. Czubryt, *Emerging concepts in cardiac matrix biology.* Can J Physiol Pharmacol, 2009. **87**(12): p. 996-1008.
8. Lloyd-Jones, D.M., et al., *Lifetime risk for developing congestive heart failure: the Framingham Heart Study.* Circulation, 2002. **106**(24): p. 3068-72.

9. Roger, V.L., et al., *Heart disease and stroke statistics--2011 update: a report from the American Heart Association.* Circulation, 2011. **123**(4): p. e18-e209.
10. Tanaka, M., et al., *Hypoxia induces apoptosis with enhanced expression of Fas antigen messenger RNA in cultured neonatal rat cardiomyocytes.* Circ Res, 1994. **75**(3): p. 426-33.
11. Elsasser, A., K. Suzuki, and J. Schaper, *Unresolved issues regarding the role of apoptosis in the pathogenesis of ischemic injury and heart failure.* J Mol Cell Cardiol, 2000. **32**(5): p. 711-24.
12. Gabbiani, G., *The myofibroblast in wound healing and fibrocontractive diseases.* J Pathol, 2003. **200**(4): p. 500-3.
13. Jester, J.V., W.M. Petroll, and H.D. Cavanagh, *Corneal stromal wound healing in refractive surgery: the role of myofibroblasts.* Prog Retin Eye Res, 1999. **18**(3): p. 311-56.
14. Cleutjens, J.P., et al., *The infarcted myocardium: simply dead tissue, or a lively target for therapeutic interventions.* Cardiovasc Res, 1999. **44**(2): p. 232-41.
15. Tomasek, J.J., et al., *Myofibroblasts and mechano-regulation of connective tissue remodelling.* Nat Rev Mol Cell Biol, 2002. **3**(5): p. 349-63.
16. Porter, K.E. and N.A. Turner, *Cardiac fibroblasts: at the heart of myocardial remodeling.* Pharmacol Ther, 2009. **123**(2): p. 255-78.
17. Lijnen, P. and V. Petrov, *Transforming growth factor-beta 1-induced collagen production in cultures of cardiac fibroblasts is the result of the appearance of myofibroblasts.* Methods Find Exp Clin Pharmacol, 2002. **24**(6): p. 333-44.
18. Hinz, B. and G. Gabbiani, *Mechanisms of force generation and transmission by myofibroblasts.* Curr Opin Biotechnol, 2003. **14**(5): p. 538-46.
19. Martin, P., *Wound healing--aiming for perfect skin regeneration.* Science, 1997. **276**(5309): p. 75-81.
20. Gabbiani, G., et al., *Granulation tissue as a contractile organ. A study of structure and function.* J Exp Med, 1972. **135**(4): p. 719-34.
21. Cleutjens, J.P., et al., *Collagen remodeling after myocardial infarction in the rat heart.* Am J Pathol, 1995. **147**(2): p. 325-38.
22. Desmouliere, A., et al., *Apoptosis mediates the decrease in cellularity during the transition between granulation tissue and scar.* Am J Pathol, 1995. **146**(1): p. 56-66.
23. Willems, I.E., et al., *The alpha-smooth muscle actin-positive cells in healing human myocardial scars.* Am J Pathol, 1994. **145**(4): p. 868-75.
24. Takemura, G., et al., *Role of apoptosis in the disappearance of infiltrated and proliferated interstitial cells after myocardial infarction.* Circ Res, 1998. **82**(11): p. 1130-8.
25. Spinale, F.G. and M.R. Zile, *Integrating the myocardial matrix into heart failure recognition and management.* Circ Res, 2013. **113**(6): p. 725-38.
26. Brown, R.D., et al., *The cardiac fibroblast: therapeutic target in myocardial remodeling and failure.* Annu Rev Pharmacol Toxicol, 2005. **45**: p. 657-87.
27. Coker, R.K. and G.J. Laurent, *Pulmonary fibrosis: cytokines in the balance.* Eur Respir J, 1998. **11**(6): p. 1218-21.
28. Balsano, C., A. Alisi, and V. Nobili, *Liver fibrosis and therapeutic strategies: the goal for improving metabolism.* Curr Drug Targets, 2009. **10**(6): p. 505-12.
29. Schnaper, H.W., *Balance between matrix synthesis and degradation: a determinant of glomerulosclerosis.* Pediatr Nephrol, 1995. **9**(1): p. 104-11.
30. Pfeffer, M.A. and E. Braunwald, *Ventricular remodeling after myocardial infarction. Experimental observations and clinical implications.* Circulation, 1990. **81**(4): p. 1161-72.
31. Pfeffer, M.A., *Left ventricular remodeling after acute myocardial infarction.* Annu Rev Med, 1995. **46**: p. 455-66.

32. Alcon, A., E. Cagavi Bozkulak, and Y. Qyang, *Regenerating functional heart tissue for myocardial repair.* Cell Mol Life Sci, 2012. **69**(16): p. 2635-56.
33. Leone, A.M., et al., *Mobilization of bone marrow-derived stem cells after myocardial infarction and left ventricular function.* Eur Heart J, 2005. **26**(12): p. 1196-204.
34. Menasche, P., et al., *Autologous skeletal myoblast transplantation for severe postinfarction left ventricular dysfunction.* J Am Coll Cardiol, 2003. **41**(7): p. 1078-83.
35. Herreros, J., et al., *Autologous intramyocardial injection of cultured skeletal muscle-derived stem cells in patients with non-acute myocardial infarction.* Eur Heart J, 2003. **24**(22): p. 2012-20.
36. Assmus, B., et al., *Transplantation of Progenitor Cells and Regeneration Enhancement in Acute Myocardial Infarction (TOPCARE-AMI).* Circulation, 2002. **106**(24): p. 3009-17.
37. Chen, S.L., et al., *Effect on left ventricular function of intracoronary transplantation of autologous bone marrow mesenchymal stem cell in patients with acute myocardial infarction.* Am J Cardiol, 2004. **94**(1): p. 92-5.
38. Beltrami, A.P., et al., *Adult cardiac stem cells are multipotent and support myocardial regeneration.* Cell, 2003. **114**(6): p. 763-76.
39. Doss, M.X., et al., *Embryonic stem cells: a promising tool for cell replacement therapy.* J Cell Mol Med, 2004. **8**(4): p. 465-73.
40. He, Q., et al., *Fate of undifferentiated mouse embryonic stem cells within the rat heart: role of myocardial infarction and immune suppression.* J Cell Mol Med, 2009. **13**(1): p. 188-201.
41. Mangi, A.A., et al., *Mesenchymal stem cells modified with Akt prevent remodeling and restore performance of infarcted hearts.* Nat Med, 2003. **9**(9): p. 1195-201.
42. Murry, C.E., L.J. Field, and P. Menasche, *Cell-based cardiac repair: reflections at the 10-year point.* Circulation, 2005. **112**(20): p. 3174-83.
43. Murry, C.E., et al., *Haematopoietic stem cells do not transdifferentiate into cardiac myocytes in myocardial infarcts.* Nature, 2004. **428**(6983): p. 664-8.
44. Murry, C.E., et al., *Skeletal myoblast transplantation for repair of myocardial necrosis.* J Clin Invest, 1996. **98**(11): p. 2512-23.
45. Nelson, T.J., et al., *Repair of acute myocardial infarction by human stemness factors induced pluripotent stem cells.* Circulation, 2009. **120**(5): p. 408-16.
46. Smits, A.M., et al., *The role of stem cells in cardiac regeneration.* J Cell Mol Med, 2005. **9**(1): p. 25-36.
47. Leri, A., et al., *Myocardial regeneration and stem cell repair.* Curr Probl Cardiol, 2008. **33**(3): p. 91-153.
48. Lionetti, V. and C. Ventura, *Regenerative medicine approach to repair the failing heart.* Vascul Pharmacol, 2013. **58**(3): p. 159-63.
49. Chavakis, E., M. Koyanagi, and S. Dimmeler, *Enhancing the outcome of cell therapy for cardiac repair: progress from bench to bedside and back.* Circulation, 2010. **121**(2): p. 325-35.
50. Adzick, N.S. and M.T. Longaker, *Scarless fetal healing. Therapeutic implications.* Ann Surg, 1992. **215**(1): p. 3-7.
51. Harrison, M.R. and N.S. Adzick, *The fetus as a patient. Surgical considerations.* Ann Surg, 1991. **213**(4): p. 279-91; discussion 277-8.
52. Badylak, S.F., *Regenerative medicine and developmental biology: the role of the extracellular matrix.* Anat Rec B New Anat, 2005. **287**(1): p. 36-41.
53. Hinderer, S., et al., *Engineering of fibrillar decorin matrices for a tissue-engineered trachea.* Biomaterials, 2012. **33**(21): p. 5259-66.
54. Kim, H., et al., *Hybrid scaffolds composed of hyaluronic acid and collagen for cartilage regeneration.* Tissue Engineering and Regenerative Medicine, 2012. **9**(2): p. 57-62.

55. Seif-Naraghi, S.B., et al., *Safety and efficacy of an injectable extracellular matrix hydrogel for treating myocardial infarction.* Sci Transl Med, 2013. **5**(173): p. 173ra25.
56. Hinderer, S. and K. Schenke-Layland, *Tracheal tissue engineering: building on a strong foundation.* Expert Rev Med Devices, 2013. **10**(1): p. 33-5.
57. Thomson, J.A., *Embryonic Stem Cell Lines Derived from Human Blastocysts.* Science, 1998. **282**(5391): p. 1145-1147.
58. Reubinoff, B.E., et al., *Embryonic stem cell lines from human blastocysts: somatic differentiation in vitro.* Nat Biotechnol, 2000. **18**(4): p. 399-404.
59. Pera, M.F., B. Reubinoff, and A. Trounson, *Human embryonic stem cells.* J Cell Sci, 2000. **113 (Pt 1)**: p. 5-10.
60. Amit, M., et al., *Clonally derived human embryonic stem cell lines maintain pluripotency and proliferative potential for prolonged periods of culture.* Dev Biol, 2000. **227**(2): p. 271-8.
61. Evseenko, D., et al., *Identification of the critical extracellular matrix proteins that promote human embryonic stem cell assembly.* Stem Cells Dev, 2009. **18**(6): p. 919-28.
62. Thomson, J.A., et al., *Embryonic stem cell lines derived from human blastocysts.* Science, 1998. **282**(5391): p. 1145-7.
63. Gerecht-Nir, S., et al., *Human embryonic stem cells as an in vitro model for human vascular development and the induction of vascular differentiation.* Lab Invest, 2003. **83**(12): p. 1811-20.
64. Yang, L., et al., *Human cardiovascular progenitor cells develop from a KDR+ embryonic-stem-cell-derived population.* Nature, 2008. **453**(7194): p. 524-8.
65. Hynes, R.O., *Integrins: bidirectional, allosteric signaling machines.* Cell, 2002. **110**(6): p. 673-87.
66. Horak, V. and J.E. Flechon, *Immunocytochemical characterisation of rabbit and mouse embryonic fibroblasts.* Reprod Nutr Dev, 1998. **38**(6): p. 683-95.
67. Xu, C., et al., *Feeder-free growth of undifferentiated human embryonic stem cells.* Nat Biotechnol, 2001. **19**(10): p. 971-4.
68. Ludwig, T.E., et al., *Derivation of human embryonic stem cells in defined conditions.* Nat Biotechnol, 2006. **24**(2): p. 185-7.
69. Amit, M., et al., *Feeder layer- and serum-free culture of human embryonic stem cells.* Biol Reprod, 2004. **70**(3): p. 837-45.
70. Braam, S.R., et al., *Recombinant vitronectin is a functionally defined substrate that supports human embryonic stem cell self-renewal via alphavbeta5 integrin.* Stem Cells, 2008. **26**(9): p. 2257-65.
71. Jones, M.B., et al., *Proliferation and pluripotency of human embryonic stem cells maintained on type I collagen.* Stem Cells Dev, 2010. **19**(12): p. 1923-35.
72. Nagaoka, M., et al., *Culture of human pluripotent stem cells using completely defined conditions on a recombinant E-cadherin substratum.* BMC Dev Biol, 2010. **10**: p. 60.
73. Prowse, A.B., et al., *Long term culture of human embryonic stem cells on recombinant vitronectin in ascorbate free media.* Biomaterials, 2010. **31**(32): p. 8281-8.
74. Rodin, S., et al., *Long-term self-renewal of human pluripotent stem cells on human recombinant laminin-511.* Nat Biotechnol, 2010. **28**(6): p. 611-5.
75. Yap, L.Y., et al., *Defining a threshold surface density of vitronectin for the stable expansion of human embryonic stem cells.* Tissue Eng Part C Methods, 2011. **17**(2): p. 193-207.
76. Yoon, T.M., et al., *Human embryonic stem cells (hESCs) cultured under distinctive feeder-free culture conditions display global gene expression patterns similar to hESCs from feeder-dependent culture conditions.* Stem Cell Rev, 2010. **6**(3): p. 425-37.

77. Melkoumian, Z., et al., *Synthetic peptide-acrylate surfaces for long-term self-renewal and cardiomyocyte differentiation of human embryonic stem cells.* Nat Biotechnol, 2010. **28**(6): p. 606-10.
78. Zhang, J., et al., *Extracellular Matrix Promotes Highly Efficient Cardiac Differentiation of Human Pluripotent Stem Cells: The Matrix Sandwich Method.* Circ Res, 2012.
79. Schenke-Layland, K., et al., *Collagen IV induces trophoectoderm differentiation of mouse embryonic stem cells.* Stem Cells, 2007. **25**(6): p. 1529-38.
80. Schenke-Layland, K., et al., *Reprogrammed mouse fibroblasts differentiate into cells of the cardiovascular and hematopoietic lineages.* Stem Cells, 2008. **26**(6): p. 1537-46.
81. Yamashita, J., et al., *Flk1-positive cells derived from embryonic stem cells serve as vascular progenitors.* Nature, 2000. **408**(6808): p. 92-6.
82. McCloskey, K.E., S.L. Stice, and R.M. Nerem, *In vitro derivation and expansion of endothelial cells from embryonic stem cells.* Methods Mol Biol, 2006. **330**: p. 287-301.
83. Nishikawa, S.I., et al., *Progressive lineage analysis by cell sorting and culture identifies FLK1+VE-cadherin+ cells at a diverging point of endothelial and hemopoietic lineages.* Development, 1998. **125**(9): p. 1747-57.
84. Itskovitz-Eldor, J., et al., *Differentiation of human embryonic stem cells into embryoid bodies compromising the three embryonic germ layers.* Mol Med, 2000. **6**(2): p. 88-95.
85. Ng, E.S., et al., *A protocol describing the use of a recombinant protein-based, animal product-free medium (APEL) for human embryonic stem cell differentiation as spin embryoid bodies.* Nat Protoc, 2008. **3**(5): p. 768-76.
86. Desbaillets, I., et al., *Embryoid bodies: an in vitro model of mouse embryogenesis.* Exp Physiol, 2000. **85**(6): p. 645-51.
87. Doetschman, T.C., et al., *The in vitro development of blastocyst-derived embryonic stem cell lines: formation of visceral yolk sac, blood islands and myocardium.* J Embryol Exp Morphol, 1985. **87**: p. 27-45.
88. Schuldiner, M., et al., *Effects of eight growth factors on the differentiation of cells derived from human embryonic stem cells.* Proc Natl Acad Sci U S A, 2000. **97**(21): p. 11307-12.
89. Draper, J.S. and V. Fox, *Human embryonic stem cells: multilineage differentiation and mechanisms of self-renewal.* Arch Med Res, 2003. **34**(6): p. 558-64.
90. Kennedy, M., et al., *Development of the hemangioblast defines the onset of hematopoiesis in human ES cell differentiation cultures.* Blood, 2007. **109**(7): p. 2679-87.
91. Lu, S.J., et al., *Generation of functional hemangioblasts from human embryonic stem cells.* Nat Methods, 2007. **4**(6): p. 501-9.
92. Willems, E., et al., *Small-molecule inhibitors of the Wnt pathway potently promote cardiomyocytes from human embryonic stem cell-derived mesoderm.* Circ Res, 2011. **109**(4): p. 360-4.
93. Chan, C.K., et al., *Differentiation of cardiomyocytes from human embryonic stem cells is accompanied by changes in the extracellular matrix production of versican and hyaluronan.* J Cell Biochem, 2010. **111**(3): p. 585-96.
94. Courtman, D.W., B.F. Errett, and G.J. Wilson, *The role of crosslinking in modification of the immune response elicited against xenogenic vascular acellular matrices.* J Biomed Mater Res, 2001. **55**(4): p. 576-86.
95. Schernthaner, G., *Immunogenicity and allergenic potential of animal and human insulins.* Diabetes Care, 1993. **16 Suppl 3**: p. 155-65.
96. MEYER, A.A., et al., *Antibody Response to Xenogeneic Proteins in Burned Patients Receiving Cultured Keratinocyte Grafts.* Journal of Trauma and Acute Care Surgery, 1988. **28**(7): p. 1054-1059.
97. Nandi, J., M.A. Zhou, and T.K. Ray, *Purification and partial characterization of the (H+,K+)-transporting adenosinetriphosphatase from fundic mucosa.* Biochemistry, 1987. **26**(14): p. 4264-72.

98. Urlaub, G., et al., *Deletion of the diploid dihydrofolate reductase locus from cultured mammalian cells.* Cell, 1983. **33**(2): p. 405-12.
99. Seth, G., et al., *Engineering cells for cell culture bioprocessing--physiological fundamentals.* Adv Biochem Eng Biotechnol, 2006. **101**: p. 119-64.
100. Korke, R., et al., *Genomic and proteomic perspectives in cell culture engineering.* J Biotechnol, 2002. **94**(1): p. 73-92.
101. Wurm, F.M., *Production of recombinant protein therapeutics in cultivated mammalian cells.* Nat Biotechnol, 2004. **22**(11): p. 1393-8.
102. Palomares, L.A., S. Estrada-Mondaca, and O.T. Ramirez, *Production of recombinant proteins: challenges and solutions.* Methods Mol Biol, 2004. **267**: p. 15-52.
103. Bhatia, P.K. and A. Mukhopadhyay, *Protein glycosylation: implications for in vivo functions and therapeutic applications.* Adv Biochem Eng Biotechnol, 1999. **64**: p. 155-201.
104. Zhu, M., M. Mollet, and R. Hubert, *Industrial Production of Therapeutic Proteins: Cell Lines, Cell Culture, and Purification*, in *Kent and Riegel's Handbook of Industrial Chemistry and Biotechnology*, J. Kent, Editor. 2007, Springer US. p. 1421-1448.
105. Omasa, T., M. Onitsuka, and W.D. Kim, *Cell engineering and cultivation of chinese hamster ovary (CHO) cells.* Curr Pharm Biotechnol, 2010. **11**(3): p. 233-40.
106. Sinacore, M.S., D. Drapeau, and S.R. Adamson, *Adaptation of mammalian cells to growth in serum-free media.* Mol Biotechnol, 2000. **15**(3): p. 249-57.
107. Urlaub, G. and L.A. Chasin, *Isolation of Chinese hamster cell mutants deficient in dihydrofolate reductase activity.* Proc Natl Acad Sci U S A, 1980. **77**(7): p. 4216-20.
108. Kellems, R.E., *Gene amplification in mammalian cells: strategies for protein production.* Curr Opin Biotechnol, 1991. **2**(5): p. 723-9.
109. Wurm, F.M., K.A. Gwinn, and R.E. Kingston, *Inducible overproduction of the mouse c-myc protein in mammalian cells.* Proc Natl Acad Sci U S A, 1986. **83**(15): p. 5414-8.
110. Chunduru, S.K., et al., *Methotrexate-resistant variants of human dihydrofolate reductase. Effects of Phe31 substitutions.* J Biol Chem, 1994. **269**(13): p. 9547-55.
111. Zhou, Z., et al., *Enhanced expression of a recombinant malaria candidate vaccine in Escherichia coli by codon optimization.* Protein Expr Purif, 2004. **34**(1): p. 87-94.
112. Ikemura, T., *Correlation between the abundance of Escherichia coli transfer RNAs and the occurrence of the respective codons in its protein genes.* J Mol Biol, 1981. **146**(1): p. 1-21.
113. Gu, M.B., et al., *Effect of amplification of dhfr and lac Z genes on growth and beta-galactosidase expression in suspension cultures of recombinant CHO cells.* Cytotechnology, 1992. **9**(1-3): p. 237-45.
114. Yamaguchi, Y. and E. Ruoslahti, *Expression of human proteoglycan in Chinese hamster ovary cells inhibits cell proliferation.* Nature, 1988. **336**(6196): p. 244-6.
115. Gossen, M., et al., *Transcriptional activation by tetracyclines in mammalian cells.* Science, 1995. **268**(5218): p. 1766-9.
116. Urlinger, S., et al., *Exploring the sequence space for tetracycline-dependent transcriptional activators: novel mutations yield expanded range and sensitivity.* Proc Natl Acad Sci U S A, 2000. **97**(14): p. 7963-8.
117. Sheehan, D. and S. O'Sullivan, *Fast Protein Liquid Chromatography*, in *Protein Purification Protocols*, P. Cutler, Editor. 2004, Humana Press. p. 253-258.
118. Mukhopadhyay, A., *Inclusion bodies and purification of proteins in biologically active forms.* Adv Biochem Eng Biotechnol, 1997. **56**: p. 61-109.
119. Yip, T.T. and T.W. Hutchens, *Immobilized metal ion affinity chromatography.* Mol Biotechnol, 1994. **1**(2): p. 151-64.

120. Hochuli, E., H. Dobeli, and A. Schacher, *New metal chelate adsorbent selective for proteins and peptides containing neighbouring histidine residues.* J Chromatogr, 1987. **411**: p. 177-84.
121. Porath, J., et al., *Metal chelate affinity chromatography, a new approach to protein fractionation.* Nature, 1975. **258**(5536): p. 598-9.
122. Yip, T.T., Y. Nakagawa, and J. Porath, *Evaluation of the interaction of peptides with Cu(II), Ni(II), and Zn(II) by high-performance immobilized metal ion affinity chromatography.* Anal Biochem, 1989. **183**(1): p. 159-71.
123. Livak, K.J. and T.D. Schmittgen, *Analysis of relative gene expression data using real-time quantitative PCR and the 2(-Delta Delta C(T)) Method.* Methods, 2001. **25**(4): p. 402-8.
124. Schenke-Layland, K., et al., *Increased degradation of extracellular matrix structures of lacrimal glands implicated in the pathogenesis of Sjogren's syndrome.* Matrix Biol, 2008. **27**(1): p. 53-66.
125. Russell, H.K., Jr., *A modification of Movat's pentachrome stain.* Arch Pathol, 1972. **94**(2): p. 187-91.
126. Ng, E.S., et al., *Forced aggregation of defined numbers of human embryonic stem cells into embryoid bodies fosters robust, reproducible hematopoietic differentiation.* Blood, 2005. **106**(5): p. 1601-3.
127. Chadwick, K., et al., *Cytokines and BMP-4 promote hematopoietic differentiation of human embryonic stem cells.* Blood, 2003. **102**(3): p. 906-15.
128. Zhang, Z., et al., *Recombinant human decorin inhibits TGF-beta1-induced contraction of collagen lattice by hypertrophic scar fibroblasts.* Burns, 2009. **35**(4): p. 527-37.
129. Levin, J. and F.B. Bang, *THE ROLE OF ENDOTOXIN IN THE EXTRACELLULAR COAGULATION OF LIMULUS BLOOD.* Bull Johns Hopkins Hosp, 1964. **115**: p. 265-74.
130. Elin, R.J. and J. Hosseini, *Clinical utility of the Limulus amebocyte lysate (LAL) test.* Prog Clin Biol Res, 1985. **189**: p. 307-27.
131. Bayrak, A., et al., *Human immune responses to porcine xenogeneic matrices and their extracellular matrix constituents in vitro.* Biomaterials, 2010. **31**(14): p. 3793-803.
132. Murry, C.E., H. Reinecke, and L.M. Pabon, *Regeneration gaps: observations on stem cells and cardiac repair.* J Am Coll Cardiol, 2006. **47**(9): p. 1777-85.
133. Roger, V.L., et al., *Heart disease and stroke statistics--2012 update: a report from the American Heart Association.* Circulation, 2012. **125**(1): p. e2-e220.
134. Taylor, D.A., et al., *Regenerating functional myocardium: improved performance after skeletal myoblast transplantation.* Nat Med, 1998. **4**(8): p. 929-33.
135. Pouzet, B., et al., *Factors affecting functional outcome after autologous skeletal myoblast transplantation.* Ann Thorac Surg, 2001. **71**(3): p. 844-50; discussion 850-1.
136. Jain, M., et al., *Cell therapy attenuates deleterious ventricular remodeling and improves cardiac performance after myocardial infarction.* Circulation, 2001. **103**(14): p. 1920-7.
137. Amado, L.C., et al., *Cardiac repair with intramyocardial injection of allogeneic mesenchymal stem cells after myocardial infarction.* Proc Natl Acad Sci U S A, 2005. **102**(32): p. 11474-9.
138. Bearzi, C., et al., *Human cardiac stem cells.* Proc Natl Acad Sci U S A, 2007. **104**(35): p. 14068-73.
139. Zaruba, M.M., et al., *Cardiomyogenic potential of C-kit(+)-expressing cells derived from neonatal and adult mouse hearts.* Circulation, 2010. **121**(18): p. 1992-2000.
140. Chimenti, I., et al., *Relative roles of direct regeneration versus paracrine effects of human cardiosphere-derived cells transplanted into infarcted mice.* Circ Res, 2010. **106**(5): p. 971-80.
141. Andersen, D.C., et al., *Murine "cardiospheres" are not a source of stem cells with cardiomyogenic potential.* Stem Cells, 2009. **27**(7): p. 1571-81.

142. Etzion, S., et al., *Influence of embryonic cardiomyocyte transplantation on the progression of heart failure in a rat model of extensive myocardial infarction.* J Mol Cell Cardiol, 2001. **33**(7): p. 1321-30.
143. Li, R.K., et al., *Cardiomyocyte transplantation improves heart function.* Ann Thorac Surg, 1996. **62**(3): p. 654-60; discussion 660-1.
144. Scorsin, M., et al., *Comparison of the effects of fetal cardiomyocyte and skeletal myoblast transplantation on postinfarction left ventricular function.* J Thorac Cardiovasc Surg, 2000. **119**(6): p. 1169-75.
145. Fujii, T., et al., *Cell transplantation to prevent heart failure: a comparison of cell types.* Ann Thorac Surg, 2003. **76**(6): p. 2062-70; discussion 2070.
146. Hutcheson, K.A., et al., *Comparison of benefits on myocardial performance of cellular cardiomyoplasty with skeletal myoblasts and fibroblasts.* Cell Transplant, 2000. **9**(3): p. 359-68.
147. Kocher, A.A., et al., *Neovascularization of ischemic myocardium by human bone-marrow-derived angioblasts prevents cardiomyocyte apoptosis, reduces remodeling and improves cardiac function.* Nat Med, 2001. **7**(4): p. 430-6.
148. Balsam, L.B., et al., *Haematopoietic stem cells adopt mature haematopoietic fates in ischaemic myocardium.* Nature, 2004. **428**(6983): p. 668-73.
149. Menard, C., et al., *Transplantation of cardiac-committed mouse embryonic stem cells to infarcted sheep myocardium: a preclinical study.* Lancet, 2005. **366**(9490): p. 1005-12.
150. Christman, K.L. and R.J. Lee, *Biomaterials for the treatment of myocardial infarction.* J Am Coll Cardiol, 2006. **48**(5): p. 907-13.
151. Rane, A.A. and K.L. Christman, *Biomaterials for the treatment of myocardial infarction: a 5-year update.* J Am Coll Cardiol, 2011. **58**(25): p. 2615-29.
152. Nelson, D.M., et al., *Intra-myocardial biomaterial injection therapy in the treatment of heart failure: Materials, outcomes and challenges.* Acta Biomater, 2011. **7**(1): p. 1-15.
153. Sarig, U. and M. Machluf, *Engineering cell platforms for myocardial regeneration.* Expert Opin Biol Ther, 2011. **11**(8): p. 1055-77.
154. Nakamuta, J.S., et al., *Cell therapy attenuates cardiac dysfunction post myocardial infarction: effect of timing, routes of injection and a fibrin scaffold.* PLoS One, 2009. **4**(6): p. e6005.
155. Guo, H.D., et al., *Transplantation of marrow-derived cardiac stem cells carried in fibrin improves cardiac function after myocardial infarction.* Tissue Eng Part A, 2011. **17**(1-2): p. 45-58.
156. Danoviz, M.E., et al., *Rat adipose tissue-derived stem cells transplantation attenuates cardiac dysfunction post infarction and biopolymers enhance cell retention.* PLoS One, 2010. **5**(8): p. e12077.
157. Zhang, X., et al., *Preservation of the cardiac function in infarcted rat hearts by the transplantation of adipose-derived stem cells with injectable fibrin scaffolds.* Exp Biol Med (Maywood), 2010. **235**(12): p. 1505-15.
158. Zhang, G., et al., *Enhancing efficacy of stem cell transplantation to the heart with a PEGylated fibrin biomatrix.* Tissue Eng Part A, 2008. **14**(6): p. 1025-36.
159. Leor, J., et al., *Intracoronary injection of in situ forming alginate hydrogel reverses left ventricular remodeling after myocardial infarction in Swine.* J Am Coll Cardiol, 2009. **54**(11): p. 1014-23.
160. Landa, N., et al., *Effect of injectable alginate implant on cardiac remodeling and function after recent and old infarcts in rat.* Circulation, 2008. **117**(11): p. 1388-96.
161. Hao, X., et al., *Angiogenic effects of sequential release of VEGF-A165 and PDGF-BB with alginate hydrogels after myocardial infarction.* Cardiovasc Res, 2007. **75**(1): p. 178-85.

162. Ruvinov, E., J. Leor, and S. Cohen, *The promotion of myocardial repair by the sequential delivery of IGF-1 and HGF from an injectable alginate biomaterial in a model of acute myocardial infarction.* Biomaterials, 2011. **32**(2): p. 565-78.
163. Yu, J., et al., *The effect of injected RGD modified alginate on angiogenesis and left ventricular function in a chronic rat infarct model.* Biomaterials, 2009. **30**(5): p. 751-6.
164. Ou, L., et al., *Intracardiac injection of matrigel induces stem cell recruitment and improves cardiac functions in a rat myocardial infarction model.* J Cell Mol Med, 2011. **15**(6): p. 1310-8.
165. Laflamme, M.A., et al., *Cardiomyocytes derived from human embryonic stem cells in pro-survival factors enhance function of infarcted rat hearts.* Nat Biotechnol, 2007. **25**(9): p. 1015-24.
166. Zhao, Z.Q., et al., *Improvement in cardiac function with small intestine extracellular matrix is associated with recruitment of C-kit cells, myofibroblasts, and macrophages after myocardial infarction.* J Am Coll Cardiol, 2010. **55**(12): p. 1250-61.
167. Okada, M., et al., *Differential efficacy of gels derived from small intestinal submucosa as an injectable biomaterial for myocardial infarct repair.* Biomaterials, 2010. **31**(30): p. 7678-83.
168. Singelyn, J.M., et al., *Catheter-deliverable hydrogel derived from decellularized ventricular extracellular matrix increases endogenous cardiomyocytes and preserves cardiac function post-myocardial infarction.* J Am Coll Cardiol, 2012. **59**(8): p. 751-63.
169. Singelyn, J.M., et al., *Naturally derived myocardial matrix as an injectable scaffold for cardiac tissue engineering.* Biomaterials, 2009. **30**(29): p. 5409-16.
170. Seif-Naraghi, S.B., et al., *Design and characterization of an injectable pericardial matrix gel: a potentially autologous scaffold for cardiac tissue engineering.* Tissue Eng Part A, 2010. **16**(6): p. 2017-27.
171. Petersen, T.H., et al., *Matrix composition and mechanics of decellularized lung scaffolds.* Cells Tissues Organs, 2012. **195**(3): p. 222-31.
172. Schenke-Layland, K., et al., *Impact of decellularization of xenogeneic tissue on extracellular matrix integrity for tissue engineering of heart valves.* J Struct Biol, 2003. **143**(3): p. 201-8.
173. Mammoto, T. and D.E. Ingber, *Mechanical control of tissue and organ development.* Development, 2010. **137**(9): p. 1407-20.
174. Hinderer, S., et al., *Engineering of a bio-functionalized hybrid off-the-shelf heart valve.* Biomaterials, 2014. **35**(7): p. 2130-9.
175. Schenke-Layland, K., et al., *Recapitulation of the embryonic cardiovascular progenitor cell niche.* Biomaterials, 2011. **32**(11): p. 2748-56.
176. Hanjaya-Putra, D., et al., *Spatial control of cell-mediated degradation to regulate vasculogenesis and angiogenesis in hyaluronan hydrogels.* Biomaterials, 2012. **33**(26): p. 6123-31.
177. Kim, T.G., H. Shin, and D.W. Lim, *Biomimetic Scaffolds for Tissue Engineering.* Advanced Functional Materials, 2012. **22**(12): p. 2446-2468.
178. Hopkins, A.M., et al., *Silk Hydrogels as Soft Substrates for Neural Tissue Engineering.* Advanced Functional Materials, 2013. **23**(41): p. 5140-5149.
179. Olguin, H.C., C. Santander, and E. Brandan, *Inhibition of myoblast migration via decorin expression is critical for normal skeletal muscle differentiation.* Dev Biol, 2003. **259**(2): p. 209-24.
180. Lee, H.K., et al., *Nidogen plays a role in the regenerative axon growth of adult sensory neurons through Schwann cells.* J Korean Med Sci, 2009. **24**(4): p. 654-9.
181. Li, Y., et al., *Decorin gene transfer promotes muscle cell differentiation and muscle regeneration.* Mol Ther, 2007. **15**(9): p. 1616-22.

182. Krusius, T. and E. Ruoslahti, *Primary structure of an extracellular matrix proteoglycan core protein deduced from cloned cDNA.* Proc Natl Acad Sci U S A, 1986. **83**(20): p. 7683-7.
183. Ruoslahti, E., *Structure and biology of proteoglycans.* Annu Rev Cell Biol, 1988. **4**: p. 229-55.
184. Jarvelainen, H., et al., *A role for decorin in cutaneous wound healing and angiogenesis.* Wound Repair Regen, 2006. **14**(4): p. 443-52.
185. Reed, C.C. and R.V. Iozzo, *The role of decorin in collagen fibrillogenesis and skin homeostasis.* Glycoconj J, 2002. **19**(4-5): p. 249-55.
186. Hakkinen, L., et al., *A role for decorin in the structural organization of periodontal ligament.* Lab Invest, 2000. **80**(12): p. 1869-80.
187. Kalamajski, S. and A. Oldberg, *The role of small leucine-rich proteoglycans in collagen fibrillogenesis.* Matrix Biol, 2010. **29**(4): p. 248-53.
188. Schaefer, L. and R.V. Iozzo, *Biological functions of the small leucine-rich proteoglycans: from genetics to signal transduction.* J Biol Chem, 2008. **283**(31): p. 21305-9.
189. Bernfield, M., et al., *Functions of cell surface heparan sulfate proteoglycans.* Annu Rev Biochem, 1999. **68**: p. 729-77.
190. Casu, B. and U. Lindahl, *Structure and biological interactions of heparin and heparan sulfate.* Adv Carbohydr Chem Biochem, 2001. **57**: p. 159-206.
191. Dellett, M., et al., *Small leucine rich proteoglycan family regulates multiple signalling pathways in neural development and maintenance.* Dev Growth Differ, 2012. **54**(3): p. 327-40.
192. Waddington, R.J., et al., *Differential roles for small leucine-rich proteoglycans in bone formation.* Eur Cell Mater, 2003. **6**: p. 12-21; discussion 21.
193. Rada, J.A., et al., *Proteoglycan composition in the human sclera during growth and aging.* Invest Ophthalmol Vis Sci, 2000. **41**(7): p. 1639-48.
194. Zhao, J., et al., *Adenovirus-mediated decorin gene transfer prevents TGF-beta-induced inhibition of lung morphogenesis.* Am J Physiol, 1999. **277**(2 Pt 1): p. L412-22.
195. Border, W.A., et al., *Natural inhibitor of transforming growth factor-beta protects against scarring in experimental kidney disease.* Nature, 1992. **360**(6402): p. 361-4.
196. Yamaguchi, Y., D.M. Mann, and E. Ruoslahti, *Negative regulation of transforming growth factor-beta by the proteoglycan decorin.* Nature, 1990. **346**(6281): p. 281-4.
197. Cheifetz, S. and J. Massague, *Transforming growth factor-beta (TGF-beta) receptor proteoglycan. Cell surface expression and ligand binding in the absence of glycosaminoglycan chains.* J Biol Chem, 1989. **264**(20): p. 12025-8.
198. Hildebrand, A., et al., *Interaction of the small interstitial proteoglycans biglycan, decorin and fibromodulin with transforming growth factor beta.* Biochem J, 1994. **302 (Pt 2)**: p. 527-34.
199. Isaka, Y., et al., *Gene therapy by skeletal muscle expression of decorin prevents fibrotic disease in rat kidney.* Nat Med, 1996. **2**(4): p. 418-23.
200. Stander, M., et al., *Decorin gene transfer-mediated suppression of TGF-beta synthesis abrogates experimental malignant glioma growth in vivo.* Gene Ther, 1998. **5**(9): p. 1187-94.
201. Stander, M., et al., *Transforming growth factor-beta and p-21: multiple molecular targets of decorin-mediated suppression of neoplastic growth.* Cell Tissue Res, 1999. **296**(2): p. 221-7.
202. Kolb, M., et al., *Proteoglycans decorin and biglycan differentially modulate TGF-beta-mediated fibrotic responses in the lung.* Am J Physiol Lung Cell Mol Physiol, 2001. **280**(6): p. L1327-34.
203. Baghy, K., et al., *Ablation of the decorin gene enhances experimental hepatic fibrosis and impairs hepatic healing in mice.* Lab Invest, 2011. **91**(3): p. 439-51.

204. Maciejewski, C.C., et al., *Differential expression of class I small leucine-rich proteoglycans in an animal model of partial bladder outlet obstruction.* J Urol, 2012. **188**(4 Suppl): p. 1543-8.
205. Honardoust, D., et al., *Small leucine-rich proteoglycans, decorin and fibromodulin, are reduced in postburn hypertrophic scar.* Wound Repair Regen, 2011. **19**(3): p. 368-78.
206. Imanishi, J., et al., *Growth factors: importance in wound healing and maintenance of transparency of the cornea.* Prog Retin Eye Res, 2000. **19**(1): p. 113-29.
207. Mohan, R.R., et al., *Apoptosis, necrosis, proliferation, and myofibroblast generation in the stroma following LASIK and PRK.* Exp Eye Res, 2003. **76**(1): p. 71-87.
208. Netto, M.V., et al., *Stromal haze, myofibroblasts, and surface irregularity after PRK.* Exp Eye Res, 2006. **82**(5): p. 788-97.
209. Stramer, B.M., et al., *Molecular mechanisms controlling the fibrotic repair phenotype in cornea: implications for surgical outcomes.* Invest Ophthalmol Vis Sci, 2003. **44**(10): p. 4237-46.
210. Wilson, S.E., et al., *The wound healing response after laser in situ keratomileusis and photorefractive keratectomy: elusive control of biological variability and effect on custom laser vision correction.* Arch Ophthalmol, 2001. **119**(6): p. 889-96.
211. Mohan, R.R., et al., *Decorin transfection suppresses profibrogenic genes and myofibroblast formation in human corneal fibroblasts.* Exp Eye Res, 2010. **91**(2): p. 238-45.
212. Giri, S.N., et al., *Antifibrotic effect of decorin in a bleomycin hamster model of lung fibrosis.* Biochem Pharmacol, 1997. **54**(11): p. 1205-16.
213. Kolb, M., et al., *Transient transgene expression of decorin in the lung reduces the fibrotic response to bleomycin.* Am J Respir Crit Care Med, 2001. **163**(3 Pt 1): p. 770-7.
214. Li, L., et al., *Postinfarction gene therapy with adenoviral vector expressing decorin mitigates cardiac remodeling and dysfunction.* Am J Physiol Heart Circ Physiol, 2009. **297**(4): p. H1504-13.
215. Toole, B.P., *Solubility of collagen fibrils formed in vitro in the presence of sulphated acid mucopolysaccharide-protein.* Nature, 1969. **222**(5196): p. 872-3.
216. Toole, B.P. and D.A. Lowther, *Dermatan sulfate-protein: isolation from and interaction with collagen.* Arch Biochem Biophys, 1968. **128**(3): p. 567-78.
217. Danielson, K.G., et al., *Targeted disruption of decorin leads to abnormal collagen fibril morphology and skin fragility.* J Cell Biol, 1997. **136**(3): p. 729-43.
218. Timpl, R., *Structure and biological activity of basement membrane proteins.* Eur J Biochem, 1989. **180**(3): p. 487-502.
219. Miosge, N., et al., *Nidogen-1 and nidogen-2 are found in basement membranes during human embryonic development.* Histochem J, 2001. **33**(9-10): p. 523-30.
220. Ries, A., et al., *Recombinant domains of mouse nidogen-1 and their binding to basement membrane proteins and monoclonal antibodies.* Eur J Biochem, 2001. **268**(19): p. 5119-28.
221. Shamhart, P.E. and J.G. Meszaros, *Non-fibrillar collagens: key mediators of post-infarction cardiac remodeling?* J Mol Cell Cardiol, 2010. **48**(3): p. 530-7.
222. Kohfeldt, E., et al., *Nidogen-2: a new basement membrane protein with diverse binding properties.* J Mol Biol, 1998. **282**(1): p. 99-109.
223. Yurchenco, P.D. and J.C. Schittny, *Molecular architecture of basement membranes.* FASEB J, 1990. **4**(6): p. 1577-90.
224. Zhou, J., et al., *Embryoid bodies formation and differentiation from mouse embryonic stem cells in collagen/Matrigel scaffolds.* J Genet Genomics, 2010. **37**(7): p. 451-60.
225. Baharvand, H., et al., *The effect of extracellular matrix on embryonic stem cell-derived cardiomyocytes.* J Mol Cell Cardiol, 2005. **38**(3): p. 495-503.

226. Kleinman, H.K., et al., *Basement membrane complexes with biological activity.* Biochemistry, 1986. **25**(2): p. 312-8.
227. Funanage, V.L., S.M. Smith, and M.A. Minnich, *Entactin promotes adhesion and long-term maintenance of cultured regenerated skeletal myotubes.* J Cell Physiol, 1992. **150**(2): p. 251-7.
228. Rasooly, R., B. Hernlem, and M. Friedman, *Low levels of aflatoxin B1, ricin, and milk enhance recombinant protein production in mammalian cells.* PLoS One, 2013. **8**(8): p. e71682.
229. Chen, S., et al., *Production of Recombinant Proteins in Mammalian Cells*, in *Current Protocols in Protein Science*. 2001, John Wiley & Sons, Inc.
230. Murnane, J.P., *The role of recombinational hotspots in genome instability in mammalian cells.* Bioessays, 1990. **12**(12): p. 577-81.
231. Marshall, E., *Gene Therapy Death Prompts Review of Adenovirus Vector.* Science, 1999. **286**(5448): p. 2244-2245.
232. Sherman, W., et al., *Catheter-based delivery of cells to the heart.* Nat Clin Pract Cardiovasc Med, 2006. **3 Suppl 1**: p. S57-64.
233. Gyongyosi, M. and N. Dib, *Diagnostic and prognostic value of 3D NOGA mapping in ischemic heart disease.* Nat Rev Cardiol, 2011. **8**(7): p. 393-404.
234. Masuda, H., Y. Takakura, and M. Hashida, *Pharmacokinetics and disposition characteristics of recombinant decorin after intravenous injection into mice.* Biochim Biophys Acta, 1999. **1426**(3): p. 420-8.
235. Tufvesson, E. and G. Westergren-Thorsson, *Biglycan and decorin induce morphological and cytoskeletal changes involving signalling by the small GTPases RhoA and Rac1 resulting in lung fibroblast migration.* J Cell Sci, 2003. **116**(Pt 23): p. 4857-64.
236. Merle, B., et al., *Decorin inhibits cell attachment to thrombospondin-1 by binding to a KKTR-dependent cell adhesive site present within the N-terminal domain of thrombospondin-1.* J Cell Biochem, 1997. **67**(1): p. 75-83.
237. Winnemoller, M., G. Schmidt, and H. Kresse, *Influence of decorin on fibroblast adhesion to fibronectin.* Eur J Cell Biol, 1991. **54**(1): p. 10-7.
238. Winnemoller, M., et al., *Interactions between thrombospondin and the small proteoglycan decorin: interference with cell attachment.* Eur J Cell Biol, 1992. **59**(1): p. 47-55.
239. Bidanset, D.J., et al., *Regulation of cell substrate adhesion: effects of small galactosaminoglycan-containing proteoglycans.* J Cell Biol, 1992. **118**(6): p. 1523-31.
240. Morita, M., et al., *Modification of infarct material properties limits adverse ventricular remodeling.* Ann Thorac Surg, 2011. **92**(2): p. 617-24.
241. Ryan, L.P., et al., *Dermal filler injection: a novel approach for limiting infarct expansion.* Ann Thorac Surg, 2009. **87**(1): p. 148-55.
242. Lu, S., et al., *Both the transplantation of somatic cell nuclear transfer- and fertilization-derived mouse embryonic stem cells with temperature-responsive chitosan hydrogel improve myocardial performance in infarcted rat hearts.* Tissue Eng Part A, 2010. **16**(4): p. 1303-15.
243. Yoon, S.J., et al., *Regeneration of ischemic heart using hyaluronic acid-based injectable hydrogel.* J Biomed Mater Res B Appl Biomater, 2009. **91**(1): p. 163-71.

7.4 Curriculum Vitae

Monika Holeiter
Ifflandstr. 20, 70563 Stuttgart, Germany

PERSONAL INFORMATION

Born on 14th July 1984 in Sathmar (Rumania), Nationality: German

EDUCATION

since 07/2010	PhD thesis at the University of Stuttgart (IGVP) c/o Fraunhofer IGB, Fraunhofer Attract Group “Bio-inspired Cardiovascular Regeneration” in the Department of Cell and Tissue Engineering.
07/2011 – 11/2011	Project at the University of California, Los Angeles (UCLA), funded by a Boehringer Ingelheim Fonds Travel Grant. Title: Impact of human pluripotent stem cell-derived extracellular matrix proteins on cell fate decision.
10/2004 – 04/2010	Studies of Technical Biology at the University of Stuttgart, Graduation: Dipl.-Biol. (t.o.), (grade: 1.0).
08/2009 – 04/2010	Diploma Thesis at the University of Stuttgart, Institute for Cell Biology and Immunology. Title: Influence of sphingomyeline synthases on epidermal growth factor receptor signaling.
05/2008 – 09/2008	Semester Project at the University of Cardiff, Brain Repair Group, Wales, UK, funded by an ERASMUS scholarship. Title: Identification of stem cell markers for cell replacement therapy in Huntington disease.
1995 – 2004	Heinrich-Heine-Gymnasium, Ostfildern, Esslingen. General qualification for university entrance, (grade: 1.4). Prize for outstanding achievements in the subject Biology.

ADDITIONAL TRAINING

04/2009 – 06/2009	Internship at Roche Diagnostics in Mannheim, in the area of marketing and lab-diagnostics.
08/2006 – 12/2007	Discontinuously: student research assistant at the University of Stuttgart, Institute for Cell Biology and Immunology.
08/2006 – 04/2007	Attendance of the optional course: Preparing for the TOEFL at the Language-center of the University of Stuttgart, (grade: 1.3).

7.5 Academic contributions

With the results of this PhD thesis the following patents were filed:

Shannon Layland (34%), Katja Schenke-Layland (33%), **Monika Holeiter** (33%), Glycosylated protein of an extracellular matrix for use in a method of treating an ischemic heart of a human or animal subject, # EP 13178951.3-1456 patent pending and # PCT/EP2014/066497 patent pending.

To date, academic contributions containing results of this PhD thesis were severely restricted, in order not to forestall and jeopardize the pending patent approvals.

Peer-reviewed publications

Heering J, Weis N, **Holeiter M**, Neugart F, Staebler A, Fehm TN, Bischoff A, Schiller J, Duss S, Schmid S, Korte T, Herrmann A, Olayioye MA. *Loss of the ceramide transfer protein augments EGF receptor signaling in breast cancer*. Cancer Res. 2012 Jun 1;72(11):2855-66. doi: 10.1158/0008-5472.CAN-11-3069. Epub 2012 Apr 3.

Groeber F, **Holeiter M**, Hampel M, Hinderer S, Schenke-Layland K. *Skin tissue engineering--in vivo and in vitro applications*. Adv Drug Deliv Rev. 2011 Apr 30;63(4-5):352-66. doi: 10.1016/j.addr.2011.01.005. Epub 2011 Jan 15. Review.

Holeiter M, Knopf A, Bluguermann C, Evseenko D, Crooks G, Schenke-Layland K. *Identification of the cardio-inductive potential of Nidogen-1 and its role in cardiac regeneration post MI.* In preparation.

Holeiter M, Sudrow K, Che N, Knopf A, Layland S L, Seifert M, Schenke-Layland K. *Biogenesis of the human extracellular matrix protein decorin for applications in regenerative medicine and immune reaction in a human in vitro test system.* In preparation.

Oral presentations

Holeiter M, Bluguermann C, Evseenko D, Crooks G, Schenke-Layland K. *Impact of human pluripotent stem cell-derived extracellular matrix proteins on cardiac cell fate decision.* Experimental Biology, Boston, USA, April 2013.

Poster presentations

Holeiter M, Bluguermann C, Evseenko D, Crooks G, Schenke-Layland K. *Impact of human pluripotent stem cell-derived extracellular matrix proteins on cardiac cell fate decision*. Hilton Head Conference, Hilton Head, USA, March 2012.

Holeiter M, Bluguermann C, Evseenko D, Crooks G, Schenke-Layland K. *Impact of human pluripotent stem cell-derived extracellular matrix proteins on cardiac cell fate decision*. Annual Meeting of the German Society for Matrix Biology (DGMB), Tübingen, Germany, March 2013.

Holeiter M, Bluguermann C, Evseenko D, Crooks G, Schenke-Layland K. *Impact of human pluripotent stem cell-derived extracellular matrix proteins on cardiac cell fate*. Annual Meeting of the German Society for Matrix Biology (DGMB), Regensburg, Germany, March 2013.

License for the use of human embryonic stem cells

Based on the results of this thesis, we successfully applied at the Robert Koch Institute for the license to import and use human embryonic stem cells in the laboratories of Prof. Dr. Katja Schenke-Layland at the Eberhard Karls University Tübingen and the Fraunhofer IGB in 2013: “Antrag auf Einfuhr und Verwendung humaner embryonaler Stammzellen nach Stammzellgesetz – StZG”. Title: “Kardioinduktive Wirkung von Proteinen der extrazellulären Matrix auf humane embryonale Stammzellen in einem 3D Trägergerüst“.

7.6 Acknowledgments

During this PhD thesis I have experienced a lot of support from my colleagues at the University of Stuttgart (IGVP), Fraunhofer IGB and the University of California (UCLA). I wish to thank all those who helped me bring this work to a successful conclusion. I particularly thank…

… Prof. Dr. Thomas Hirth and Prof. Dr. Günter Tovar for providing the possibility to accomplish my PhD thesis at the IGVP of the University of Stuttgart and the Fraunhofer IGB.

… Prof. Dr. Günter Tovar for being the first assessor of my PhD work. Thank you for your friendly support and trust in my scientific work.

… Prof. Dr. Thomas Hirth and Prof. Dr. Katja Schenke-Layland for being the second assessors of my PhD work. Thank you for your help and support.

… Prof. Dr. Katja Schenke-Layland for the supervision of this work. You enabled me to conduct a part of this work at the UCLA, which was invaluable for my PhD thesis and for me personally. I thank you for your constructive advice during this whole time and for all the opportunities you gave me. You taught me to “think big”.

… Prof. Dr. Peter Scheurich who kindly agreed to chair my PhD examination.

… Prof. Dr. Gay Crooks, Prof. Dr. Denis Evseenko and MD. Ali Nsair from the University of California for their support and input to this work. I also thank Carolina Bluguermann and Brooke Latour for the pleasant working atmosphere.

… Nam Che from the University of California for his help and advice for the stable clone generation. Although on a different continent I could always count on your support.

… Anne Knopf for her motivated work and great support throughout this time.

… PD Dr. Martina Seifert and Katrin Sudrow for their great work with the in vitro immune tests and Stefanie Weisser for her support with the dermal equivalent contraction assay.

… all my colleagues in the department Cell and Tissue Engineering, especially Claudia, Alex, Florian, Susanne and Michael for the great working atmosphere.

… my friends and

especially my family. You always stand behind me and I cannot thank you enough.

7.7 Erklärung

Hiermit versichere ich, dass ich die vorliegende Arbeit selbst und lediglich unter Verwendung der angegebenen Quellen und Hilfsmittel verfasst habe.

Monika Holeiter